Geophys. J. Int. (1996) **125**, 639–678

Seismic moment assessment of earthquakes in stable continental regions—II. Historical seismicity

Arch C. Johnston

Center for Earthquake Research and Information (CERI), The University of Memphis, Memphis, TN 38152, *USA*

Accepted 1995 December 18. Received 1995 December 14; in original form 1994 October 17

SUMMARY

Seismic intensity observations contain sufficient information about the earthquake source to quantitatively constrain its scalar seismic moment, M_0, and hence moment magnitude, **M**, within useful limits. This is valuable, especially in the pre-instrumental and early instrumental seismic eras, but also in the modern era. This study is limited to stable continental regions where intensity data are especially important for seismic hazard assessment, but the methodology is generic and can be applied to other tectonically active regions. It builds on regression techniques developed in the Part I analysis (Johnston 1996) and applies them to isoseismal area (A_i) data. Derived regression relations for modified Mercalli isoseismal areas for levels felt to VIII yield a predicted $\log(M_0)$ or **M** value within specified 1σ uncertainty bounds. Standard linear and polynomial regressions are tested against a new functional regression form proposed by Frankel (1994), which contains both geometrical spreading and anelastic attenuation terms. Goodness-of-fit statistics are similar, but the Frankel regression form is preferred because it is derived from physical principles of wave propagation. The A_{felt}–A_{IV} regressions, with most data at epicentral distance $r > 100$ km, are controlled by surface-wave (L_g) geometrical spreading and attenuation characteristics. For the A_{VII} and A_{VIII} regressions, r is mainly less than 100 km and body-wave propagation dominates, although near-source site and path effects are significant. The A_{V} and A_{VI} regressions are transitional between the L_g and body-wave domains. With either the Frankel or quadratic regression, individual isoseismal areas can constrain the source event's moment magnitude within an estimated ± 0.30–0.45 **M** units except at the regression extremes. If a suite of isoseismal areas is available for the same earthquake, these uncertainties can be approximately halved by weighted averaging. This means that when good-quality isoseismal data exist for an event, they are capable of constraining its seismic moment estimate within the same order of uncertainty as individual instrumental magnitude readings. Hence, historical seismicity data may usefully be combined with instrumental data in seismic hazard analyses. A hierarchy of methods to recover an earthquake's M_0 or **M** combines the instrumental results of Part I with the isoseismal area results of this study. Finally, regressions on $I_{\max}$ and number of recording stations provide the means to estimate **M** to within $\sim \pm 0.45$–0.55 M units when no other data are available.

Key words: earthquake intensity, seismic moment, stable continental regions.

INTRODUCTION

Prior to the beginning of the instrumental era of seismology in the 1890s, the occurrence of earthquakes and their characteristics were known only through their effects on people, structures and the land. Our knowledge of historical earthquakes is, therefore, necessarily qualitative and does not lend itself to quantitative analysis. Constrained size estimates of pre-instrumental earthquakes, however, are an important element in seismic hazard assessment. This is true even in highly active plate-boundary seismic zones, where the average repeat times of the larger earthquakes usually exceed a century. Moreover, the importance of pre-instrumental data is inversely proportional to the seismic activity level of a region because for less-active (i.e. lower strain rate) regions, the recurrence intervals are longer, moving an increasing percentage of

larger earthquakes to the pre-instrumental or historical seismic era.

In this paper I examine the historical seismicity of some of the Earth's least active regions, the stable continental plate interiors. A companion paper (Johnston 1996, hereafter referred to as Part I) treats the instrumental seismicity of these areas, collectively called stable continental regions, or SCRs. SCRs are defined briefly in Part I and extensively in Kanter (1994), so I will not repeat the complete development here. They are the continental nuclei, the Archaean cratons of North and South America, Africa, Europe, Asia, India, Australia, and Antarctica, and their associated Proterozoic terranes, Palaeozoic fold belts and Mesozoic/Cenozoic passive margins. They constitute nearly two-thirds of all continental crust and are the host lands for $\sim$60 per cent of the world's population. In global terms their seismicity is negligible, yet more than 100 moment magnitude $\mathbf{M} \geq 6$ earthquakes have been documented in SCRs (Johnston 1994a). This, coupled with the large population, leads to a significant SCR seismic risk. The Killari–Latur earthquake of September 1993 in the SCR of peninsular India (Gupta 1993) provides a recent and fatal example.

To assess the seismic hazard of stable continental regions, reliance on the historical earthquake record is unavoidable. For example, of the ten largest known earthquakes in onshore SCR North America (my rankings, Johnston 1994a), eight occurred in the historical period and none during the modern seismic era (1964–present). Moreover, many moderate earthquakes of the early instrumental era ($\sim$1900–1963) are known only through their macroseismic effects, as reported in terms of intensity data. The purpose of this paper is to provide the analytical tools to obtain constrained moment–magnitude estimates of SCR earthquakes from intensity data, thus yielding an improved combined historical and instrumental seismicity database for seismic hazard assessment.

Most of the regression analysis methodology developed in Part I for recovering **M** from the logarithm of seismic-wave amplitude (instrumental magnitude) applies equally well to intensity data in the form of the logarithm of isoseismal area. Therefore, for topics such as outlier evaluation, chi-square goodness-of-fit criteria and error propagation analysis that are common to both data sets, I refer the reader to Part I for the complete treatment. Other topics unique to intensity data, such as estimating the uncertainty of isoseismal areas and choice of the regression functional form, are fully developed here.

Regression on isoseismal area to recover seismic moment is not new to this study. Earlier regional applications include Hanks, Hileman & Thatcher (1975), Wesnousky, Scholz & Shimazaki (1982) and Wesnousky *et al.* (1984) in tectonically active zones, and Herrmann, Cheng & Nuttli (1978) and Bollinger, Chapman & Sibol (1993) in the central and eastern United States. What is new, however, is a global scope, an extensive examination of regression functional form, and a detailed assessment of uncertainty. It turns out that, unsurprisingly, isoseismal areas are not able to predict an earthquake's seismic moment M_0 (or **M**) as reliably as teleseismic instrumental magnitudes. What may be suprising, however, is how well the intensity data are able to constrain the seismic moment of the source earthquake. If several isoseismal areas of different intensity levels are available for an earthquake, a robust estimate of M_0 is possible, one that often is comparable to estimates from regional or even short-period teleseismic magnitudes. To reach this conclusion requires extensive analysis of the SCR data provided in the Appendix. Such an analysis for modified Mercalli levels felt to VIII, for maximum intensity, and for number of recording stations is the subject of this paper.

THE SCR SEISMIC MOMENT–ISOSEISMAL AREA DATABASE

SCR isoseismal data

Table A3 in the Appendix contains the isoseismal area data for all SCR earthquakes that have both mapped (and published) isoseismal area(s) and a directly determined seismic moment. The adopted seismic-moment values and associated uncertainties are extracted directly from the Part I seismic-moment data base, which consists of 177 SCR events with directly determined M_0. The subset with published isoseismal data consists of 84 earthquakes (47 per cent) of which 51 events (61 per cent) are from North America, where more earthquakes of small-to-moderate M_0 have been analysed by waveform modelling than in other SCRs. North America is listed separately in Table A3(a) and the appendix bibliography, and a separate set of North American SCR regressions is developed in Part III. Table B1 in Part I gives the hypocentral data and faulting mechanisms for all SCR events. All entries of the Part I and Part II databases are fully referenced in their respective appendix bibliographies.

The basic datum for this regression analysis is the (base 10) logarithm of a modified Mercalli isoseismal (MMI) area for intensity levels felt to VIII. Above VIII we run out of data—and the MMI VII and VIII regressions are marginal in this regard. This study is not sensitive to the choice of the modified Mercalli intensity scale (Wood & Neumann 1931), nor to proposed modifications to the Wood & Neumann scale, such as those by Richter (1958) or Brazee (1978). Following standard practice [e.g. the explanatory text for the Preliminary Determination of Epicenters (NEIC 1963–1994)], I take the major European scales, Medvedev–Sponheuer–Kárník (MSK) and Mercalli–Cancanni–Seiberg (MCS), as equivalent to the modified Mercalli scale of Wood & Neumann. The conversion of the Rossi–Forel (RF) scale to MMI is also a long-recognized standard (Richter 1958; NEIC 1963–1994). The Japanese intensity scale is not applicable to stable continental regions.

Global studies such as this are, of necessity, dependent on data published in the literature. No original sources (mainly newspapers or field survey reports) have been consulted for re-evaluation of intensity observations for any of the earthquakes in the database. Table A3 does not include quoted isoseismal areas or radii; a requirement was that each isoseismal area could be measured from scaled isoseismal maps. Together, measurement and map-scaling errors should be less than 5–10 per cent and are minor in comparison to the other major isoseismal uncertainties discussed below, which can exceed a factor of two (100 per cent). Many events in the SCR database had multiple published isoseismal maps. Data not used in the regression are identified with a dagger (†) in Table A3. The final regression isoseismal values (bold type) are a mixture of weighted-average and single-source data. All data, used and unused, are included in Table A3 so the interested reader may judge the variability among multiple sources, similar to the procedure for the $\log(M_0)$ data in Part I. Those results are transferred to this study as the assigned $\log(M_0)$ values in Table A3.

Appendix Table A4 contains additional SCR isoseismal data

used in the regression analysis. The three initial criteria for an earthquake to be included were:

(1) that it occurred in stable continental crust;
(2) that it had a directly determined M_0;
(3) that it had an isoseismal map.

I have relaxed these criteria for nine SCR earthquakes without a direct M_0 determination and for three large earthquakes that occurred on SCR borders (Table A4). For the former I assigned M_0 and associated uncertainty from the Part I regressions on teleseismic M_s and m_b. The border events, which had direct M_0 determinations, had isoseismal areas largely within the adjacent SCR (Fig. 1) so that stable continental attenuation and scattering governed the isoseismal contours. The rationale for including these 12 events is that the advantages afforded by the additional control on the regression curve fits outweigh the disadvantages of the increased uncertainty associated with these data.

Isoseismal area uncertainty

Uncertainty of isoseismal area (A_i, i = felt–VIII) data is treated in the same manner as seismic moment in Part I. For logarithmic data such as $\log(M_0)$ or $\log(A_i)$, uncertainty is the standard deviation of the log value, for example $\sigma^{\pm}_{\log}$, which is related to the uncertainty in A_i via a multiplicative error factor MEF such that:

$$\sigma^{+}_{\log} = \log(\mathrm{MEF}); \quad (A_i)(\mathrm{MEF}) = A_i + \sigma^{+},$$
$$\sigma^{-}_{\log} = \log(\mathrm{MEF}); \quad \frac{A_i}{\mathrm{MEF}} = A_i - \sigma^{-}. \tag{1}$$

The MEFs for M_0 in appendix Table A3 are adopted directly from Part I but MEFs for A_i are developed here, as described next.

The assignment of A_i data uncertainty was the most qualitative aspect of this study. None of the data sources of Table A3 estimates errors or uncertainties. For the majority of

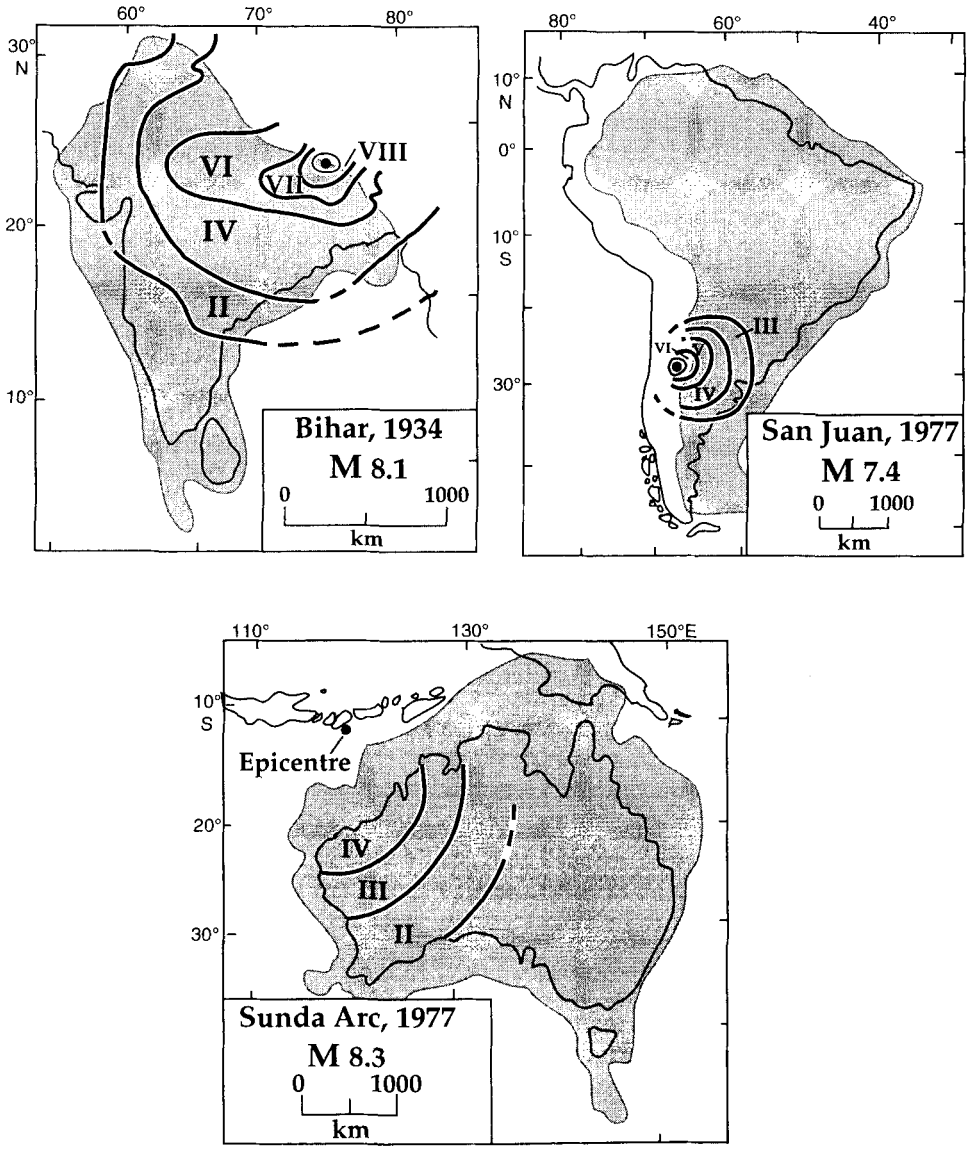

Figure 1. Modified Mercalli intensity maps of the three SCR border events included in this study. These earthquakes are either plate boundary or active intraplate, but their isoseismal areas are predominantly in SCR crust (shaded). See appendix Table A4 for data sources.

the maps only isoseismal contours are given, not the individual data points. None of the maps has a specific uncertainty assigned to a given contour, nor is there any discussion of the range of the contour allowed by the observations. To provide uncertainty for such data, I consider two separate potential error sources: contour error and intensity observation error. Contour error assumes the intensity data are correct, but the intermingling of observations of different intensities or the lack of observations over large areas within the contour (e.g. oceanic or unpopulated regions) forces the investigator to interpolate and/or extrapolate the contour. Abundant data of good quality interpreted by an experienced analyst might limit contour error to $\sim$10 per cent (MEF = 1.1), while for poor data and haphazard analysis, contour error could reach 50 per cent (MEF = 1.5) or worse.

Observation error is potentially more serious. In the worst case, systematic misassignment of intensity values could result in isoseismal contours that are displaced by an entire intensity unit. To 'calibrate' A_i uncertainties, I combine contour and observation error and let this worst case represent $2\sigma_{\log}$ uncertainty for an isoseismal area rated of poor quality. The ratings good, fair and poor in Table A3 are judgments of the event's average contour quality based on the following criteria.

Isoseismal contour quality	No. of data points	Fraction of total area contoured	General reliability
poor	none	$\lesssim 1/3$	small or unreliable distance scale MMI/RF/other scale uncertainty old or unknown authors or sources
fair	few to none	$\sim 1/3$–$2/3$	reliable distance scale MMI or MSK or equivalent more recent analysis
good	few to many	$\gtrsim 2/3$	accurate latitude/longitude and scale standardized and documented analysis recent; experienced analysts

These contour quality ratings are combined with observation error to yield the final assigned MEF uncertainty for each Table A3 source. If an isoseismal contour can be in error by an entire intensity level, then uncertainty for a poor contour becomes $2\sigma^{\pm}_{\log} = \log(A_{i+1}) - \log(A_i) = \Delta \log(A_i)$. For fair- and good-quality contours, I take 75 per cent and 50 per cent, respectively, of $\Delta \log(A_i)$. From eqs (1), this yields the following for the total A_i uncertainty assignments:

$$[\mathrm{MEF}_{A_i}]_{\mathrm{poor}} = 10^{(\Delta \log A_i)/2},$$
$$[\mathrm{MEF}_{A_i}]_{\mathrm{fair}} = 10^{3(\Delta \log A_i)/8}, \quad (2)$$
$$[\mathrm{MEF}_{A_i}]_{\mathrm{good}} = 10^{(\Delta \log A_i)/4}.$$

Values of $\Delta \log(A_i)$ vary for different pairs of isoseismal contours; hence assigned uncertainties will also vary. Fig. 2 illustrates this for a typical **M** = 6.0 suite of isoseismal contours. Note that the small inner isoseismals exhibit higher $\Delta \log(A_i)$ values, hence greater observational uncertainty, than the larger outer contours. This is a general pattern that holds to varying degrees throughout the entire magnitude range. Table 1 summarizes the final A_i MEF uncertainties used in this study, as computed from eqs (2) and averaged for the $\Delta \log(A_i)$ value for contours both above and below a given A_i. I assigned each individual A_i in Table A3 a contour quality rating with an MEF from Table 1.

Assigned A_i uncertainty affects the $\log(M_0)$–$\log(A_i)$ regressions in two ways. It directly affects the least-squares fit when the data are weighted by the reciprocal of their uncertainty, although I found this effect was minor and usually not significant, as have other investigators performing geophysical data regressions (e.g. Singh, Bazan & Esteva 1980; Bonilla, Mark & Lienkaemper 1984; Wells & Coppersmith 1994). This is because the intrinsic variability of the intensity data is high, so that event-to-event differences (aleatory uncertainty) dominate over measurement errors (epistemic uncertainty). Even if contour and observation errors were zero, there would still be significant scatter in the regression data arising from such variables as hypocentral depth differences, attenuation and site-effect differences, and source differences in stress drop, radiation pattern, and directivity. I examine the important cases of stress drop and attenuation variability in a later section. The second

Table 1. Isoseismal area uncertainty assignments.

M	log(M_0)	A_{felt} G	F	P	A_{III} G	F	P	A_{IV} G	F	P	A_V G	F	P	A_{VI} G	F	P	A_{VII} G	F	P	A_{VIII} G	F	P
4.0	22.05	†1.3	1.4	1.5	1.3	1.4	1.6	1.5	1.8	2.1	2.6	3.5	4.3	—	—	—	—	—	—	—	—	—
4.5	22.80	1.2	1.4	1.5	1.3	1.4	1.5	1.4	1.7	1.9	2.2	2.8	3.4	4.4	6.6	9.8	—	—	—	—	—	—
5.0	23.55	1.2	1.3	1.4	1.2	1.3	1.4	1.3	1.5	1.7	2.1	2.6	3.1	4.0	5.5	7.0	5.5	7.8	10.0	—	—	—
5.5	24.30	1.2	1.2	1.3	1.2	1.3	1.4	1.3	1.4	1.5	1.9	2.3	2.7	2.8	3.7	4.6	3.7	5.1	6.4	4.5	6.3	8.0
6.0	25.05	1.1	1.2	1.3	1.2	1.3	1.3	1.2	1.4	1.5	1.7	2.0	2.4	2.1	2.7	3.2	2.7	3.5	4.4	4.0	5.5	7.0
6.5	25.80	1.1	1.2	1.2	1.1	1.2	1.3	1.2	1.3	1.4	1.5	1.8	2.1	1.8	2.2	2.6	2.1	2.6	3.2	3.2	4.2	5.3
7.0	26.55	1.1	1.1	1.2	1.1	1.2	1.2	1.2	1.3	1.3	1.4	1.6	1.8	1.6	1.9	2.2	1.8	2.2	2.5	2.5	3.3	4.1
7.5	27.30	1.1	1.1	1.15	1.1	1.151.2		1.151.2	1.3		1.3	1.5	1.6	1.5	1.7	1.9	1.6	1.9	2.3	2.3	2.9	3.5
8.0	28.05	1.05	1.1	1.1	1.1	1.1	1.15	1.1	1.2	1.2	1.2	1.3	1.4	1.4	1.5	1.7	1.6	1.8	2.1	2.0	2.5	3.0
8.5	28.80	1.05	1.1	1.1	1.05	1.1	1.1	1.1	1.151.2		1.15	1.2	1.3	1.3	1.4	1.6	1.5	1.7	2.0	1.8	2.1	2.5

G = good, F = fair, P = poor

†all values are multiplicative error factors (MEF) from eq. (2), averaged for $\Delta\log(A_i) = \log(A_{i+1}) - \log(A_i)$ and $\Delta\log(A_i) = \log(A_i) - \log(A_{i-1})$. The A_i's are representative values for a given log(M_0) taken from the regressions.

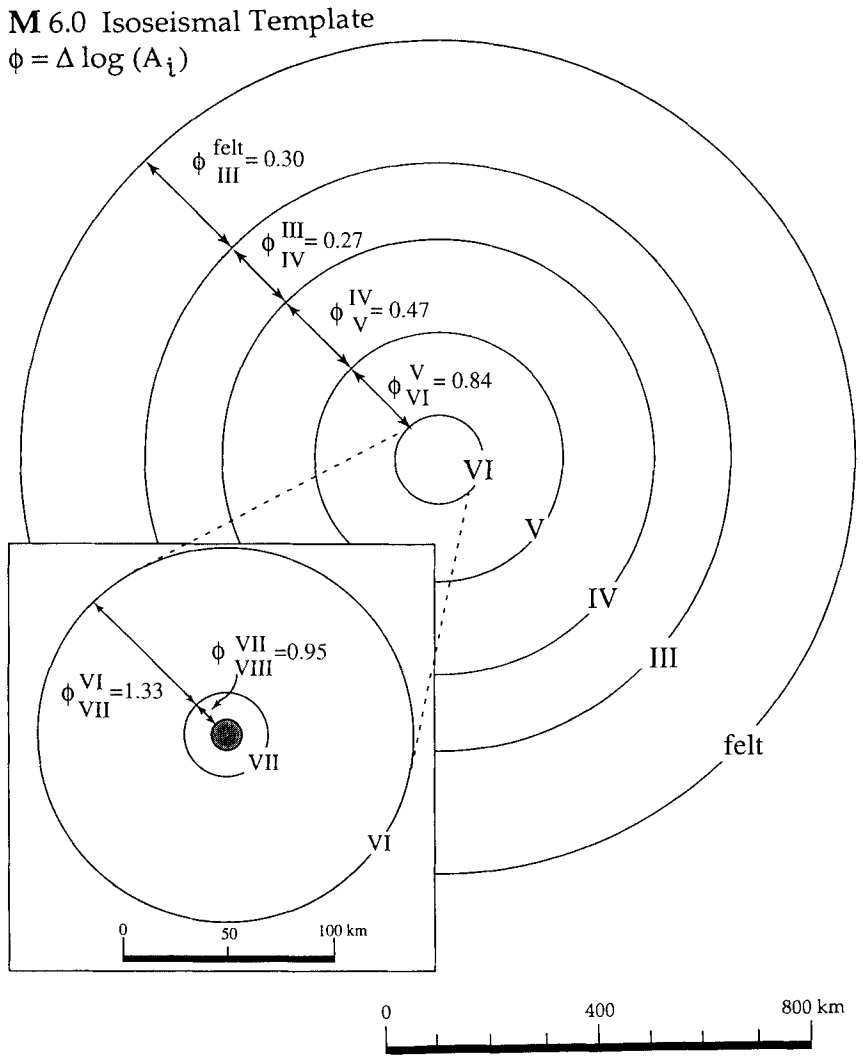

Figure 2. Illustration of isoseismal area uncertainty assignment for a representative M 6.0 earthquake. Isoseismal radii are taken from Table 3. The $\phi^i_{i+1} = \Delta \log(A_i)$ is the basis for the $2\sigma^{\pm}_{\log}$ uncertainty assignment for the A_i database of Table A3 (see text and eq. 2). The trend of increasing ϕ^i_{i+1} for smaller inner isoseismals holds true for all magnitude ranges (Table 1).

effect of A_i uncertainty is to control the assessment of the reliability of the regression. When data are weighted according to their uncertainties, the weights determine regression parameter variance, confidence limits for the regression as a whole, and chi-square assessment of goodness of fit, topics that are developed in Appendix A of Part I.

REGRESSION ANALYSIS

Application of Part I development

Once the SCR isoseismal data set is compiled and individual isoseismal area uncertainties assigned, the analysis follows closely the Part I regression procedures. Specifically, I followed the same four-step method:

(1) estimation of observational uncertainties (previous section);

(2) outlier identification and removal;

(3) chi-square analysis for the best type of regression curve fit;

(4) generation of full regression and prediction uncertainty statistics.

One departure from Part I is in step (3), where I adopt a new functional regression form specific to intensity data (Frankel 1994), a significant development that merits its own section (see below).

Outlier analysis (step 2) again utilizes Chauvenet's criterion (e.g. Bevington & Robinson 1992). For normally distributed errors this yields an outlier limit $C = \pm z\sigma_{res}$, where σ_{res} is the standard deviation of the regression residuals, and z is determined from integral tables of Gaussian probability (Part I, Appendix A2). Outlying data points and the outlier limit are shown on each regression residual graph of Fig. 3.

As in Part I, I judged the suitability of a particular functional regression form by the reduced chi-square statistic χ^2_v (step 3):

$$\chi^2_v = \frac{\chi^2}{v} = \frac{\chi^2}{N-K}, \tag{3}$$

where v is the number of degrees of freedom for fitting N data with K parameters. If the data are properly weighted by the

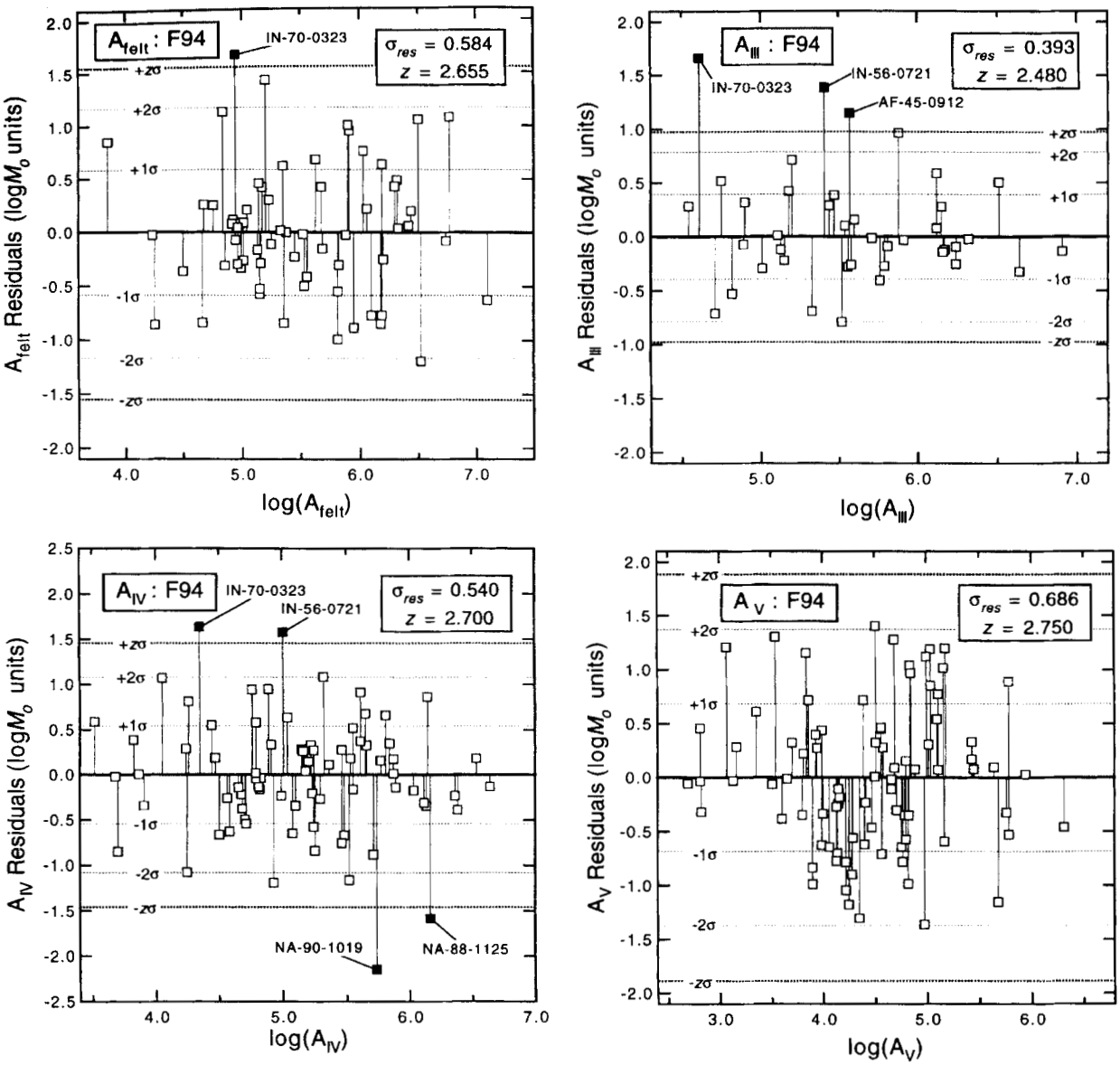

Figure 3. Residual plots of the isoseismal area regressions. The outlier limit C, as defined by Chauvenet's criterion, is $C = z\sigma_{res}$ (on plots, shortened to $z\sigma$), where σ_{res} is the standard deviation of the residuals [observed minus computed $\log(M_0)$ values] for each regression. Residuals (open symbols) are in $\log(M_0)$ units; identified outliers are solid symbols. Outlier identification is keyed to Table A3.

reciprocal of their standard error, χ_v^2 will lie close to unity, which yields an integrated chi-square probability $P_{\chi_v^2}$ close to 50 per cent. A higher χ_v^2 produces a lower $P_{\chi_v^2}$, meaning that there is a greater probability that random fits to the data will represent the parent data population equally well. I tested linear, quadratic, and cubic regression curve fits, as well as the Frankel (1994) functional form, designated F94, on all the isoseismal data. The results, along with those for I_{max} and number of recording stations, are tabulated in Table 2.

The χ_v^2 is sensitive to the weighting of individual data points. Basically, all data are weighted by the reciprocal of the standard error or uncertainty of the dependent variable, which is $1/\log(\mathrm{MEF}_{M_0}) = (\sigma_{M_0})^{-1}$. However, the weighting is modified to incorporate uncertainty in A_i, which makes a large but indirect contribution, σ_I, to the total $\log(M_0)$ uncertainty. Since M_0 and A_i errors are uncorrelated, it is appropriate to combine them in quadrature: $\sigma_{tot} = \sqrt{\sigma_{M_0}^2 + \sigma_I^2}$. The σ_I is determined by propagation of errors (*cf.* Part I):

$$\sigma_I = \sigma_{A_i} \frac{d(\log M_0)}{d(\log A_i)}.$$

I represent the dependence of $\log(M_0)$ on $\log(A_i)$ by the linear regression curve fits of Table 2. Then,

$$\frac{d(\log M_0)}{d(\log A_i)} \simeq k1,$$

the second regression parameter. Therefore, the total uncertainty of a data point is

$$\sigma_{tot} \simeq \sqrt{(\sigma_{M_0})^2 + (k1\sigma_{A_i})^2}. \quad (4)$$

The $k1$ for the A_i linear regressions in Table 2 varies from 0.8 to 2.5, and from Table A3 the average $\mathrm{MEF}_{M_0} = 1.75$ (average $\sigma_{M_0} = 0.24$) and the average $\mathrm{MEF}_{A_i} = 2.10$ (average $\sigma_{A_i} = 0.32$). An average data point will therefore have an

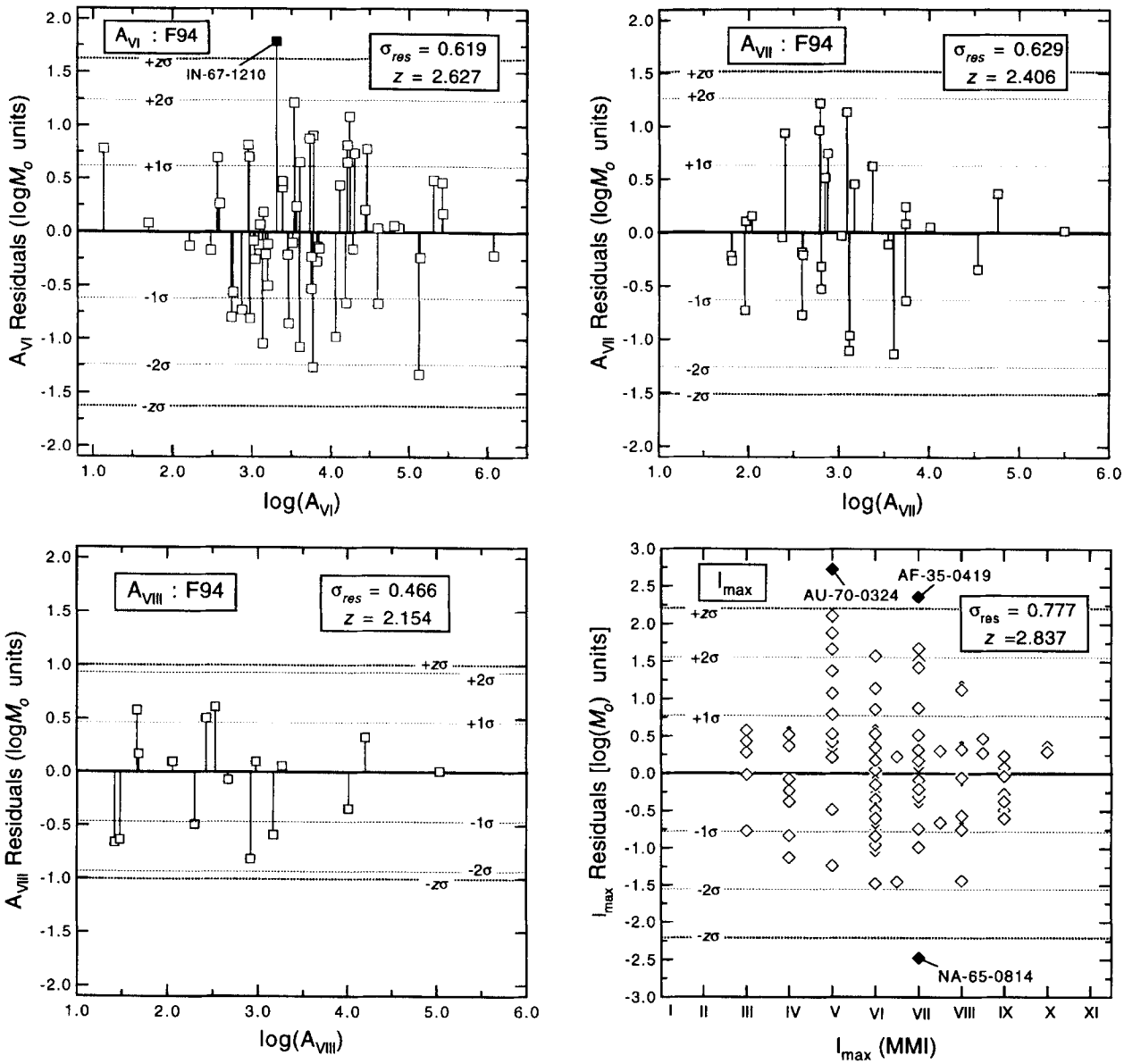

Figure 3. (*Continued.*)

uncertainty σ_{tot} of 0.35 to 0.84 $\log(M_0)$ units, depending on the $k1$ value, with the $\log(A_i)$ uncertainty dominating that of $\log(M_0)$ (53–92 per cent of σ_{tot}). Eq. (4) yields the standard weighting factor for chi-square statistics to have absolute meaning:

$$W_i \simeq \frac{1}{(\sigma_{tot})_i}, \tag{5}$$

where the equality is approximate because σ_{tot} is not known but estimated as described above.

The Frankel (1994) A_{felt} regression

In previously published regressions (Johnston 1989; Hanks & Johnston 1992; Johnston 1994a), I employed second-order polynomial or quadratic curve fits to accommodate the non-linear relation between $\log(M_0)$ and $\log(A_i)$. A quadratic regression form also proved an effective approximation to the theoretical relation between amplitude magnitudes and $\log(M_0)$ in Part I. Recently, Frankel (1994) proposed a new functional regression form specifically for **M** or $\log(M_0)$ on A_{felt} that has the great attraction of being based on the physical principles of seismic-wave propagation, whereas the quadratic functional form is not. Because of the importance of this advance, I will briefly review the derivation, changing a few symbols to agree with usage in this study.

Seismic intensities should be proportional to the amplitude a of seismic waves: the larger a is, the higher the intensity level, ignoring for the moment the complications of frequency dependence. The value of a at distance r from the source depends on the interplay of geometrical spreading and anelastic attenuation and scattering:

$$a \propto a_0 r^{-n} e^{-mr}, \tag{6}$$

where a_0 is a reference amplitude dependent on M_0, n is the geometrical spreading exponent for epicentral distance r, and

Table 2. Regression parameters for A_i, I_{max} and number of recording stations.

A_i	type of fit	k0	k1	k2	k3	ν	χ^2_ν	$P(\chi^2_\nu)$	Difference(†)	σ_{res} ($\log M_o$ units)	No. of outliers	z
A_{felt}	F94	17.31	+0.959	+0.00126	——	60	1.078	0.318	—	0.584	1	2.655
	quadratic	35.03	-6.277	+0.751	——	60	1.156	0.193	NS	0.588	1	2.655
	cubic	-21.36	+23.94	-4.582	+0.310	59	1.080	0.314	NS			
	linear	10.87	+2.308	——	——	61	1.815	<0.001	SW			
A_{III}	F94	17.59	+1.020	+0.00139	——	35	0.502	0.996	—	0.393	3	2.480
	quadratic	34.94	-6.185	+0.759	——	35	0.495	0.998	NS	0.391	3	2.480
	cubic	15.65	+4.314	-1.122	+0.111	34	0.501	0.995	NS			
	linear	10.56	+2.482	——	——	36	1.032	0.417	SW			
A_{IV}	F94	18.10	+0.971	+0.00194	——	69	1.062	0.340	—	0.540	4	2.700
	quadratic	31.31	-5.000	+0.686	——	69	1.067	0.330	NS	0.541	4	2.700
	cubic	13.25	+5.734	-1.403	+0.133	68	1.061	0.340	NS			
	linear	12.40	+2.263	——	——	70	1.702	<0.001	SW			
A_V	F94	19.83	+0.788	+0.00260	——	81	0.734	0.962	—	0.686	0	2.750
	quadratic	26.47	-2.737	+0.474	——	81	0.696	0.982	NS	0.668	0	2.750
	cubic	29.60	-4.952	+0.981	-0.038	80	0.703	0.980	NS			
	linear	16.90	+1.591	——	——	82	0.899	0.726	SW			
A_{VI}	F94	20.23	+1.032	+0.00176	——	55	0.779	0.879	—	0.619	1	2.627
	quadratic	20.66	+0.708	+0.0823	——	55	0.783	0.874	NS	0.609	1	2.627
	cubic	20.81	+0.573	+0.119	-0.0032	54	0.797	0.854	NS			
	linear	19.34	+1.384	——	——	56	0.790	0.864	NS			
A_{VII}	F94	23.22	+0.559	+0.00328	——	28	1.242	0.181	—	0.629	0	2.406
	quadratic	23.92	-0.067	+0.140	——	28	1.333	0.115	NS	0.642	0	2.406
	cubic	13.44	+9.620	-2.684	+0.260	27	1.128	0.295	NS			
	linear	22.20	+0.947	——	——	29	1.352	0.100	NS			
A_{VIII}	F94	24.05	+0.440	+0.00586	——	13	0.631	0.827	—	0.466	0	2.154
	quadratic	24.70	-0.226	+0.173	——	13	0.739	0.725	NS	0.492	0	2.154
	cubic	18.98	+6.177	-2.016	+0.230	12	0.542	0.886	NS			
	linear	23.13	+0.878	——	——	14	0.815	0.653	SW			
I_{max}	quadratic	19.36	+0.481	+0.0244	——	107	0.995	0.494	—	0.777	3	2.837
	linear	18.47	+0.789	——	——	108	0.996	0.491	NS			
N_{st}/N_{mx}	exponential	22.38	+5.049	+2.107	——	173	0.862	0.903	—	0.709	0	2.987
N_{20}/N_{20mx}	exponential	22.16	+5.110	+1.542	——	168	0.950	0.652	—	0.632	2	2.976

format

polynomial: $\log(M_0) = k0 + k1*X + k2*X^2 + k3*X^3$

$X = \log A_i$ or I_{max}

F94: $\log(M_0) = k0 + k1*\log A_i + k2*(A_i)^{1/2}$

exponential: $\log(M_0) = k0 + k1*\exp[k2*R]$

$R = \log(N_{st}/N_{mx})$ or

$R = \log(N_{20}/N_{20mx})$

Key: ν = no. degrees of freedom = $N - K$

N = no. of data points; K = no. of regression parameters

(†) statistical grade of regression relative to the first listed

NS not significantly different

SB significantly better

SW significantly worse

σ_{res} standard deviation of residuals

z : outlier limit = $z\sigma_{res}$

e^{-mr} expresses anelastic attenuation and scattering. The m parameter contains frequency f, shear-wave quality factor Q, and shear-wave velocity β, terms:

$$m = \frac{\pi f}{Q\beta}. \tag{7}$$

With application of a number of assumptions, Frankel (1994) demonstrates that eq. (6) leads to the following relation between **M** and felt area A_{felt} (Frankel's eq. 6):

$$\mathbf{M} = n \log(A_{felt}/\pi) + \frac{2m}{2.3\sqrt{\pi}}\sqrt{A_{felt}} + B, \tag{8}$$

where B is a constant. Frankel's moment magnitude, $\mathbf{M} = (2/3)\log M_0 - 10.7$ (Hanks & Kanamori 1979), is the same as used in this study and in Part I. The principal assumptions of Frankel to obtain eq. (8) from eq. (6) were: (1) the average frequency f of felt perceptibility is above (i.e. on the high-frequency side of) the earthquake source spectrum's corner frequency; (2) stress drop is constant for varying M_0 and (3) the specific frequency dominating eq. (8) occurs at the spectral peak of the product of the ground-motion spectrum and the spectrum of human sensitivity. Recast in terms of $\log(M_0)$ and incorporating the $-\log(\pi)$ term in the constant $k0$ parameter, we have

$$\log(M_0) = k0 + k1 \log(A_i) + k2\sqrt{A_i}. \tag{9}$$

This is Frankel's eq. (6) with $\log(M_0)$ instead of **M** and generalized isoseismal area A_i instead of specifically A_{felt}. It will serve as the functional form (F94) for one class of SCR regressions in the following sections. For $\beta = 3.5$ km s^{-1}, the relationship between the regression parameters $k0$–$k2$ and the exponent of geometrical spreading n and the anelastic attenuation term (f/Q) is

$$k0 = 1.5(B - 0.497n + 10.7),$$
$$k1 = 1.5n, \qquad (10)$$
$$k2 = 0.660(f/Q).$$

For $A_i = A_{\text{felt}}$, Frankel fixed the exponent of geometrical spreading n at 0.5, which fixes $k1$ at 0.75. I shall let $k0$–$k2$ vary freely for intensities A_i, i = felt–VIII, and then examine how well they recover reasonable values of n and Q for stable continental regions. When $\log(M_0)$ is regressed on the independent variable A_i, it yields a nearly linear slope on $\log(A_i)$ for small A_i. In this range the regression is controlled by the geometrical spreading term $k1\log(A_i)$. It is only for large A_i, that is, for large epicentral distances, that the attenuation term, $k2(A_i)^{1/2}$, becomes significant and increases the slope of the $\log(M_0)$–A_i regression.

As we shall see in the following sections, the quadratic regression does a good job of emulating the physically based F94 functional form except for very small A_i or M_0 values. It is in this range—generally around **M** 4.0–4.3—that the quadratic curve fits go through an inflection point and begin increasing in $\log(M_0)$ with decreasing $\log(A_i)$, a physically unacceptable behaviour. Therefore, quadratic regressions suffer the necessity of a small M_0–small A_i cut-off, whereas the F94 regressions do not. Also, for very large A_i, the quadratic regression increases more slowly than F94, leading to slightly smaller predicted M_0 or **M** values.

Regression, prediction and weighted average uncertainty

Up to this point considerations of uncertainty have concerned only the input data on which regressions are performed. In this section I describe how the uncertainty of the output of regression analysis—a predicted value of $\log(M_0)$ or **M**—is expressed. It takes three forms: regression uncertainty, $\sigma^{\text{R}}_{\log M_0}$ or $\sigma^{\text{R}}_{\text{M}}$, prediction uncertainty, $\sigma^{\text{P}}_{\log M_0}$ or $\sigma^{\text{P}}_{\text{M}}$; and uncertainty of a final weighted average of multiple separate regressions. The order of these is important because weighted average uncertainty depends on both $\sigma^{\text{R}}_{\log M_0}$ and $\sigma^{\text{P}}_{\log M_0}$, and $\sigma^{\text{P}}_{\log M_0}$ depends on $\sigma^{\text{R}}_{\log M_0}$.

Regression uncertainty expresses the degree of confidence that a given regression relation accurately represents the parent population of a given distribution of data. The $\sigma^{\text{R}}_{\log M_0}$ is in $\log(M_0)$ units and depends on both variances and covariances of the regression parameters for least-squares curve fits. The error propagation equation (see Part I, eq. A7) and the covariance or error matrix (Part I, eq. A8) define this dependence. For a quadratic regression of the form $\log(M_0) = k1 + k2\log(A_i) + k3\log^2(A_i)$, they yield a regression uncertainty given by

$$(\sigma^{\text{R}}_{\log M_0})^2 = 1\varepsilon_{11} + \log^2(A_i)\varepsilon_{22} + \log^4(A_i)\varepsilon_{33} + 2[\log(A_i)\varepsilon_{12} + \log^2(A_i)\varepsilon_{13} + \log^3(A_i)\varepsilon_{23}], \qquad (11)$$

where ε_{ii} is the variance of the regression parameter ki, and ε_{ij} is the covariance of parameters ki and kj. A similar analysis of eq. (9) yields the uncertainty of the F94 regression:

$$(\sigma^{\text{R}}_{\log M_0})^2 = 1\varepsilon_{11} + \log^2(A_i)\varepsilon_{22} + A_i\varepsilon_{33} + 2[\log(A_i)\varepsilon_{12} + \sqrt{A_i}\varepsilon_{13} + \log(A_i)\sqrt{A_i}\varepsilon_{23}]. \qquad (12)$$

Finally, for the exponential regression used for number of recording stations, the functional form is $\log(M_0) = k0 + k1\exp(k2X)$ and the uncertainty is

$$(\sigma^{\text{R}}_{\log M_0})^2 = 1\varepsilon_{11} + \exp(2k2X)\varepsilon_{22} + (k1X)^2\exp(2k2X)\varepsilon_{33} + 2[\exp(k2X)\varepsilon_{12} + (k1X)\exp(k2X)\varepsilon_{13} + (k1X)\exp(2k2X)\varepsilon_{23}], \qquad (13)$$

where X represents the logarithm of the normalized number of recording stations. Application of eqs (11)–(13) over the range of the independent variable generates the regression confidence limits. For random errors, 68 per cent confidence that the obtained regression truly represents the parent data distribution is just $\pm\sigma^{\text{R}}_{\log M_0}$ and 95 per cent confidence is $\pm 2\sigma^{\text{R}}_{\log M_0}$. Figs 4–10, 13 and 15 display the 95 per cent confidence limits obtained for each regression of this study.

The regression uncertainty does not represent the total uncertainty of a predicted dependent variable value. The total prediction uncertainty is given by the sum of the regression and residual variances (*cf.* Part I, eq. A10):

$$(\sigma^{\text{P}}_{\log M_0})^2 = (\sigma^{\text{R}}_{\log M_0})^2 + (\sigma_{\text{res}})^2. \qquad (14)$$

Appendix Table A1 lists $\sigma^{\text{P}}_{\log M_0}$ and $\sigma^{\text{P}}_{\text{M}}$ for all regressions, and Figs 4–10, 13 and 15 display them graphically. Eq. (14) gives the prediction uncertainty of $\log(M_0)$ expected from applying a regression relation to a single isoseismal area measurement. In practice, however, usually more than one area is contoured. Multiple A_i of different MMI level contribute much additional data that should be valuable for reducing the uncertainty in the event's predicted seismic moment. The proper way to exploit multiple A_i data is, however, not clear-cut and some discussion is warranted.

Consider an earthquake for which N A_i measurements exist, each at a different intensity level. Each is used as the input value for its appropriate regression and a predicted moment magnitude is obtained with uncertainty estimated from eq. (14). In the framework of this study these may be regarded as N separate measurements of the earthquake's M_0 or **M**. If the data are separate and independent then a straightforward application of the method of weighted averages is appropriate. Working with **M** rather than $\log(M_0)$ for simplicity, the best-estimate **M**, based on N A_i values that yield N $\mathbf{M}_i$ estimates, is the weighted average,

$$\mathbf{M}_{\text{best}} = \frac{\sum_{i=1}^{N} w_i\mathbf{M}_i}{\sum_{i=1}^{N} w_i}, \qquad (15)$$

where the weights w_i are the reciprocals of the individual prediction variances (squares of the prediction uncertainties):

$$w_i = \frac{1}{(\sigma^{\text{P}}_{\text{M}})^2}. \qquad (16)$$

The uncertainty in $\mathbf{M}_{\text{best}}$ may be calculated using error propagation and is

$$\sigma_{\mathbf{M}_{\text{best}}} = \left[\sum_{i=1}^{N} w_i\right]^{-1/2}. \qquad (17)$$

If the w_i are all equal, eq. (17) reduces to the familiar standard deviation of the mean $\sigma_m = \sigma_M^P/\sqrt{N}$. For $N \geq 5$ a trimmed mean in which the highest and lowest $\mathbf{M}_i$ are discarded before applying eq. (15) may be preferable.

The weighted average and particularly its uncertainty $\sigma_{M_{best}}$ are strictly valid only if the input $\mathbf{M}_i$ from $\log(A_i)$ regressions are from separate and independent measurements. An argument can be made for A_i data independence. For a given earthquake, each A_i represents an area affected by a different seismic intensity level; its outer boundary, which determines its value, is controlled by observation points at the outer perimeter of A_i and within the innermost portion of A_{i-1}. These points are geographically separate and independent from those that control the outer boundaries of other A_i for the same event. If only these factors apply, then eq. (17) is appropriate and provides the best estimate for the total prediction uncertainty.

For the particular case of isoseismal data, eq. (17) is almost certainly too optimistic because there is a strong potential for systematic error. The two most important potential contributors to systematic error are the source properties of the earthquake and the seismic intensity analyst. Faulting mechanism, focal depth, rupture duration and directivity, and stress drop of the source earthquake can all affect isoseismal patterns in a complex, but often systematic, manner. Analyst influence is probably systematic because for a given earthquake it is usually the same analyst(s) evaluating and then contouring the intensity data. Numerous subjective judgements are necessary to progress from a collection of descriptions or observations of seismic effects at geographically dispersed locales to a final contoured isoseismal map. Thus, even though the observation points of a given isoseismal area are independent of those for other A_i, their analysis is not. Therefore I take eq. (17) to represent only the *random* error component of the weighted average final **M** and allow for the possibility of *systematic* error as great as the random component. Combining the variances of these components yields, for the final weighted average and uncertainty estimates,

$$\mathbf{M}_{final} = \mathbf{M}_{best},$$
$$\sigma_{M_{final}} = \sqrt{(\sigma_{M_{best}})^2 + (\sigma_{sys})^2} \simeq \sqrt{2}\sigma_{M_{best}}. \quad (18)$$

Eqs (15)–(18) provide the framework for combining multiple isoseismal area data for a single earthquake into a final estimate of its moment magnitude with specified uncertainty bounds.

THE SCR INTENSITY DATA REGRESSIONS

This section describes the regressions for $\log(M_0)$ on isoseismal areas A_{felt} to A_{VIII} and on maximum intensity I_{max}. For each isoseismal area, I examined four regression functional forms: linear, quadratic, cubic, and the Frankel (1994) relation, F94. Results for all are reported in Table 2, but only the F94 and quadratic regressions are examined in detail, and full uncertainty statistics are given in Table A1 only for F94.

Isoseismal area regressions

Log(M_0*)–Log(*A_{felt}*)*

A total of 64 earthquakes in the SCR database (Appendix A, Tables A3 and A4) have A_{felt} reported. The A_{felt} regression is one of the more important ones because for many historical events only the felt limit (radius or area) is reported. The felt limit is most often MMI II or I–II, but it is not uncommon for it to be MMI III or unspecified. Only one event (IN-70-0323) qualified as an outlier (Fig. 3). Table 2 summarizes the results of four regressions performed on the remaining 63 $\log(A_{felt})$ values. The F94, quadratic and cubic curve fits have similar reduced chi-square χ_ν^2 statistics. The differences are not statistically significant—unlike the significantly worse linear fit—and I take the F94 fit as the primary A_{felt} regression because of its physical basis. Fig. 4(a) shows the F94 and quadratic regressions with their associated 95 per cent confidence limits and the A_{felt} data points. Fig. 4(b) gives the corresponding regression and prediction uncertainties, also tabulated in Table A1 for F94. The prediction uncertainty is dominated by the data scatter component; this holds true for all except the A_{III} and A_{VIII} regressions.

There are several aspects of the A_{felt} regression results that are characteristic of all the A_i regressions. The F94 and quadratic fits overlay each other through the midrange of the data. For very large areas ($\log A_i > 6.5$), F94 and quadratic remain close but F94 predicts slightly larger $\log(M_0)$. At small A_i (or $\log M_0 \lesssim 22.5$) F94 and quadratic behave quite differently: F94 continues to decrease smoothly in $\log(M_0)$, while the quadratic fit goes through an inflection point and begins to increase. This non-physical behaviour of the quadratic was the reason for the low-magnitude cut-off imposed on the regressions of Johnston (1994a). Since F94 is the preferred functional form, the quadratic regressions are not illustrated for the remaining A_i regressions, but they are summarized in Fig. 11.

A characteristic behaviour of A_i regression uncertainties is also evident in Fig. 4(b). Uncertainties of both the F94 and quadratic regressions are relatively low over the midrange of the data, with σ_M^R only ± 0.05–0.07 **M** units and $\sigma_M^P = \sim \pm 0.40$ **M** units. Regression uncertainty begins to increase at both high and low $\log(A_i)$ values where data become sparse, but the quadratic increase at low $\log(A_i)$ is greater than that of F94, and F94 uncertainty increases much more rapidly at high $\log(A_i)$. One would expect such behaviour from eqs (11) and (12) for σ_M^R: at large A_i, the $\sqrt{A_i}$ and A_i terms of eq. (12) for F94 progressively dominate the $\log^3(A_i)$ and $\log^4(A_i)$ terms of eq. (11) for quadratic, while the opposite is usually true at small A_i.

Log(M_0*)–Log(*A_{III}*)*

If A_{felt} is reported for an earthquake, more often than not A_{III} is omitted. This is the primary reason that, at 41 observations, A_{III} has the smallest regression data set, excepting the sparse A_{VII} and A_{VIII} data. The low residual scatter ($\sigma_{res} = 0.39 \log M_0$ units) led to a relatively small outlier limit that disqualified three events as small area outliers: the same low-stress-drop Indian event (IN-70-0323) that was an A_{felt} outlier; an African event (AF-45-0912) with a very poorly known A_{III}; and, surprisingly, the high-stress-drop Anjar earthquake (IN-56-0721). The interesting case of the Anjar event is discussed below in the data scatter section. Residuals and outliers are shown in Fig. 3 and the final F94 regression in Fig. 5(a). Again, only the linear fit was significantly worse than the other regressions (Table 2). The smaller data set gives A_{III} a greater regression uncertainty than A_{felt} over the central data range, but the

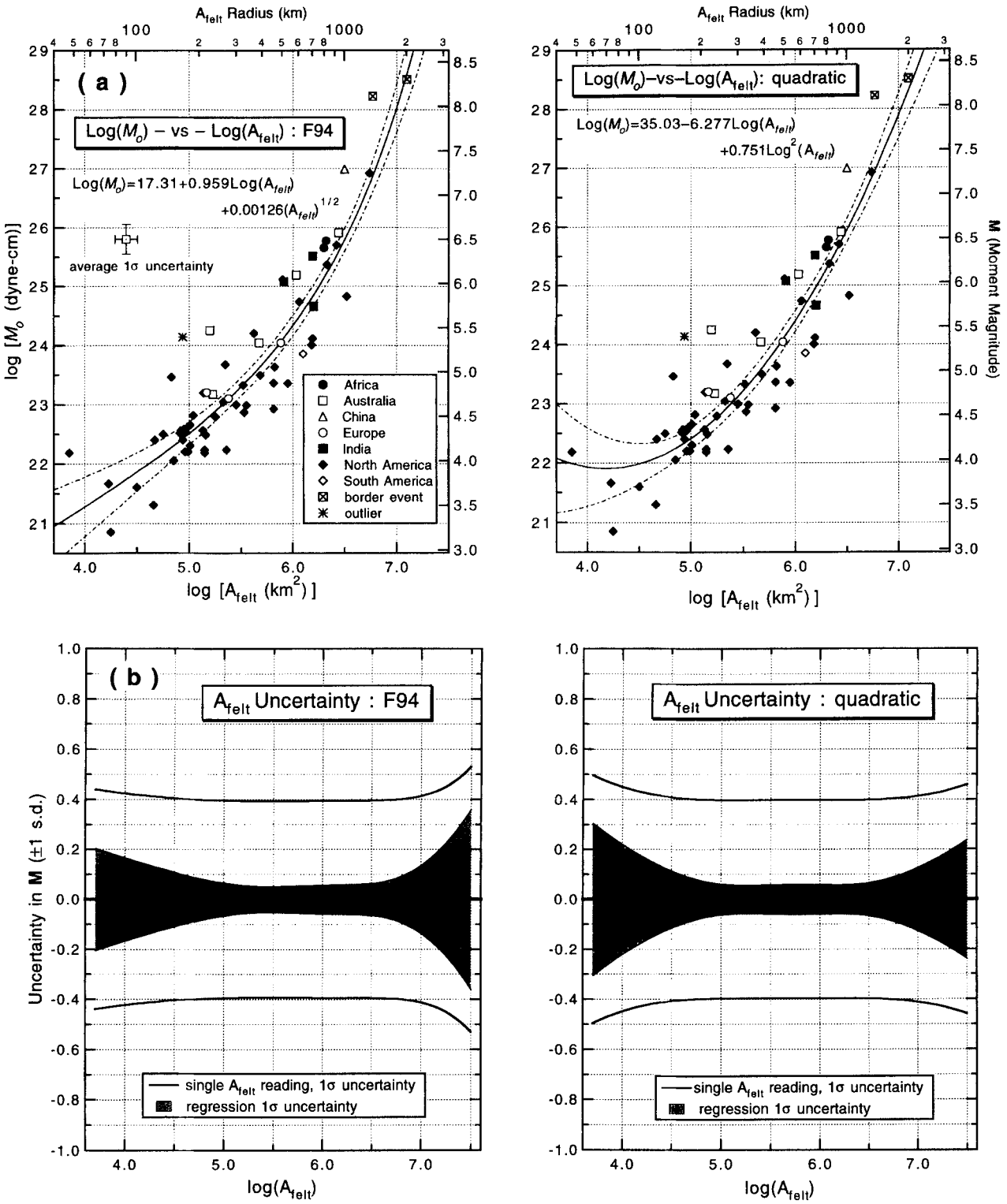

Figure 4. (a) log(M_0)–log(A_{felt}) regression for both F94 (Frankel 1994) and quadratic curve fits. The light dash–dot curves are the 95 per cent ($\pm 2\sigma$) confidence limits of the regression. Data points are identified by their continental SCR affiliation. The length of the error bars representing data point uncertainty is the average 1σ uncertainty derived from the assigned MEFs of the log(M_0) and log(A_{felt}) data, as listed in Table A3. (b) Graphical display of log(A_{felt}) regression and prediction uncertainty in moment magnitude (M) units. The shaded zone is the 68 per cent ($\pm 1\sigma$) confidence limit on the regression relation. The quadratic sum (eq. 14) of this limit and σ_{res}, the residual standard deviation, yields the prediction uncertainty of a single log(A_{felt}) measurement (heavy line). The uncertainty of the F94 regression exceeds the quadratic for high log(A_{felt}) values but is less for low log(A_{felt}) values. This same pattern holds for all the log(A_i) regressions (Figs 5–10, which do not display the quadratic regression).

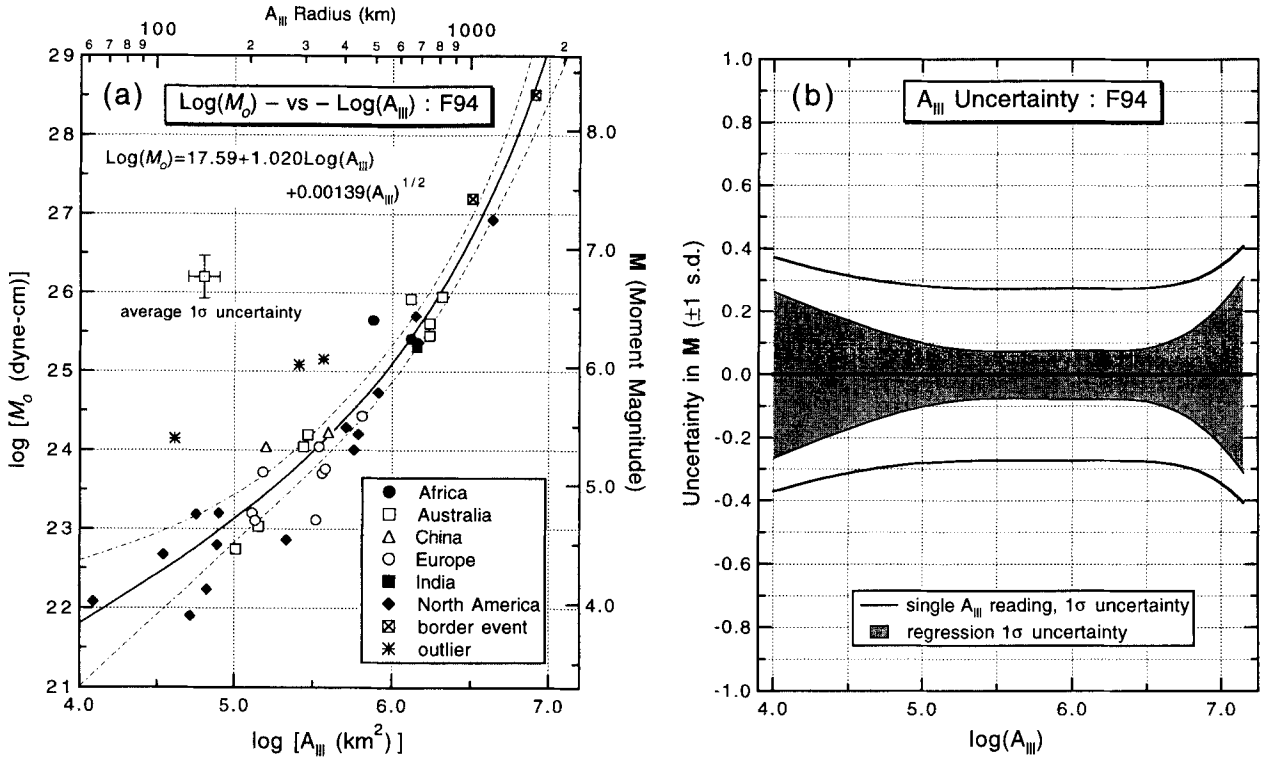

Figure 5. (a) The F94 $\log(M_0)$–$\log(A_{III})$ regression. Explanation of symbols is the same as for Fig. 4(a). (b) Graphical display of the F94 $\log(A_{III})$ regression and prediction uncertainty in moment magnitude (**M**) units. Explanation is the same as for Fig. 4(b).

smaller σ_{res} yields a lower σ_M^P of only ~0.27 **M** units (Fig. 5b). This is the smallest prediction uncertainty of all the A_i regressions.

Log(M_0*)–Log(*A_{IV}*)*

The A_{IV} regression begins the analysis of the midrange of isoseismal data (MMI IV–VI) where intensities are clearly stronger than perceptible (MMI I–III), yet still below structural damage levels (MMI ≥ VII). There were 76 $\log(M_0)$–$\log(A_{IV})$ observations (Tables A3 and A4); the total would have been higher but for the common practice in the United States of combining MMI I–IV data into one isoseismal area. The A_{IV} data set with the final F94 regression is shown in Fig. 6(a); Fig. 6(b) displays the A_{IV} regression and prediction uncertainties tabulated in Table A1. A Chauvenet analysis identified four outliers (Fig. 3): the same two Indian events that were low-A_{III} outliers and two high-A_{IV}, high-stress-drop North American events. As with A_{felt} and A_{III}, the χ_ν^2 statistics of the F94, quadratic and cubic curve fits were similar, and the linear fit was significantly worse (Table 2). F94 regression uncertainties are depicted in Fig. 6(a) by $\pm 2\sigma$ (95 per cent) confidence limits in $\log(M_0)$ units and in Fig. 6(b) in **M** units. The prediction uncertainty is ±0.36–0.40 **M** units over the $\log(A_{IV})$ range 4.0–6.7, higher than A_{III} but comparable to A_{felt}.

Log(M_0*)–Log(*A_V*)*

The A_V regression closely mirrors that of A_{IV}, except its data dispersion is significantly higher, leading to greater prediction uncertainty. In fact, for reasons that remain unclear, the A_V data exhibit the highest residual scatter ($\sigma_{res} = 0.686 \log M_0$ units) of all the A_i regressions. I suggest this may be due to the incremental nature of all the descriptive categories of MMI V: the number of persons actually feeling the quake, the number awakened or frightened, the degree that hanging objects swing or small objects move or liquids spill or trees and bushes shake. All these categories are shared with MMI IV and VI and depend on modifiers such as *slight*, *moderate*, *few*, *some*, *many*, *some instances*, *generally*, and so on, hence there is greater opportunity for subjective interpretation at MMI V than perhaps at any other intensity level.

The large dispersion of the 84 A_V data points resulted in a outlier limit $C = z\sigma_{res}$ too large for any of the data to qualify as outliers (Fig. 3). Goodness-of-fit statistics follow the familiar pattern (Table 2), with only the linear curve fit significantly different (worse) than the others. Fig. 7(a) displays the A_V data and the principal F94 regression; Table A1 and Fig. 7(b) detail its associated uncertainty. Because of the large σ_{res} the prediction uncertainty is high: $\sigma_M^P = \sim \pm 0.46$–$0.55$ **M** units over the central A_V data range.

Log(M_0*)–Log(*A_{VI}*)*

The F94 regression on the 59 events with A_{VI} data is shown in Fig. 8(a). Outlier analysis identified only one outlier candidate, the low-stress-drop Koyna earthquake (IN-67-1210) with a very small A_{VI} (Fig. 3). Comparison of regression types (Table 2) shows the F94 curve fit had the best χ_ν^2 statistics, but it was not significantly better than any of the others, including the linear curve fit. Fig. 8(b) shows both regression and prediction uncertainties in **M** units. The moderately high σ_{res} for A_{VI} yields a prediction uncertainty of $\sigma_M^P \simeq 0.43$–0.50 **M** units for $\log(A_{VI}) \simeq 1.0$–5.5.

The A_{VI} regression is the first one examined for which the

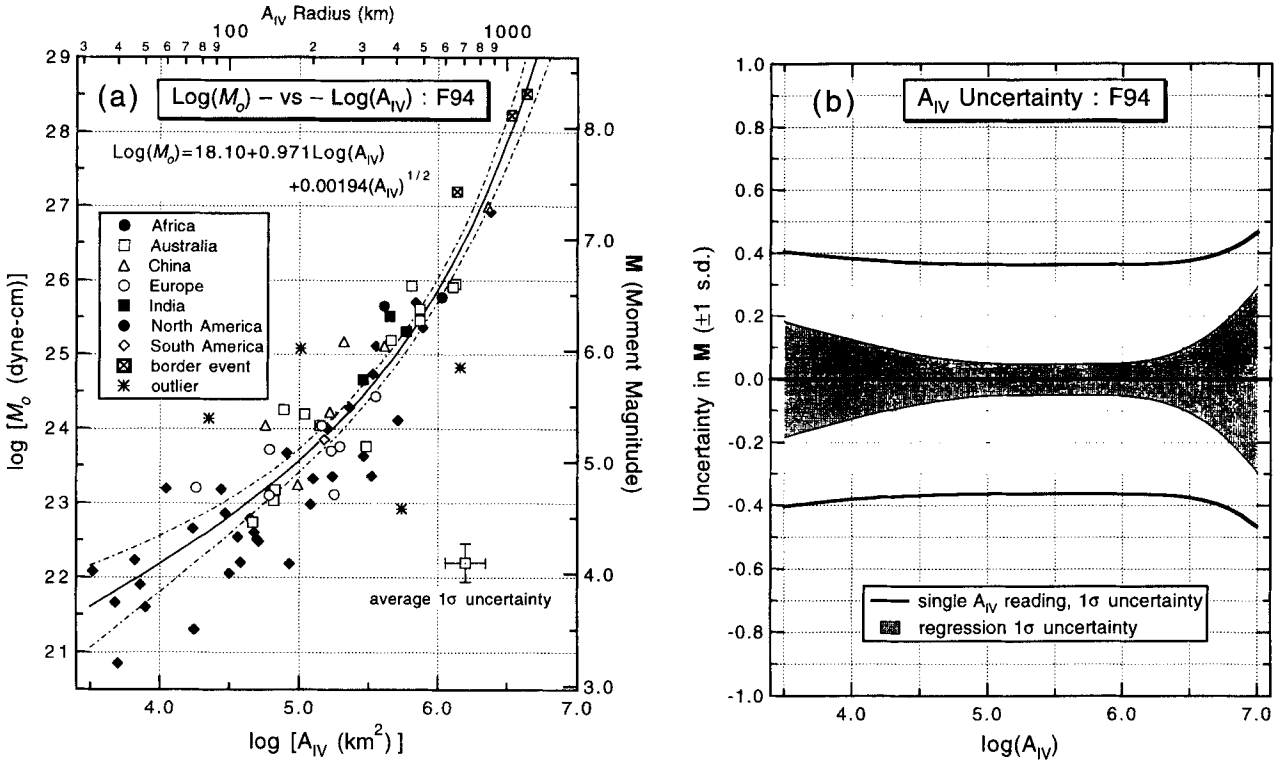

Figure 6. (a) The F94 $\log(M_0)$–$\log(A_{IV})$ regression. Explanation of symbols is the same as for Fig. 4(a). (b) Graphical display of the F94 $\log(A_{IV})$ regression and prediction uncertainty in moment magnitude (**M**) units. Explanation is the same as for Fig. 4(b).

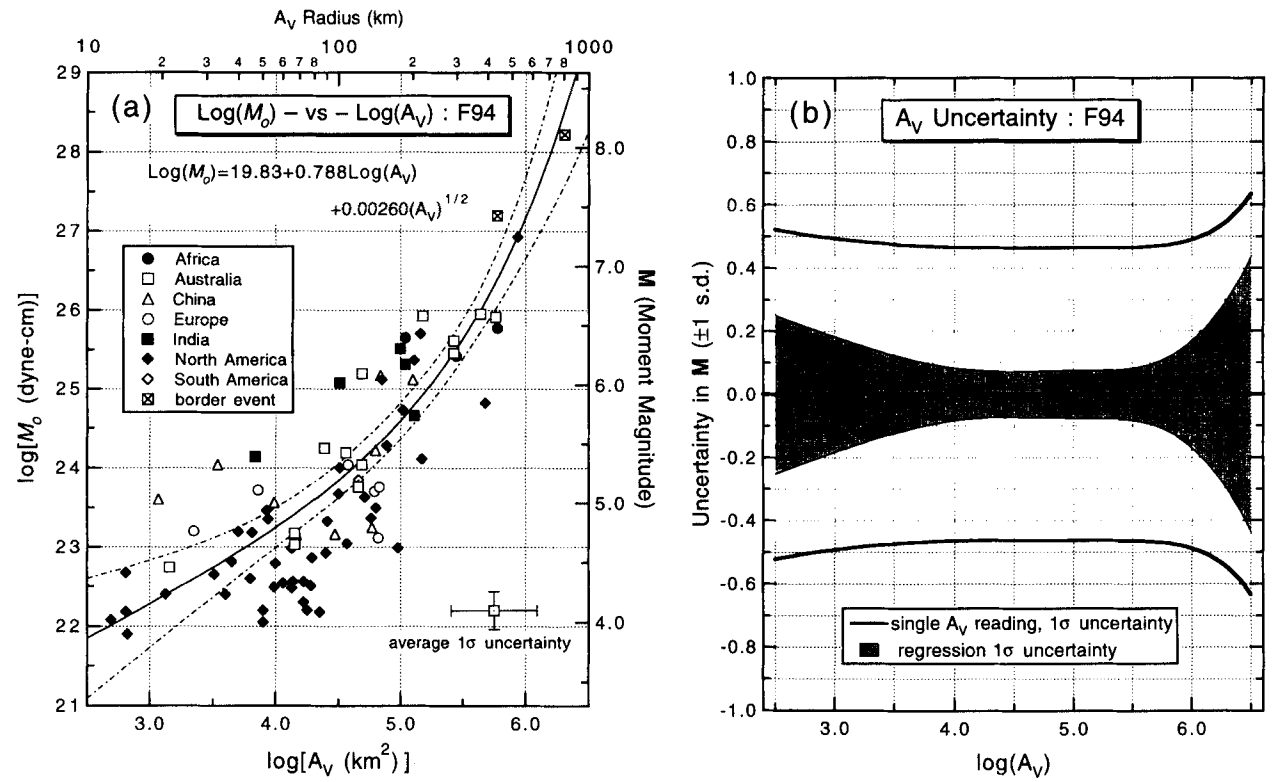

Figure 7. (a) The F94 $\log(M_0)$–$\log(A_V)$ regression. Explanation of symbols is the same as for Fig. 4(a). (b) Graphical display of the F94 $\log(A_V)$ regression and prediction uncertainty in moment magnitude (**M**) units. Explanation is the same as for Fig. 4(b).

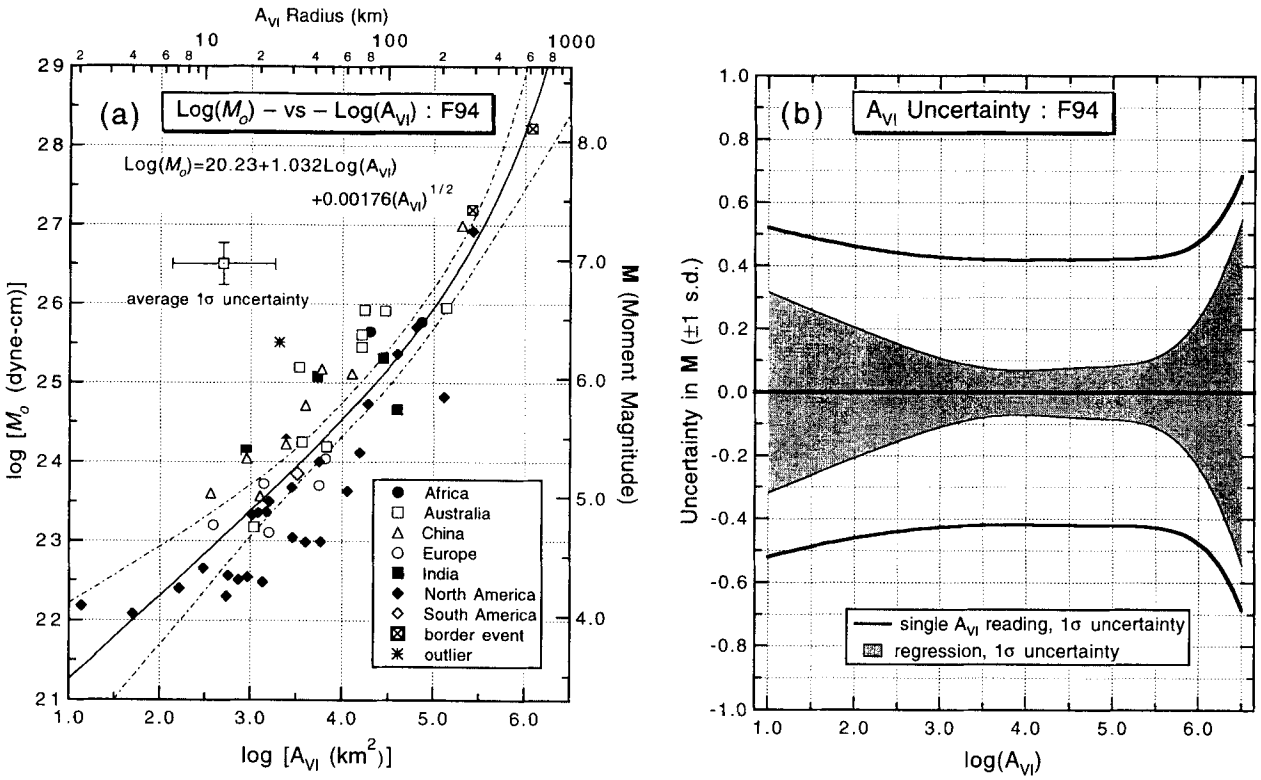

Figure 8. (a) The F94 $\log(M_0)$–$\log(A_{VI})$ regression Explanation of symbols is the same as for Fig. 4(a). (b) Graphical display of the F94 $\log(A_{VI})$ regression and prediction uncertainty in moment magnitude (**M**) units. Explanation is the same as for Fig. 4(b).

bulk of the data represent isoseismal areas of equivalent radius r less than 100–150 km (Fig. 8a). It is within this distance range that the influence of geometrical spreading dominates that of anelastic attenuation and scattering (*cf.* Hanks & Johnston 1992; see the data-scatter section below), so the linear form of the A_{VI} regression out to $\log(A_{VI}) \sim 5.0$ ($r \sim 175$ km) is not unexpected. Also, from eqs (9) and (10) the slope of the regression when the $k2$ term is negligible yields the geometrical spreading exponent n: $k1 = 1.5n$ or $n = 0.69$ for A_{VI}. At $r \lesssim 100$ km, dominant ground motions are expected from S body waves, for which $r^{-1}(n = 1)$ spherical spreading is appropriate; the A_{VI} $n = 0.69$ is significantly less than this value.

For A_i with $r \gtrsim 100$ km, surface or L_g waves dominate ground motions. If L_g is a simple single-mode Airy phase, the theoretical time-domain geometrical spreading follows a $r^{-5/6}$ dependence; in the frequency domain, such as the Frankel (1994) F94 development, $r^{-0.5}$ spreading is expected for the entire dispersed wave train (Herrmann & Kijko 1983). The A_{VI} regression suggests that for $r < 100$ km ($A_i \geq A_{VI}$) a spreading factor intermediate between $n = 0.5$ and $n = 1.0$ is appropriate for stable continental regions. For A_{felt} to A_V, the average n from the $k1$ parameter is $n_{av} = 0.62$, roughly consistent with the theoretically predicted $n = 0.5$ for $r \gtrsim 100$ km.

The Log(A_{VII}) and Log(A_{VIII}) regressions

There were only 31 and 16 data points available for the respective A_{VII} and A_{VIII} regressions (Tables A3 and A4 and Figs 9 and 10). Residual scatter (Fig. 3) is high for A_{VII} but relatively low for the few A_{VIII} data points. This leads to a relatively low χ^2_ν for A_{VIII} (Table 2), indicating that it is easy to find a representative fit to such sparse data, each of which have high individual uncertainties (see Table 1). Surprisingly, no data points qualified as outliers, primarily because of the low z values. As previously, the linear regressions had the poorest curve fit statistics (Table 2); differences among F94, quadratic and cubic curve fits were not significant.

Regression uncertainties for A_{VII} and A_{VIII} are shown in $\log(M_0)$ units as 68 per cent and 95 per cent confidence limits in Figs 9(a) and 10(a) and in **M** units in Figs 9(b) and 10(b). The high limits reflect both the few data points and the high observation uncertainty. F94 prediction uncertainties (Figs 9b and 10b) average between 0.35 and 0.45 **M** units over the central range of the $\log(A_{VII})$–$\log(A_{VIII})$ data but rapidly increase above this range.

The behaviour of the A_{VII} and A_{VIII} regression parameters was different from the other A_i regressions. Their $k2$ attenuation parameter is discussed in a later section. From Table 2 and eq. (10), the A_{VII} $k1$ parameter yields a geometrical spreading coefficient of $n = 0.37$ and the A_{VIII} $k1$ yields $n = 0.29$, lower than all other regressions and much lower than the $n \sim 1$ expected for body-wave geometrical spreading ($r < 100$ km). It is probable that the short, essentially near-source ray paths involved and the undoubtedly large site effects render the theoretical concept of geometrical spreading inappropriate for A_{VII} and A_{VIII}.

Summary of A_i *regressions*

Fig. 11 is a summary plot of the F94 and quadratic regressions for the complete suite of isoseismal data, A_{felt} through A_{VII}. There were insufficient data to attempt regressions for A_{IX} and above. The shaded band on Fig. 11 at 100–150 km epicentral distance divides the plots into two ground-

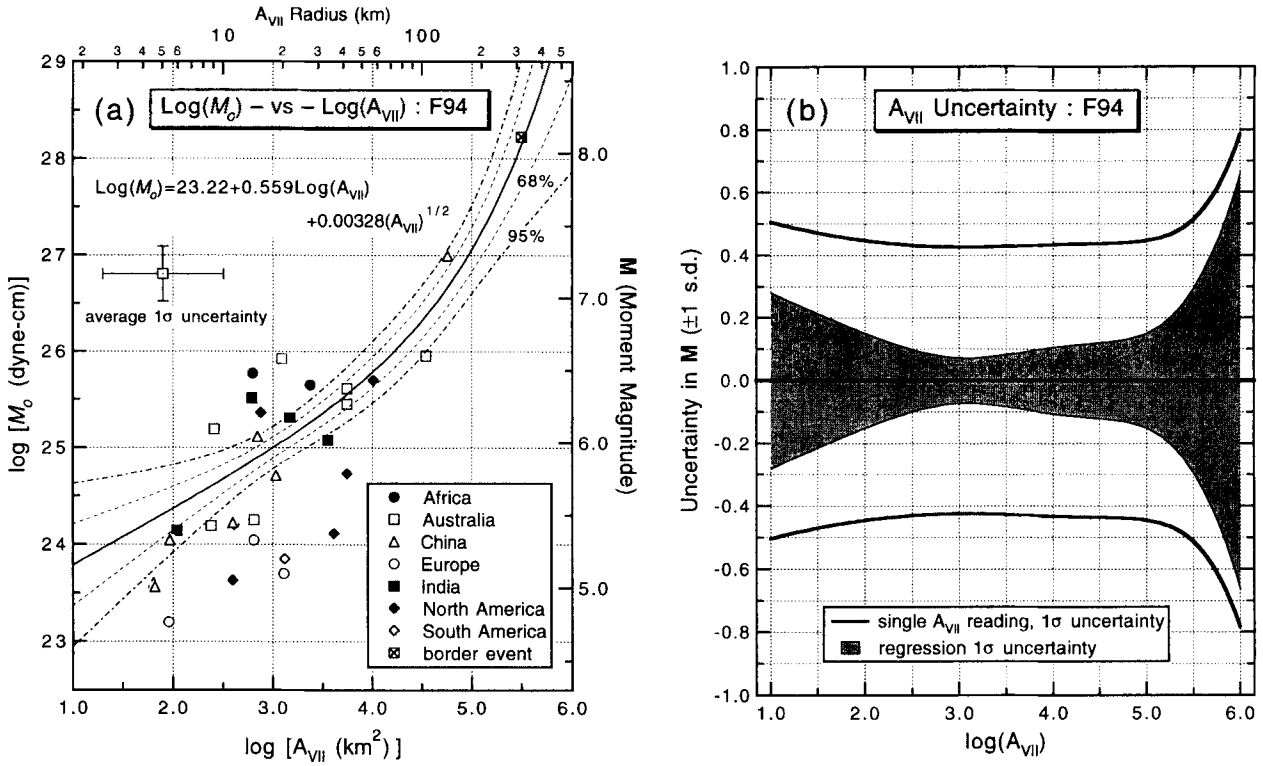

Figure 9. (a) The F94 $\log(M_0)$–$\log(A_{VII})$ regression. Explanation of symbols is the same as for Fig. 4(a). (b) Graphical display of the F94 $\log(A_{VII})$ regression and prediction uncertainty in moment magnitude (**M**) units. Explanation is the same as for Fig. 4(b).

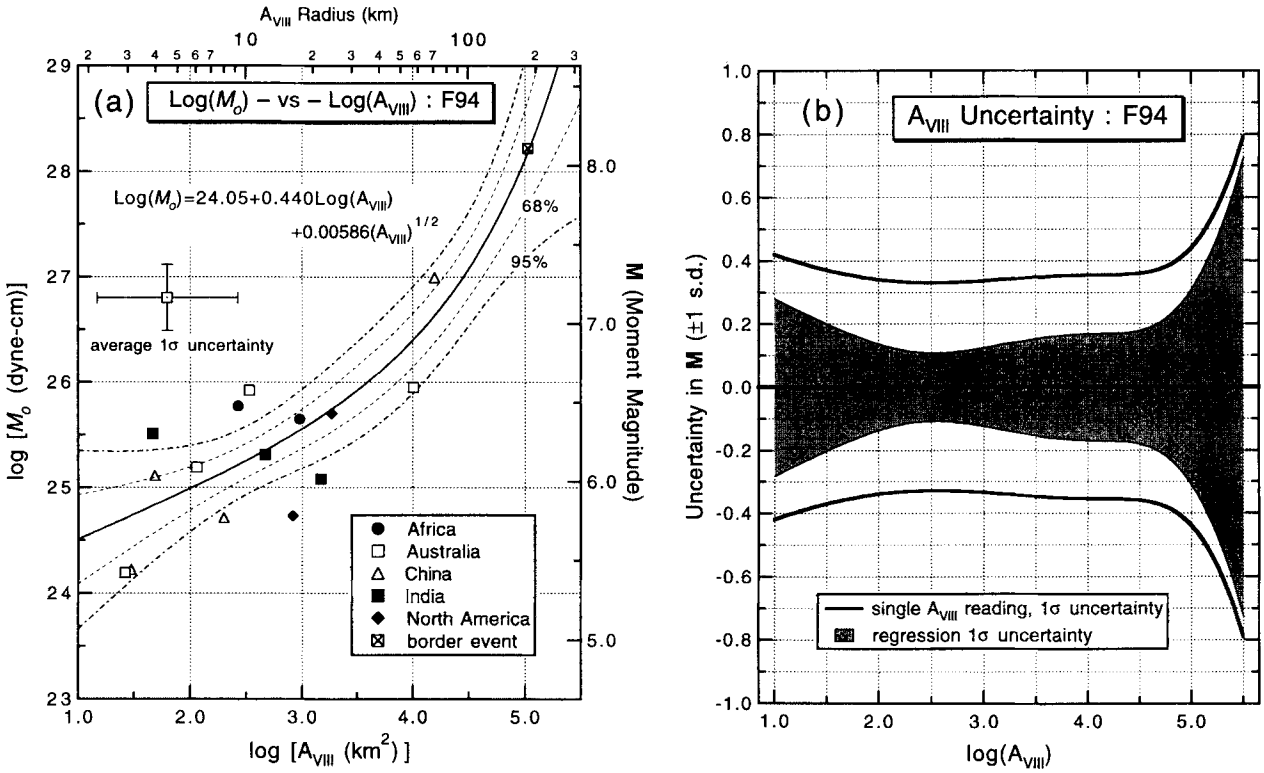

Figure 10. (a) The F94 $\log(M_0)$–$\log(A_{VIII})$ regression. Explanation of symbols is the same as for Fig. 4(a). (b) Graphical display of the F94 $\log(A_{VIII})$ regression and prediction uncertainty in moment magnitude (**M**) units. Explanation is the same as for Fig. 4(b).

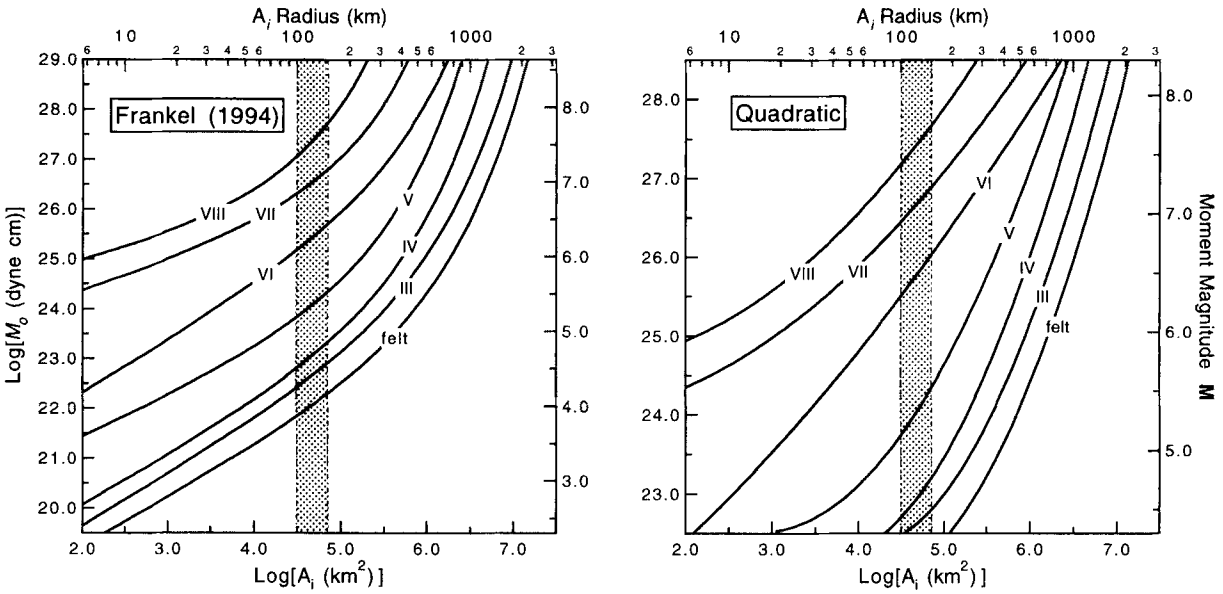

Figure 11. Summary of the F94 and quadratic regressions on SCR isoseismal data. The quadratic regressions extend to only $\log(M_0) = 22.5$ (**M** 4.3) because of their inflection behaviour at lower levels. The shaded band marks the A_i radius range of 100–150 km that separates the L_g from the body-wave ground-motion domains (see text).

motion domains: body- (*S*-)wave-dominated ground motion for $r < 100$–150 km and surface- (L_g-) wave-dominated ground motion for $r > 100$–150 km. This division assists in understanding the functional form of the various A_i regressions. There are three basic categories.

(1) L_g regressions: low intensities, A_{felt}–A_{IV}; A_V is transitional. Nearly all data are for A_i radius $r > 100$ km, therefore these regressions are nearly entirely controlled by geometrical spreading and attenuation appropriate to surface or L_g waves.

(2) Body-wave regressions: mid-range intensity, A_{VI}; again A_V is transitional. Nearly all data are for A_i radius $r < 100$ km, implying body- (*S*-) wave n and Q control behaviour.

(3) Near-source regressions: high intensities, A_{VII} and A_{VIII}. I call these regressions 'near-source' because the radii of their isoseismal areas are of the same order as their causative fault lengths (more so for A_{VIII} than for A_{VII}). Their behaviour is poorly controlled by the sparse available data, but it appears not to conform to either body- or surface-wave spreading and attenuation.

The above interpretation can qualitatively account for the regression behaviour summarized in Fig. 11. In Table 3 these regressions are used to estimate generalized predicted isoseismal areas for a given **M** for average SCR crust. Figs 4–10 show that there is high scatter about these average values. Much of the scatter is aleatory, i.e. not attributable to measurement errors, and I examine the two major sources of aleatory uncertainty in the next section.

Analysis of A_i data scatter

In the foregoing regressions, I have treated the relationship between seismic moment and isoseismal area as $A_i(M_0)$, a one-variable function dependent only on M_0, whereas in reality A_i is a multivariable function, such as $A_i(M_0, \Delta\sigma, h, Q, s, p)$. Here $\Delta\sigma$ is the stress parameter (which for this application may be considered equivalent to the Brune or static stress drop) required to match the high-frequency seismic spectrum above the corner frequency, h is hypocentral depth, Q is the *S*-wave or L_g quality factor, and s and p are generalized parameters representing site effects and population distribution/construction effects, respectively. These six parameters can easily account for the dispersion of data about a $\log(M_0)$–$\log(A_i)$ relation, but which parameters are more or less important in a given situation is a complex question.

Variations in hypocentral depth, site effects, population distribution, and construction type are all potentially significant contributors to A_i variability (especially for $i \geq$ VII). There is, for example, a long history of using macroseismic data to estimate h (e.g. Blake 1941; Kárník 1969). SCR database limitations preclude quantitative analysis of the precise effects of these parameters, so for this study they remain as recognized but unquantified contributors to A_i data scatter. Theoretical considerations, however, would lead one to expect stress drop, $\Delta\sigma$, to play a prominent, perhaps dominant role, in A_i variability, and we have already seen in the functional form of the F94 regression (eqs 7–10) that Q is important, especially at large epicentral distances.

Stress drop

Seismic ground motions have a strong dependence on stress drop, but the predicted dependence will vary according to what aspect of ground motion intensity actually measures. Potential types of motion include maximum ground acceleration, a_{max}, root-mean-square acceleration, a_{rms}, peak ground velocity, v_{max}, and rms velocity, v_{rms}. Moreover, the dominant ground-motion contributor to intensity may change: low intensities based on degree of human perception may be attributable to a different type of ground motion than high intensities based on damage effects. Here I will follow Frankel (1994) and Atkinson & Hanks (1994) and assume that human perception intensities relate to a high-frequency (i.e. greater than the

Table 3. Average effects of earthquakes: stable continental regions.

M	[1]A_{felt}	A_{III}	A_{IV}	A_V	A_{VI}	A_{VII}	A_{VIII}	I_{max}	[4]N_{ISS}^{total} (year: 1925)	N_{ISS}^{20} (year: 1925)	N_{ISC}^{total} (year: 1992)	N_{ISC}^{20} (year: 1992)
3.0	2,000 F[2] (25)	750 F (15)	300 F (10)	[3]——	——	——	——	2.5 Q	——	——	——	——
3.5	11,000 F (59)	3,600 F (34)	1,600 F (23)	70 F (5)	——	——	——	3.5 Q	——	——	——	——
4.0	46,000 F (120)	16,000 F (71)	7,700 F (50)	550 F (13)	60 F (4)	——	——	4.5 Q	——	——	——	——
4.5	160,000 F (230)	60,000 F (140)	31,000 F (99)	3,700 F (34)	290 F (10)	——	——	5.5 Q	7 E	5 E	60 E	38 E
5.0	460,000 F (380)	180,000 F (240)	98,000 F (180)	19,000 F (78)	1,400 F (21)	5 F (1.3)	——	6.5 Q	22 E	15 E	186 E	120 E
5.5	970,000 F (560)	450,000 F (380)	250,000 F (280)	66,000 F (140)	6,500 F (45)	75 F (5)	5 F (1.3)	7.5 Q	37 E	29 E	319 E	230 E
6.0	1,900,000 F (780)	960,000 F (550)	520,000 F (410)	170,000 F (230)	25,000 F (89)	1,200 F (20)	130 F (6)	8.5 Q	54 E	45 E	458 E	360 E
6.5	3,200,000 F (1,000)	1,700,000 F (740)	950,000 F (550)	350,000 F (330)	81,000 F (160)	10,000 F (56)	2,200 F (26)	9 Q	71 E	64 E	602 E	509 E
7.0	5,000,000 F (1,300)	2,900,000 F (960)	1,300,000 F (640)	670,000 F (460)	210,000 F (260)	48,000 F (120)	14,000 F (67)	10 Q	88 E	85 E	746 E	675 E
7.5	7,300,000 F (1,500)	4,400,000 F (1,200)	2,400,000 F (870)	1,100,000 F (590)	470,000 F (390)	140,000 F (210)	43,000 F (120)	10.5 Q	106 E	106 E	893 E	845 E
8.0	10,000,000 F (1,800)	6,400,000 F (1,400)	3,400,000 F (1,000)	1,600,000 F (710)	900,000 F (540)	290,000 F (300)	95,000 F (170)	11.5 Q	108 E	106 E	920 E	845 E
8.5	14,000,000 F (2,100)	8,800,000 F (1,700)	4,700,000 F (1,200)	2,300,000 F (860)	1,500,000 F (690)	530,000 F (410)	170,000 F (230)	12 Q	108 E	106 E	920 E	845 E

(1) isoseismal areas (A_i) in km^2 rounded to 2 significant digits; equivalent radius (km) in parentheses
(2) regressions: F, F94; Q, quadratic; E, exponential
(3) symbol —— means regression should not be applied in this range
(4) last 4 columns: number of expected ISS and ISC reporting stations for given **M** for representative years 1925 and 1992; N_{mx} = 108 (1925), 920 (1992); for $\Delta \geq 20°$, N_{20mx} = 106 (1925), 845 (1992)

corner frequency f_c) spectral amplitude a_0. Then, for a Brune (1970) source spectrum with an angular frequency dependence of ω^{-2} above f_c:

$$a_0 \propto M_0^{1/3} \Delta\sigma^{2/3}. \tag{19}$$

This is the same functional dependence as that for v_{rms} (Atkinson & Hanks 1994).

In his development, Frankel assumed constant stress drop, $a_0 \propto M_0^{1/3}$, so that the formulas for a_0 and A_{felt} include no $\Delta\sigma$ term (eqs 4 and 6 of Frankel 1994; eqs 6 and 8, this study). If $\Delta\sigma$ is allowed to vary, then eq. (19) is applicable and the F94 relation must be modified to include a stress-drop term. Taking the logarithm of both sides of eq. (19) and substituting in eq. (4) of Frankel (1994) yields

$$\log(M_0) = k'0 + k1 \log(A_i) + k2\sqrt{A_i} - 2\log(\Delta\sigma), \tag{20}$$

where the nomenclature of eqs (9) and (10) applies and $\Delta\sigma$ is in bars. A reasonable assumption is that the original F94 regressions predict $\log(M_0)$ for SCR earthquakes of average $\Delta\sigma$. If $\overline{\Delta\sigma}$ is the average SCR stress drop, then

$$k'0 = k0 + 2\log(\overline{\Delta\sigma}), \tag{21}$$

where $k0$ is the constant parameter determined in the F94 least-squares fitting. When $\Delta\sigma = \overline{\Delta\sigma}$, eq. (20) reduces to the original F94 regression form (eq. 9).

Eqs (20) and (21) can be used to assess the effect of non-average stress drop on $\log(M_0)$–$\log(A_i)$ regressions. A factor of two change in $\Delta\sigma$ from its average will induce $\sim \pm 0.4$ **M** change if A_i is fixed. Johnston (1994b) determined that for Brune stress drops in SCRs, $\overline{\Delta\sigma} = 85$ bar with 1 standard deviation limits of 25 bar and 250 bar. If static stress drop and the high-frequency stress parameter behave similarly, then a $\Delta\sigma$ change over this standard deviation range will produce a change in **M** of $\sim \pm 0.65$ units for fixed A_i. Since σ_{res}, the standard deviation of the regression residuals, varies from 0.4 to 0.7 $\log(M_0)$ units (0.3–0.5 **M** units), it is clear that stress-drop variation is capable of accounting for a large percentage of the data scatter evident in the A_i regressions—provided the theoretical functional dependence of eq. (19) holds.

Strong qualitative support for the validity of eq. (19) and the primary role of stress drop in accounting for the data dispersion observed in $\log(M_0)$–$\log(A_i)$ regressions is provided by Fig. 12. In this figure, all A_i (i = felt–VIII) residuals of Fig. 3 for which $\Delta\sigma$ is available (Johnston 1994b) are plotted with symbols keyed to stress-drop range. Large A_i (negative residuals) generally correlate with high $\Delta\sigma$ and small A_i (positive residuals) with low $\Delta\sigma$. The mapping is not one-to-one but there is clearly a significant association. All of the most negative residuals are from high $\Delta\sigma$ events that exceed 250 bars, and all of the most positive residuals are from low $\Delta\sigma$ events, less than 25 bars.

Contrary to expectations from eq. (19), stress drop will be secondary to seismic moment in controlling the range of isoseismal area size because seismic moments span a much larger range than stress drops. This may be demonstrated by rewriting eq. (20) in differential form, $\Delta(A_i \text{ terms}) = \Delta\log(M_0) + 2\Delta\log(\Delta\sigma)$ and noting that $\Delta\log(M_0) \sim 8$ and $\Delta\log(\Delta\sigma) \sim 2$. The great range of M_0 has roughly twice the influence of the much smaller range of $\Delta\sigma$ on isoseismal area sizes. The total possible range of $\sim 10^{12}$ for the A_i terms is much greater than the observed range of $\sim 10^7$ ($\sim 10^6$ for A_{felt} itself) because extreme combinations are not observed, e.g. an **M** 8.5, $\Delta\sigma = 1000$ bar event.

Stress drop is not the only agent introducing data scatter

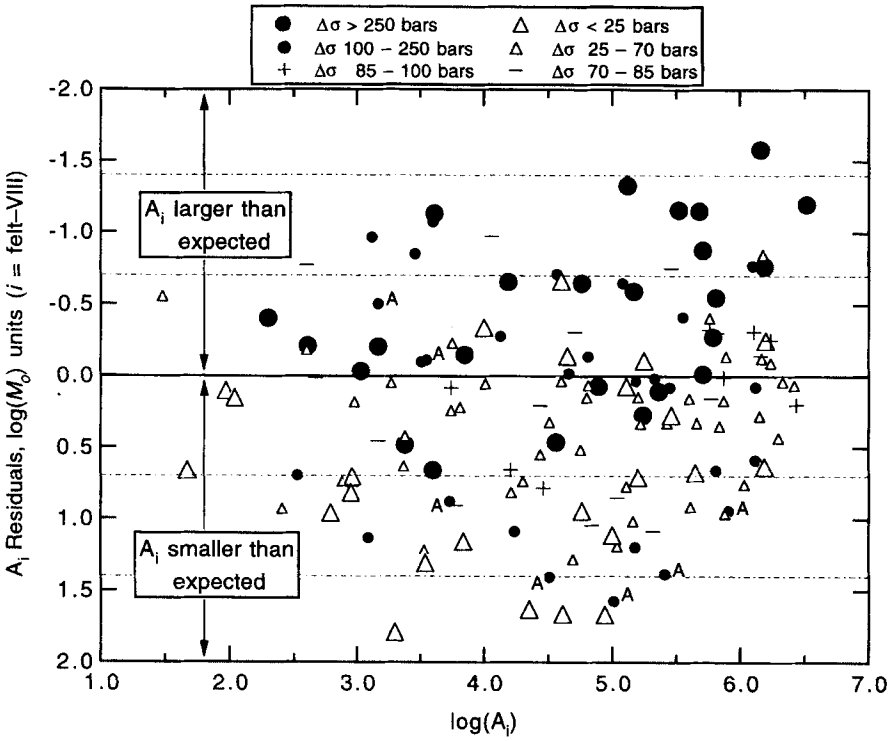

Figure 12. The A_i residuals for a subset of 30 events of the appendix Table A3 database for which stress drop $\Delta\sigma$ has been computed from the M_0 and source time functions (Johnston 1994b). All residuals from regressions A_{felt} through A_{VIII} have been combined on this single plot; dashed lines are ± 1 and ± 2 standard deviations. Average $\Delta\sigma$ is 85 bar. Residual symbols are keyed to three $\Delta\sigma$ ranges: large symbols, >1 standard deviation from average $\Delta\sigma$; small symbols, <1 standard deviation from average $\Delta\sigma$; + or −, average $\Delta\sigma \pm 15$ bar. The symbol 'A' identifies residuals of the 1956 Anjar earthquake discussed in the text.

into the $\log(M_0)$–$\log(A_i)$ relations. The residuals of the Anjar, India, earthquake (symbol A, Fig. 12) illustrate well the importance of anelastic attenuation and scattering for $\log(M_0)$–$\log(A_i)$ data dispersion. Chung & Gao (1995) determined a moderately high stress drop for this event, $\Delta\sigma = 162$ bar (or 209 bar using the application of Johnston 1994b). Its damage area isoseismals, A_{VII} and A_{VIII}, reflect this, yielding moderately negative residuals. Yet all its outer A_i, from A_{VI} to A_{felt}, yield strongly positive residuals, indicating isoseismal areas much too small for the determined M_0 and opposite to expectations for a high-$\Delta\sigma$ event. The Anjar earthquake occurred in the Kutch graben, where the crust is highly extended from Mesozoic rifting episodes. Such a crustal environment is expected to have a high associated seismic-wave attenuation, even though it is within the SCR Indian subcontinent. The Anjar isoseismal pattern strongly suggests a very low Q_β for the Kutch–Cambay graben region, a finding in accord with the occurrence there of the 1819 **M** 7.5–8.0 Kutch earthquake and the hypothesis of Jin & Aki (1988) that large intraplate earthquakes occur preferentially within low-Q regions.

Attenuation: quality factor Q

Variations in attenuation are not expected to contribute to A_i data scatter to the same degree as stress drop for a number of reasons. First, the very restrictive definition of stable continental regions (see Part I) should lead to a restricted intra-SCR Q range. (This was one motivation for defining SCR crust separately.) Second, an averaging over crustal zones of different Q naturally occurs by working with isoseismal areas rather than radii, especially for the larger, outer isoseismals. A final reason is that Q is incorporated into the F94 regression functional form, via the $k2$ regression parameter, while $\Delta\sigma$ is not (see eq. 10). Therefore, the least-squares fitting for the optimum regression parameters works to minimize Q variations, whereas a constant average stress drop is assumed.

Because Q is frequency-dependent, care must be exercised when comparing the Q of different regions or from different studies. Frankel (1994) found that the average frequency f of minimum perceptible ground motion in humans was 3 ± 1 Hz. This is the best estimate of the f of eqs (7) and (10) for the A_{felt}–A_{III} regressions; it therefore becomes the frequency at which Q is estimated in those regressions. I assume that $f = 3 \pm 1$ Hz is also the best frequency at which to estimate Q for regressions on A_{IV}–A_{VI}, since these intensity levels depend primarily on degree of human perception of ground motion. For the A_{VII} and A_{VIII} regressions, however, which depend primarily on degree of damage to structures, a better estimate for the best-applicable f is ~ 5 Hz (e.g. Nuttli & Herrmann 1984). This frequency could be higher for very stiff, brittle structures or lower if the damage region contains many large or medium- to high-rise structures.

As noted previously, the ground motions that determine intensity levels are dominated by the continental crust surface wave L_g when A_i radius $r \gtrsim 100$ km. Thus the Q under discussion is actually Q_{L_g}, and the $k2$ parameter in the L_g regressions yields an estimate for the average Q_{L_g} of stable continental crust. For $r \lesssim 100$ km, S waves probably produce the largest ground motions; this would mostly concern the A_{VI}–A_{VIII} regressions and any Q estimates from their $k2$ terms.

From Table 2 for the $k2$ parameter, the A_i regressions of this study yield the following estimates for SCR Q (eq. 10): $Q_{\text{felt}}^{3\text{Hz}} = 1570$; $Q_{\text{III}}^{3\text{Hz}} = 1420$; $Q_{\text{IV}}^{3\text{Hz}} = 1020$; $Q_{\text{V}}^{3\text{Hz}} = 760$; $Q_{\text{VI}}^{3\text{Hz}} = 1125$; $Q_{\text{VII}}^{5\text{Hz}} = 1010$; $Q_{\text{VIII}}^{5\text{Hz}} = 560$. For A_{felt}–A_{IV}, average SCR 3 Hz Q is ~1340, compared to 1150 determined by Frankel (1994) for A_{felt} with n fixed at 0.5. The Q values of the higher isoseismals are not easily interpreted, as they represent a mix of Q_{L_g}, Q_β, and for Q_{VII} and Q_{VIII}, substantial contamination from shallow low-Q path and site conditions.

Q values determined from far-field intensity data should reflect Q_{coda} determined from the coda decay of L_g waveforms since Q_{L_g} and Q_{coda} are similar in most regions (Mitchell 1995). Mitchell *et al.* (1993) and Mitchell (1995) have mapped L_g coda Q over most of the Earth's continental regions, both active and stable. They find that Q_{coda} correlates well with the average crustal accretion dates of the SCRs (Australia is an exception), if allowance is made for more recent deformational episodes. For example, North America, the oldest SCR, with craton assemblage completed by ~ 1.6–2.0×10^9 yr, exhibits the highest 1 Hz Q_{coda}, 1000–1200, but in the younger ($\lesssim 1.0 \times 10^9$ yr) surrounding crust, Q_{coda} is 700–900, and in the Mesozoic margin regions it dips to ~300–500 (Singh & Herrmann 1983). Other SCRs exhibit a similar craton-to-margin pattern, but their average Q_{coda} ranges differ, depending mainly on their assembly ages. They generally have 1 Hz Q_{coda} values intermediate between North America and Australia (1 Hz $Q_{\text{coda}} < 230$), with SCR India, South America, and the northwest portions of SCR Europe and Africa tending toward high Q_{coda} relative to western Europe, China, Asia, and southern Africa.

The above 1 Hz Q_{coda} summary for SCRs cannot be compared directly with Q obtained from this study's A_{felt}–A_{VIII} regressions because of frequency differences and spectral-domain versus time-domain considerations. The summary does, however, reveal relative levels of attenuation among the SCRs. For example, North America consistently accounts for the majority of the points below the regression curve, suggesting that North American A_i tend to be larger than average for a given M_0. There are no A_i data for the Siberian craton. The A_is for the single South American earthquake are consistently to the high A_i side of the regressions. SCR Australia, except for A_{VII} and A_{VIII}, is predominantly on the low A_i side of the regressions. SCR Europe, India, Africa, and China appear well mixed, although India has an inordinate number of low A_i outliers, perhaps due to low stress drop.

To conclude this examination of A_i data scatter, analysis of stress-drop and Q variations in stable continental regions leads to qualitative estimates of the principal sources of data dispersion in the SCR $\log(M_0)$–$\log(A_i)$ regressions. Stress-drop variation probably accounts for one-half to two-thirds of the aleatory (M_0 and A_i error-free) data scatter, variation in Q accounts for one-quarter to one-third, with focal-depth differences and site effects the next most significant uncertainty contributors.

Regression on maximum intensity, I_{max}

The I_{max} SCR data set consists of all reported maximum intensities, as listed in Table A3, plus additional observations from Tables 2 and B2 in Part I. The I_{max} may be the actual epicentral intensity I_0, but frequently it is not, or it is unclear whether I_{max} is I_0. This uncertainty, site effects (especially the presence or absence of soft alluvial soils), population density, and type of construction all contribute to the high data scatter of Fig. 13(a). Despite these large sources of error, a regression for $\log(M_0)$ on I_{max} is important because of the numerous

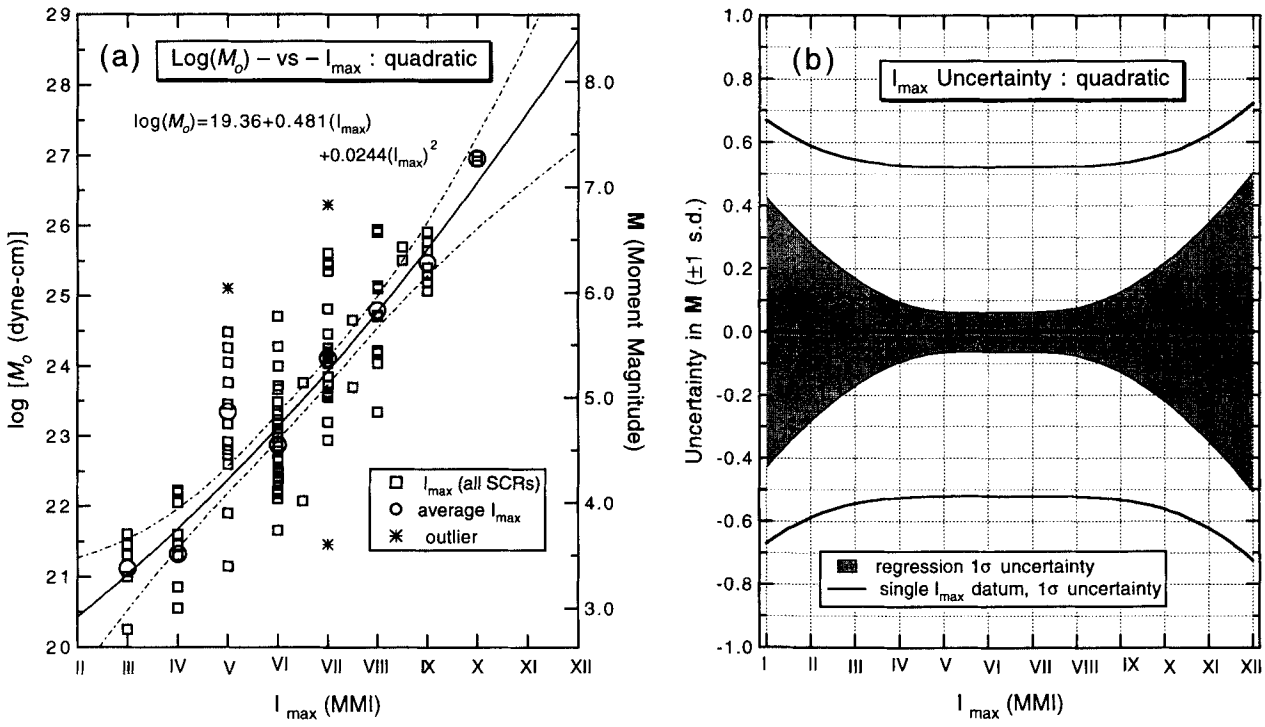

Figure 13. (a) Quadratic regression of $\log(M_0)$ on I_{max}, the maximum reported intensity which is often, but not always, the epicentral intensity I_0. Figure explanation as in Fig. 4(a), except data points are not identified with individual SCRs and average I_{max} for each MMI level is given. (b) Graphical display of I_{max} regression and prediction uncertainty in moment magnitude (**M**) units. Explanation is the same as for Fig. 4(b).

events in historical seismicity catalogues for which I_{max} is the only size indicator.

I tested both linear and quadratic regressions of $\log(M_0)$ on the I_{max} data; the F94 functional form should not be applicable here. Table 2 contains the regression parameters and chi-square information. Statistically, the two curve fits were not significantly different, but I selected the quadratic regression as primary because it fits the two $I_{max} = X$ observations better. Three outliers were identified (Fig. 3) and deleted from the regression analysis. Not surprisingly, the resulting I_{max} $\sigma_{res} = 0.78 \log(M_0)$ units represents the largest data scatter of all regressions of this study.

There is no useful way to evaluate the reliability of an individual I_{max} observation, so I weighted all I_{max} data equally. Therefore, from eq. (4) the only variation in weighting was contributed by the uncertainty of the corresponding $\log(M_0)$ value. The resulting regression uncertainty is shown as 95 per cent confidence limits in $\log(M_0)$ units in Fig. 13(a) and in **M** units in Fig. 13(b). Between I_{max} III and X the major contributor to the prediction uncertainty $\sigma^{P}_{I_{max}}$ is the large σ_{res}; beyond these limits the rapid increase of $\sigma^{R}_{I_{max}}$ dominates. Except at these extremes, Fig. 13(b) and Table A1 demonstrate that a single I_{max} value can be expected to constrain the size of the earthquake to within $\sim$0.50–0.55 **M** units 68 per cent of the time. This is the largest prediction uncertainty of any of the SCR regressions in Part I or Part II, yet it is lower than previous estimates of I_{max} reliability (e.g. Johnston 1994a). For convenience, I list here the predicted moment magnitudes from the I_{max} quadratic regression from Table A1:

I_{max}	**M**
I	2.5 ± 0.67
II	2.9 ± 0.59
III	3.3 ± 0.55
IV	3.8 ± 0.53
V	4.2 ± 0.52
VI	4.7 ± 0.52
VII	5.3 ± 0.52
VIII	5.8 ± 0.52
IX	6.4 ± 0.53
X	7.0 ± 0.56
XI	7.7 ± 0.62
XII	8.4 ± 0.72

(22)

Only SCR earthquakes were used to derive the I_{max} regression, but, unlike isoseismal areas, there are no compelling reasons that these relations should differ from an **M**– or $\log(M_0)$–I_{max} relation obtained in active tectonic regions. If this is true, a much larger database would be available to constrain the high and low ranges of the regression better.

Perhaps the most widely used relation between magnitude and maximum intensity is the Gutenberg & Richter (1954) formula $M(M_{GR} \sim \mathbf{M}) = 2I_0/3 + 1$. For $I_0(\mathrm{MM}) = $ III, IV, V, VI, VII, VIII, IX, X, XI, XII, this relation yields, respectively, $M = 3.0, 3.6, 4.3, 5.0, 5.7, 6.3, 7.0, 7.7, 8.3, 9.0$, values significantly higher for $I_0/I_{max} \geq$ VI than given by eq. (22). A non-exhaustive sampling of published formulas [China (Gu 1983); central and eastern United States (Sibol, Bollinger & Birch 1987); Persia (Ambraseys & Melville 1982); NW Europe (Ambraseys 1985); Europe (Kárník 1969, 1971); and global (Gutenberg & Richter 1954)], and converting from M_s, m_b or m_{bL_g} using Part I equations, shows that the SCR **M** from I_{max} (eq. 22) is generally in the midrange of other values from a wide variety of tectonic and cultural environments, a not unexpected result if there are no characteristics that are peculiar to SCR I_{max}, as opposed to I_{max} from other types of crust.

NUMBER OF ISS/ISC REPORTING STATIONS

In this section I give a rationale and technique for recovering seismic moment from the number of reporting seismic stations, N_{st}. The application is especially useful for the $\sim$25 000 earthquakes reported ($\sim$50 per cent were located) in the early instrumental era of the International Seismological Summary (ISS 1913–1963). The ISS did not compute magnitude so the only global magnitude sources are the large earthquake catalogues of Gutenberg & Richter (1954) and Rothé (1969). The application is extended to the International Seismological Centre (ISC) era, 1964–1993, but is less useful there.

The N_{st} for a given event is more akin to felt area (MMI A_{felt}) than to amplitude magnitude. Imagine that reporting stations are uniformly distributed over the globe and that they all have the same detection thresholds. Then, for average stress drop, N_{st} will depend on the size or seismic moment of the earthquake; larger earthquakes will produce seismic waves of greater amplitudes that will exceed detection thresholds to greater distances and thus encompass a greater number of stations. The analogy of N_{st} to felt area has limitations. The Earth's seismic-station distribution is markedly non-uniform in space, in time and in sensitivity, and teleseismic waves propagate in a different manner than the near-source body waves and L_g waves on which intensities are based. Therefore we should not necessarily expect a M_0–N_{st} regression relation to be of the F94 or quadratic type.

All but one of the SCR M_0 database events were reported in the ISS or ISC bulletins; therefore N_{st} and N_{20}, the subset of reporting stations at geocentric angular distance $\Delta \geq 20°$, are included with the instrumental data (Table B2) of Part I rather than the much shorter isoseismal database in this study. The N_{st} data, however, cannot be used directly in a regression analysis without first allowing for the tremendous variation in number of reporting stations through time. Therefore, following the work of Ambraseys & Melville (1982), I have normalized N_{st} by N_{mx}, the maximum number of seismic stations reporting a single earthquake to the ISS or ISC in a given year. The N_{mx} is a superior normalizing factor to the total number of seismic stations because it is an index of active, rather than just existing, stations. Fig. 14 shows N_{mx} and the related N_{20mx} for the ISS and ISC eras through 1992. These normalizing factors also are listed in Table A2, along with information about each N_{mx} and N_{20mx} earthquake.

For the regression analysis, I used $\log(R)$, where $R = N_{st}/N_{mx}$, as the independent variable. It quickly became evident that independent constraints would be necessary to obtain a stable curve fit. The first constraint was for small earthquakes: the ISS was not concerned with small, local earthquakes so $\log(M_0) \simeq 22.00$ ($\mathbf{M} \simeq 4.0$) was a reasonable lower threshold for $R = 0$. Very large earthquakes should saturate the global

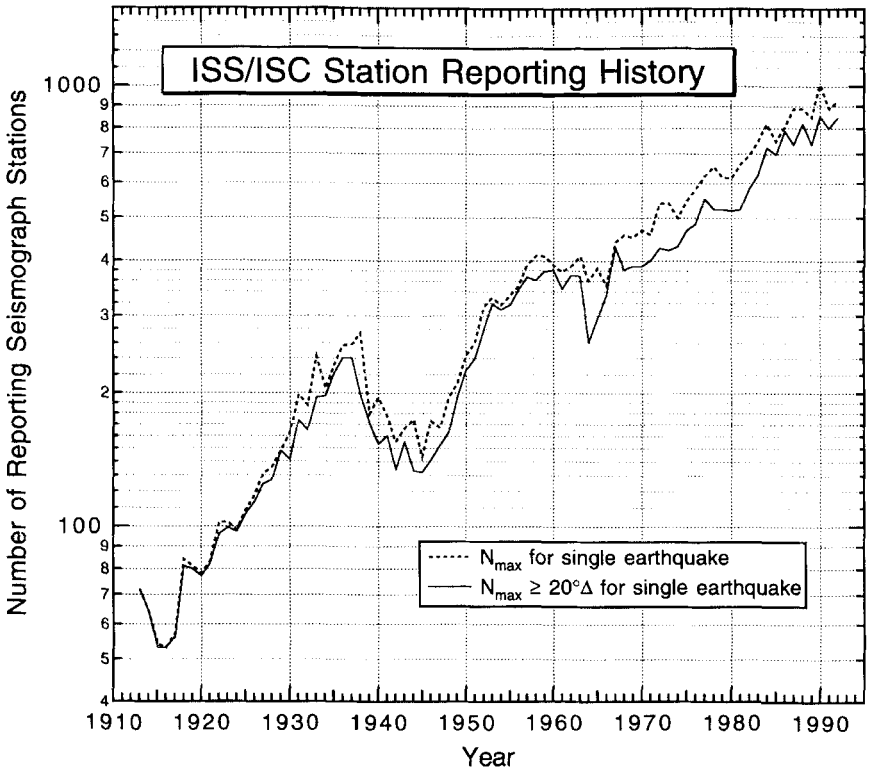

Figure 14. The station reporting history of the International Seismological Summary (1913–1963) and the International Seismological Centre (1964–1992). For a given year, the dashed line gives the maximum number of stations reporting a single earthquake, and the solid line gives the maximum number of reporting stations at epicentral distance $\geq 20^{\circ}\Delta$ (geocentric angle) for a single earthquake. For some years the two numbers will be from the same earthquake but often they are different (see Table A2). These data are used as normalizing factors for the regressions of Fig. 15.

array of stations; $R = 1$ ($\log R = 0.0$) is the large ($\log M_0 \simeq 28$) earthquake limit. An exponential regression curve satisfied both constraints.

Fig. 15(a) shows the SCR N_{st}/N_{mx} data fit with an exponential regression on $\log(R)$. As $R \rightarrow 0$, $\log(M_0) \rightarrow 22.38$ ($\mathbf{M} = 4.2$) and for $R = 1$, $\log(M_0) = 27.43$ ($\mathbf{M} = 7.6$). These **M** values are close to the desired behaviour at $R = 0$ and 1; it was not possible to achieve better behaviour at these extremes without degrading the fit to the midrange data. Table 2 lists the regression parameters and goodness-of-fit statistics for the $R = N_{st}/N_{mx}$ and $R_{20} = N_{20}/N_{20mx}$ data. Residual scatter is high, although not as dispersed as for I_{max}. There were no outliers. Unlike isoseismal areas, R and R_{20} have no uncertainty, so data points were weighted proportional only to M_0 uncertainty.

Examination of the N_{st}/N_{mx} data in Fig. 15(a) reveals a data set problem. The data points below the regression, representing earthquakes that have more reporting stations than predicted by the regression, are predominantly from North America and Europe, reflecting the high station density of these regions. Conversely, southern hemisphere events from Australia, South America, and southern Africa, as well as from China, are disproportionately unreported relative to the global SCR average. Normalization by N_{mx} removes much of the temporal variability in N_{st} but does nothing to correct for the non-uniform spatial distribution of reporting stations.

The regression on N_{20}/N_{20mx} shown in Fig. 15(c) represents an attempt to correct, or at least reduce, this station-distribution problem. By taking only reporting stations at $\Delta \geq 20^{\circ}$, the chance proximity of an earthquake to a region with a large number of stations does not inflate its N_{20} relative to events in more isolated regions. The N_{20mx} has the same epicentral distance restrictions as N_{20} and is a more stable normalizing factor than N_{mx}. The N_{mx} is sensitive to whether, in a given year, a large earthquake occurred near Japan. In most years one did; from 1930 to present, about three-quarters of the N_{mx} are from such events, whereas the N_{20mx} events are distributed essentially randomly around the globe. Thus N_{20mx} should represent a more uniform normalizing factor through time than N_{mx}.

Fig. 15(d) and Tables 2 and A1 show that the recomputation using $R_{20} = N_{20}/N_{20mx}$ was moderately successful. Data scatter is reduced from $\sigma_{res} = 0.709$ to 0.632 $\log(M_0)$ units. Regional biases in the data are not so apparent. Regression uncertainties, computed from eq. (13), may be compared in Figs 15(b) and (d) and Table A1. Prediction uncertainties (same sources) decrease from 0.48 to 0.42 **M** units over the midrange of the data. Overall, the log (R) regression can constrain **M** within limits comparable to the A_V regression, and use of the $\log(R_{20})$ relation is competitive with the A_{VI} or A_{VII} regressions. Each provides a tighter constraint on the seismic moment/moment magnitude of an earthquake than I_{max}/I_0.

APPLICATIONS AND CONCLUSIONS

Unless there is surface rupture, seismic moment cannot be estimated directly for any historical earthquakes, and it has not been determined directly for the great majority of twentieth century earthquakes. In this study I developed 10 regression equations applicable to stable continental regions for the

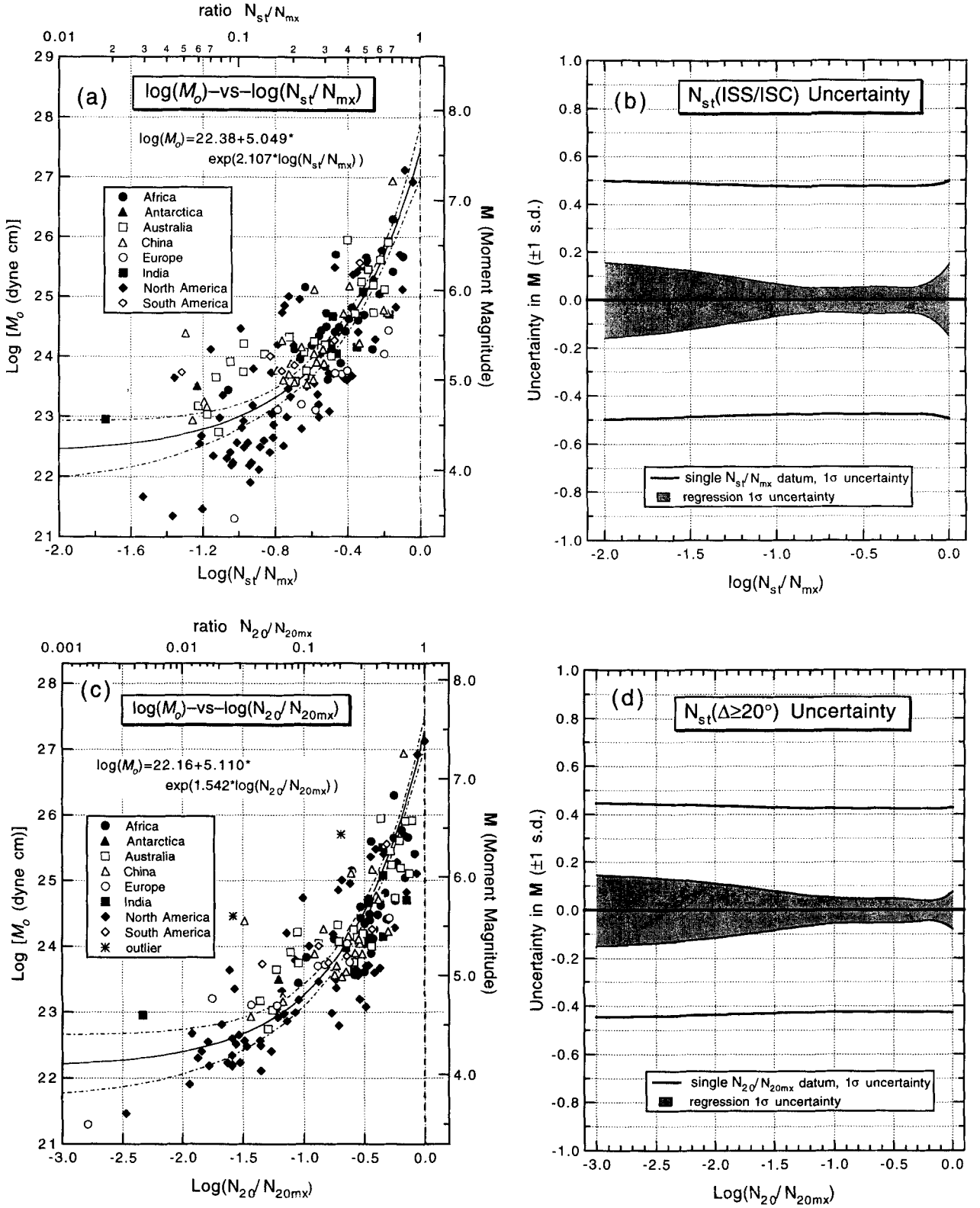

Figure 15. (a) Regression of $\log(M_0)$ on the logarithm of the number of ISS/ISC stations reporting each SCR earthquake normalized by N_{mx}, the greatest number of stations reporting an earthquake in the same year. The exponential regression curve fit has the desired quasi-asymptotic approach of $\log(N_{st}/N_{mx})$ to zero as the ratio N_{st}/N_{mx} approaches 1.0 for large earthquakes. Dash–dot lines are 95 per cent confidence limits. (b) Graphical display of $\log(N_{st}/N_{mx})$ regression and prediction uncertainty in moment magnitude (**M**) units. Explanation is the same as for Fig. 4(b). (c) Same as 15(a) but for N_{20}, the number of ISS/ISC stations at geocentric distance $\Delta \geq 20°$ reporting an SCR event normalized by N_{20mx}, the maximum number of stations of $\Delta \geq 20°$ reporting an earthquake in the same year. Several small events in the $\log(N_{st}/N_{mx})$ regression had no reporting stations at or beyond $\Delta = 20°$ and therefore could not be used in this regression. (d) Graphical display of the $\log(N_{20}/N_{20mx})$ regression and prediction uncertainty in moment magnitude (**M**) units. Explanation is the same as for Fig. 4(b).

estimation of seismic moment or **M** from intensity data or from number of reporting stations. For most of the regressions, I explored different types of curve fits, so for convenience I list here the *preferred* regression relation for each data type:

$$
\begin{aligned}
X = A_{\text{felt}} \quad & \log(M_0) = 17.31 + 0.959\log(X) + 0.00126\sqrt{X},\\
X = A_{\text{III}} \quad & \log(M_0) = 17.59 + 1.020\log(X) + 0.00139\sqrt{X},\\
X = A_{\text{IV}} \quad & \log(M_0) = 18.10 + 0.971\log(X) + 0.00194\sqrt{X},\\
X = A_{\text{V}} \quad & \log(M_0) = 19.83 + 0.788\log(X) + 0.00260\sqrt{X},\\
X = A_{\text{VI}} \quad & \log(M_0) = 20.23 + 1.032\log(X) + 0.00176\sqrt{X},\\
X = A_{\text{VII}} \quad & \log(M_0) = 23.22 + 0.559\log(X) + 0.00328\sqrt{X},\\
X = A_{\text{VIII}} \quad & \log(M_0) = 24.05 + 0.440\log(X) + 0.00586\sqrt{X},\\
X = I_{\max} \quad & \log(M_0) = 19.36 + 0.481X + 0.0244X^2,\\
X = \log(N_{\text{st}}/N_{\text{mx}}) \quad & \log(M_0) = 22.38 + 5.049\exp(2.107X),\\
X = \log(N_{20}/N_{20\text{mx}}) \quad & \log(M_0) = 22.16 + 5.110\exp(1.542X).
\end{aligned}
\tag{23}
$$

Table 3 presents the results of inverting the eq. (23) regressions to obtain the average values of isoseismal areas, maximum intensity and number of recording stations for given **M**.

The regression results of this Part II study may be combined with the Part I instrumental analysis to yield a hierarchy of methods to determine M_0 or **M** in stable continental regions. The hierarchy is based solely on the prediction uncertainty associated with each predicted **M**. From the SCR database (Table B2, Part I) the average MEF_{M_0} for all 177 SCR events with direct M_0 is MEF = 1.75. Hence $\log(\text{MEF}_{M_0}) = \sigma_{\log M_0} = 0.244$, yielding $\sigma_{\mathbf{M}} = 0.16$ **M** units. This I take as the fundamental uncertainty of **M**. Next I take the prediction uncertainty for each regression from the central range of the SCR data determined in Part I and in this study, generally $\mathbf{M} \sim 4.5$ to $\mathbf{M} \sim 7.0$, and let this represent the limiting uncertainty of each data category, yielding the following hierarchy for the determination of **M**:

independent variable		predicted **M** value ±1 standard deviation
M_0	→	$\mathbf{M}_{M_0}$ ±0.16
M_s	→	$\mathbf{M}_{M_s}$ ±0.19
m_{L_g}	→	$\mathbf{M}_{mL_g}$ ±0.23
m_b	→	$\mathbf{M}_{m_b}$ ±0.26
A_{III}	→	$\mathbf{M}_{A_{\text{III}}}$ ±0.28
A_{VIII}	→	$\mathbf{M}_{A_{\text{VIII}}}$ ±0.35
M_L	→	$\mathbf{M}_{M_L}$ ±0.35
A_{IV}	→	$\mathbf{M}_{A_{\text{IV}}}$ ±0.37
A_{felt}	→	$\mathbf{M}_{A_{\text{felt}}}$ ±0.39
A_{VI}	→	$\mathbf{M}_{A_{\text{VI}}}$ ±0.42
A_{VII}	→	$\mathbf{M}_{A_{\text{VII}}}$ ±0.43
$N_{20}/N_{20\text{mx}}$	→	$\mathbf{M}_{N_{20}}$ ±0.43
A_{V}	→	$\mathbf{M}_{A_{\text{V}}}$ ±0.47
$N_{\text{st}}/N_{\text{mx}}$	→	$\mathbf{M}_{N_{\text{st}}}$ ±0.48
$I_{\max}$	→	$\mathbf{M}_{I_{\max}}$ ±0.52

(24)

If M_0 is preferred, the same hierarchy applies, with a $\log(M_0)$ uncertainty 1.5 times the eq. (24) levels.

Predicted **M** from the low and high extremes of the indepen-

Table 4. Application of hierarchy for determining **M**.

	Variable	Value	—Ceres, South Africa (CSA) 1969— Predicted **M**	Uncertainty (±1 s.d.)	——English Channel (EC), 1580—— Predicted **M**	Uncertainty (±1 s.d.)
[I.]	$^{\dagger}M_o$	4.5×10^{25} dyne cm (Somerville 1986)	6.40 (preferred)	±0.15		
	(from Part I)	2.0×10^{25} dyne cm (Maasha & Molnar 1972)	6.17	±0.25		
		1.7×10^{26} dyne cm (Shudofsky 1985)	6.78 (not used)			
	$\Delta\sigma$	67 bars (Somerville 1986)				
[II.]	$^{\dagger}M_s$	6.3 (NEIC)	6.27	±0.18		
	$^{\dagger}m_b$	5.9 (NEIC); 5.6 (ISC)	5.94 (NEIC); 5.63 (ISC)	±0.27		
	$^{\dagger}M_L$	6.0 (station BUL)	5.57	±0.35		
	N_{st}	226 (N_{mx} = 451)	6.01	± 0.48		
	N_{20}	216 (N_{20mx} = 388)	6.39	± 0.42		
[III.]	A_{felt} (MMI II)	2,000,000 km^2	6.05	±0.39		
	A_{III}	760,000 km^2	5.83	±0.27		
	A_{IV}	407,000 km^2	5.82	±0.36		
	A_{V}	110,000 km^2 (CSA); 452,000 km^2 (EC)	5.74	±0.47	6.66	± 0.47
	A_{VI}	20,000 km^2 (CSA); 214,000 km^2 (EC)	5.91	±0.42	7.00	± 0.42
	A_{VII}	2,300 km^2 (CSA); 45,000 km^2 (EC)	6.14	±0.43	6.98	± 0.44
	A_{VIII}	955 km^2 (CSA); 11,000 km^2 (EC)	6.33	±0.33	6.93	± 0.35
	$I_{\max}$	IX (CSA); offshore (EC)	6.41	± 0.53		
[I.]	weighted average, from M_o		6.3	±0.13		
[II.]	weighted average, instrumental data: [M_s, m_b, M_L, N_{20}]		6.1	±0.13		
[III.]	weighted average, A_i data (eq. 18)		6.0	±0.20	6.9	± 0.30

$^{\dagger}M_o$, predicted **M**, and uncertainties from Part I data and regressions

dent variable will have larger uncertainties than given in eq. (24) (see Table A1). It is no surprise that **M** based on direct M_0 has the least uncertainty, nor that **M** from I_{max}/I_0 has the greatest. It is perhaps surprising just how well **M** determinations from individual isoseismal areas rank relative to instrumental magnitudes. Also, at $\mathbf{M} \pm \sim \frac{1}{2}\mathbf{M}$ units, the normalized number of recording stations and I_{max} provide useful size constraints in the absence of other data of higher rank in eq. (24).

For an individual earthquake, the regression results of Part I and eqs (23)–(24) may be applied using weighted averaging to yield a final predicted moment magnitude and uncertainty (eqs 15–18): $\mathbf{M}_{final} \pm \sigma_{\mathbf{M}_{final}}$. This can result in a substantial reduction of uncertainty, even with the allowance for systematic error in eq. (18). An example application for two earthquakes will illustrate this: these are the 1969 Ceres, South Africa earthquake, selected from Table A3 (AF-69-0929) for its complete suite of isoseismal data and well-determined M_0, and the English Channel earthquake of 1580, selected to illustrate the usual case for historical events where only incomplete isoseismal data are available. Fig. 16 shows the isoseismal maps of the two events at the same scale. The Ceres map rated fair because only about one-third of the outer isoseismals are on land. The English Channel A_i rated good, but the outer A_{felt}–A_{IV} were missing.

Table 4 summarizes the Ceres and English Channel regression results for all available data. For the Ceres event the weighted average $\mathbf{M}_{M_0} = 6.3 \pm 0.13$ is the standard of comparison for the A_i regressions, a luxury not available for the English Channel event. Part I regressions on the Ceres instrumental data yield a weighted average of **M** 6.1 ± 0.13. However, when teleseismic M_s is available, it is good practice to use only it for $\mathbf{M} \gtrsim 5.5$ and this yields $\mathbf{M}_{M_s} = 6.3 \pm 0.18$. The N_{20} regression does a very good job with this event; it substantially increases the N_{st} estimate because only 10 reporting stations were within $\Delta = 20°$, while N_{20mx} had 63 fewer stations than N_{mx}.

The Ceres A_i results were fairly stable, the low being **M** 5.74 from A_V and the high, **M** 6.33 from A_{VIII}. The weighted average of the seven A_i is $\mathbf{M} = 6.0 \pm 0.20$, moderately low with respect to $\mathbf{M}_{M_0}$. The uncertainty is smaller than usually obtained with isoseismal data because it is unusual to have a full suite of A_{felt} to A_{VIII} data. Ceres was a moderately low-stress-drop earthquake ($\Delta\sigma = 67$ bar; Somerville 1986) and South African attenuation is high for both body waves and L_g relative to the rest of SCR Africa and average stable continental crust (Frankel

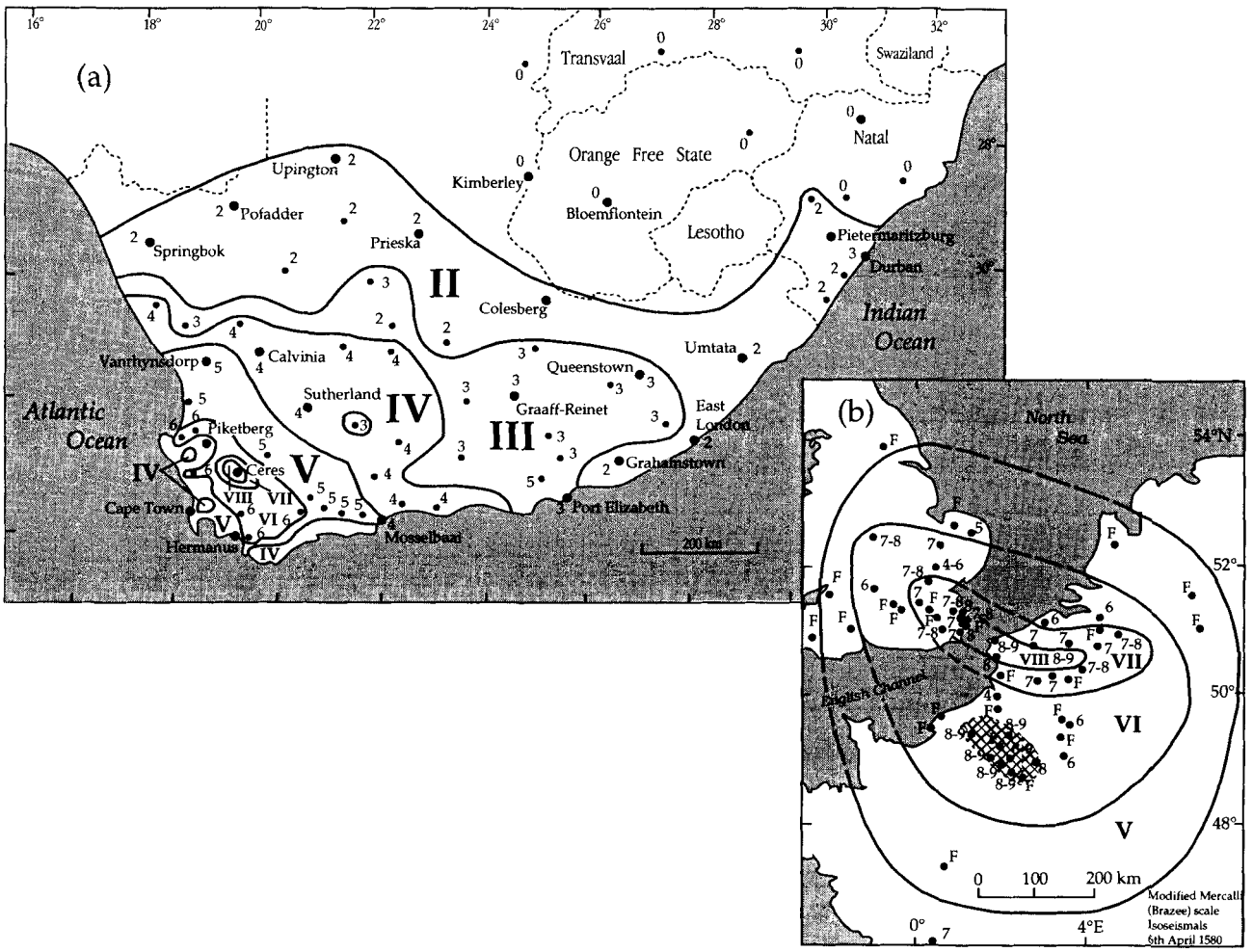

Figure 16. Two same-scale SCR isoseismal maps used to illustrate the application of the hierarchy of methods for determining **M** (see Table 4). (a) The 1969 **M** 6.4 Ceres, South Africa earthquake, for which both instrumental and intensity data (G16, appendix) are abundant. (b) The English Channel earthquake of 1580 for which four isoseismal areas and I_{max} (not I_0) are the only available data (Neilson, Musson & Burton 1984).

et al. 1990; Mitchell 1995). Despite these factors, the one standard deviations of $\mathbf{M}_{A_i}$ and $\mathbf{M}_{M_0}$ overlap for the Ceres earthquake.

Based on a comparison of the A_V–A_{VIII} contours in Fig. 16, we would expect the English Channel earthquake to be substantially larger than that of Ceres. The $\mathbf{M}_{A_i}$ estimates are stable ranging from $\mathbf{M}_{A_V} = 6.66$ to $\mathbf{M}_{A_{VI}} = 7.00$ and yielding $\mathbf{M}_{final} = 6.9 \pm 0.30$. Therefore, at $6.6 \leq \mathbf{M} \leq 7.2$ (68 per cent confidence), the English Channel event of 1580 was a very large (possibly the largest) SCR European earthquake. Accounts (Neilson, Musson & Burton 1984) of either a local tsunami or large seiches along the shores of the English Channel lend qualitative support to this assessment.

These two examples serve both to summarize the main products of this study—regressions on intensity data and number of recording stations to recover **M**—and to illustrate their versatility in terms of the wide range of data to which they may be applied. The regressions are limited mainly by the sparse M_0–A_i data of stable continental regions. A much larger database would be possible for regions of active tectonics, leading to reduced uncertainties on estimates of **M** and M_0.

ACKNOWLEDGMENTS

For a long time I, like many (most?) seismologists, did not appreciate the value of intensity data. The careful and creative work of Otto Nuttli, Gil Bollinger, Nicholas Ambraseys and Tom Hanks was the most influential in convincing me otherwise. Substantive reviews by Dave Boore, Joan Gomberg, Gail Atkinson and Gil Bollinger and the constructive criticism of associate editor Steve Ward resulted in a markedly improved manuscript. Finally those acknowledged in Part I contributed even more to this Part II study. I am grateful for the initial support of the Electric Power Research Institute and for the continuing foresight of the Tennessee Centers of Excellence program for its nurturing of basic research. This is contribution number 267 of the Center for Earthquake Research and Information (CERI), The University of Memphis.

REFERENCES

Ambraseys, N.N., 1985. Intensity–attenuation and magnitude–intensity relationships for northwest European earthquakes, *Earthq. Eng. struct. Dyn.*, **13,** 733–778.

Ambraseys, N.N. & Melville, C.P., 1982. *A History of Persian Earthquakes,* Cambridge University Press, Cambridge.

Atkinson, G.M. & Hanks, T.C., 1994. A high-frequency magnitude scale, *Bull. seism. Soc. Am.*, **85,** 825–833.

Bevington, R.R. & Robinson, D.K., 1992. *Data Reduction and Error Analysis for the Physical Sciences,* 2nd edn, McGraw-Hill, Inc., New York.

Blake, A., 1941. On the estimation of focal depth from macroseismic data, *Bull. seism. Soc. Am.*, **31,** 225–231.

Bollinger, G.A., Chapman, M.C. & Sibol, M.S., 1993. A comparison of earthquake damage areas as a function of magnitude across the United States, *Bull. seism. Soc. Am.*, **83,** 1064–1080.

Bonilla, M.G., Mark, R.K. & Lienkaemper, J.J., 1984. Statistical relations among earthquake magnitude, surface rupture length, and surface fault displacement, *Bull. seism. Soc. Am.*, **74,** 2379–2411.

Brazee, R.J., 1978. Reevaluation of modified Mercalli intensity scale for earthquakes using distance as determinant, *NOAA Tech. Mem. EDS NGSDC-4,* Nat. Oceanic Atmos. Admin., Boulder, CO.

Brune, J.N., 1970. Tectonic stress and the spectra of seismic shear waves from earthquakes, *J. geophys. Res.*, **75,** 4997–5009.

Chung, W.-Y. & Gao, H., 1995. Source mechanism of the Anjar, India, earthquake of July 21, 1956 and its seismotectonic implications for the Kutch rift basin, *Tectonophysics,* **242,** 281–292.

Frankel, A., 1994. Implications of felt area–magnitude relations for earthquake scaling and the average frequency of perceptible ground motion, *Bull. seism. Soc. Am.*, **84,** 462–465.

Frankel, A., McGarr, A., Bicknell, J., Mori, J. Seeber, L. & Cranswick, E., 1990. Attenuation of high-frequency shear waves in the crust: Measurements from New York State, South Africa and Southern California, *J. geophys. Res.*, **95,** 17 441–17 458.

Gu, G. (ed.), 1983. *Catalog of Chinese Earthquakes 1831 BC–1969 AD,* Science Press, Beijing.

Gupta, H., 1993. The deadly Latur earthquake, *Science,* **262,** 1666–1667.

Gutenberg, B. & Richter, C.F., 1954. *Seismicity of the Earth and Associated Phenomena,* 2nd edn, Princeton University Press, Princeton, NJ.

Hanks, T.C. & Johnston, A.C., 1992. Common features of the excitation and propagation of strong ground motion for North American earthquakes, *Bull. seism. Soc. Am.*, **82,** 1–23.

Hanks, T.C. & Kanamori, H., 1979. A moment magnitude scale, *J. geophys. Res.*, **84,** 2348–2350.

Hanks, T.C., Hileman, J.A. & Thatcher, W., 1975. Seismic moments of the larger earthquakes of the Southern California region, *Geol. Soc. Am. Bull.*, **86,** 1131–1139.

Herrmann, R.B. & Kijko, A., 1983. Modeling some empirical vertical component L_g relations, *Bull. seism. Soc. Am.*, **73,** 157–171.

Herrmann, R.B., Cheng, S.-H. & Nuttli, O.W., 1978. Archeoseismology applied to the New Madrid Earthquakes of 1811–1812, *Bull. seism. Soc. Am.*, **68,** 1751–1759.

International Seismological Centre (ISC), 1964–1993. *Bulletin of the International Seismological Centre,* Monthly publ. ISC, Newbury, UK.

International Seismological Summary (ISS), 1913–1963. *Publ. British Assoc. Seism. Comm.,* Kew Obs., Richmond, Surrey, UK.

Jin, A. & Aki, K., 1988. Spatial and temporal correlation between coda Q and seismicity in China, *Bull. seism. Soc. Am.*, **78,** 741–769.

Johnston, A.C., 1989. Moment magnitude estimation for stable continental earthquakes, *Seism. Res. Lett.*, **60,** 13, (abstract).

Johnston, A.C., 1994a. The stable continental region earthquake database, in *The Earthquakes of Stable Continental Regions: Assessment of Large Earthquake Potential,* pp. 3-1–3-80, ed. Schneider, J.F., *EPRI Rpt. TR-102261,* Electric Power Res. Inst., Palo Alto, CA.

Johnston, A.C., 1994b. Seismotectonic interpretations and conclusions from the stable continental region seismicity database, in *The Earthquakes of Stable Continental Regions: Assessment of Large Earthquake Potential,* pp. 4-1–4-103, ed. Schneider, J.F., *EPRI Rpt. TR-102261,* Electric Power Res. Inst., Palo Alto, CA.

Johnston, A.C., 1996. Seismic moment assessment of earthquakes in stable continental regions—I. Instrumental seismicity, *Geophys. J. Int.*, **124,** 381–414.

Kanter, L.R., 1994. Tectonic interpretation of stable continental crust, in *The Earthquakes of Stable Continental Regions: Assessment of Large Earthquake Potential,* pp. 2-1–2-98, ed. Schneider, J.F., *EPRI Rpt. TR-102261,* Electric Power Res. Inst., Palo Alto, CA.

Kárník, V., 1969. *Seismicity of the European Area, Part 1,* D. Reidel Publ. Co., Dordrecht, Holland.

Kárník, V., 1971. *Seismicity of the European Area, Part 2,* D. Reidel Publ. Co., Dordrecht, Holland.

Maasha, N. & Molnar, P., 1972. Earthquake fault parameters and tectonics in Africa, *J. geophys. Res.*, **77,** 5731–5743.

Mitchell, B.J., 1995. Anelastic structure and evolution of the continental crust and upper mantle from seismic surface wave attenuation, *Rev. Geophys.*, **33,** 441–462.

Mitchell, B.J., Pan, Y., Chen, D. & Xie, J.-K., 1993. Q and crustal evolution in stable continental regions, *Seism. Res. Lett.*, **64,** 262, (abstract).

National Earthquake Information Center (NEIC), 1963–1994. *Preliminary Determination of Epicenters,* USGS monthly publ., Golden, CO.

Neilson, G., Musson, R.M.W. & Burton, P.W., 1984. The 'London' earthquake of 1580, April 6, *Eng. Geol.,* **20,** 113–141.

Nuttli, O.W. & Herrmann, R.B., 1984. Ground motion of Mississippi Valley earthquakes, *J. tech. Topics civ. Eng.,* **110,** 54–69.

Richter, C.F., 1958. *Elementary Seismology,* W.H. Freeman & Co., San Francisco, CA.

Rothé, J.P., 1969. *The Seismicity of the Earth, 1953–1965,* UNESCO, Paris.

Shudofsky, G.N., 1985. Source mechanisms and focal depths of East African earthquakes using Rayleigh-wave inversion and body-wave modelling, *Geophys. J. R. astr. Soc.,* **83,** 563–614.

Sibol, M.S., Bollinger, G.A. & Birch, J.B., 1987. Estimation of magnitudes in central and eastern North America using intensity and felt area, *Bull. seism. Soc. Am.,* **77,** 1635–1654.

Singh, S.K. & Herrmann, R.B., 1983. Regionalization of crustal coda Q in the continental United States, *J. geophys. Res.,* **88,** 527–538.

Singh, S.K., Bazan, E. & Esteva, L., 1980. Expected earthquake magnitude from a fault, *Bull. seism. Soc. Am.,* **70,** 903–914.

Somerville, P., 1986. Source-scaling relations of eastern North American earthquakes, *EPRI NP-4790 Final Report,* Electric Power Res. Inst., Palo Alto, CA.

Wells, D.L. & Coppersmith, K.J., 1994. Updated empirical relationships among magnitude, rupture length, rupture area, and surface displacement, *Bull. seism. Soc. Am.,* **84,** 974–1002.

Wesnousky, S., Scholz, C. & Shimazaki, K., 1982. Deformation of an island arc; rates of moment release and crustal shortening in intraplate Japan determined from seismicity and Quaternary fault data, *J. geophys. Res.,* **87,** 6929–6852.

Wesnousky, S., Jones, L., Scholz, C. & Deng, Q., 1984. Historical seismicity and rates of crustal deformation along the margins of the Ordos block, North China, *Bull. seism. Soc. Am.,* **74,** 1767–1783.

Wood, H.O. & Neumann, F., 1931. Modified Mercalli intensity scale of 1931, *Bull. seism. Soc. Am.,* **21,** 277–283.

APPENDIX A

Table A1. Regression results and prediction uncertainties. Explanation for use.

Isoseismal area A_i is in km^2; seismic moment M_0 is in dyne-cm.
Superscripts R and P denote regression and prediction uncertainty, respectively.
Subscripts log M_0 and **M** denote standard deviation σ in log(M_0) units and **M** units, respectively.
Numbers in bold type denote the range of the data on which the regression is based; non-bold listings are an extrapolation of the regression results beyond the data range. No values are listed for log(A_i) that are judged unrealistic extrapolations for the given intensity level.
To use with an isoseismal map, select the proper MMI regression and enter the table under the proper log(A_i) value. The predicted seismic moment and moment magnitude are given by log(M_0) and **M**, respectively, for that row. The 1σ (68 per cent) uncertainties for these values are given by $\sigma^P_{\log M_0}$ and σ^P_M, respectively.
If several isoseismal areas of different intensity levels are available for an earthquake, a predicted log(M_0) or **M** value should be obtained separately for each one. The weighted average using the prediction uncertainties as weights then yields the final predicted value and its associated uncertainty via eqs (15)–(18).

	A_{felt} regression						A_{III} regression					
log(A_i)	log(M_0)	$\sigma^R_{\log M_0}$	$\sigma^P_{\log M_0}$	**M**	σ^R_M	σ^P_M	log(M_0)	$\sigma^R_{\log M_0}$	$\sigma^P_{\log M_0}$	**M**	σ^R_M	σ^P_M
1.0												
1.1												
1.2												
1.3												
1.4												
1.5												
1.6												
1.7												
1.8												
1.9												
2.0	19.24	0.659	0.881	2.13	0.439	0.587	19.64	1.052	1.123	2.40	0.702	0.749
2.1	19.34	0.638	0.865	2.19	0.425	0.576	19.75	1.018	1.091	2.47	0.679	0.728
2.2	19.44	0.616	0.849	2.26	0.411	0.566	19.85	0.984	1.060	2.53	0.656	0.706
2.3	19.53	0.595	0.834	2.32	0.397	0.556	19.96	0.950	1.028	2.60	0.633	0.685
2.4	19.63	0.574	0.819	2.39	0.383	0.546	20.06	0.916	0.997	2.67	0.611	0.664
2.5	19.73	0.553	0.804	2.45	0.369	0.536	20.16	0.882	0.966	2.74	0.588	0.644
2.6	19.83	0.532	0.790	2.52	0.354	0.527	20.27	0.848	0.935	2.81	0.565	0.623
2.7	19.93	0.511	0.776	2.59	0.340	0.517	20.38	0.814	0.904	2.88	0.543	0.603
2.8	20.03	0.490	0.762	2.65	0.326	0.508	20.48	0.781	0.874	2.95	0.521	0.583
2.9	20.13	0.469	0.749	2.72	0.313	0.499	20.59	0.748	0.845	3.02	0.498	0.563
3.0	20.23	0.448	0.736	2.78	0.299	0.491	20.69	0.714	0.815	3.10	0.476	0.543
3.1	20.33	0.427	0.724	2.85	0.285	0.482	20.80	0.681	0.786	3.17	0.454	0.524
3.2	20.43	0.407	0.712	2.92	0.271	0.475	20.91	0.648	0.758	3.24	0.432	0.505
3.3	20.53	0.387	0.700	2.99	0.258	0.467	21.02	0.616	0.730	3.31	0.410	0.487
3.4	20.63	0.366	0.689	3.06	0.244	0.460	21.13	0.583	0.703	3.39	0.389	0.469
3.5	20.74	0.346	0.679	3.12	0.231	0.453	21.24	0.551	0.677	3.46	0.367	0.451
3.6	20.84	0.326	0.669	3.19	0.218	0.446	21.35	0.519	0.651	3.53	0.346	0.434
3.7	20.95	0.307	0.660	3.27	0.205	0.440	21.46	0.488	0.626	3.61	0.325	0.418
3.8	**21.05**	**0.287**	**0.651**	**3.34**	**0.192**	**0.434**	21.58	0.457	0.603	3.68	0.305	0.402
3.9	**21.16**	**0.268**	**0.643**	**3.41**	**0.179**	**0.428**	21.69	0.426	0.580	3.76	0.284	0.387
4.0	**21.27**	**0.250**	**0.635**	**3.48**	**0.166**	**0.423**	**21.81**	**0.396**	**0.558**	**3.84**	**0.264**	**0.372**
4.1	**21.38**	**0.231**	**0.628**	**3.56**	**0.154**	**0.419**	**21.93**	**0.367**	**0.538**	**3.92**	**0.245**	**0.358**
4.2	**21.50**	**0.213**	**0.622**	**3.63**	**0.142**	**0.415**	**22.05**	**0.338**	**0.518**	**4.00**	**0.225**	**0.346**
4.3	**21.61**	**0.196**	**0.616**	**3.71**	**0.131**	**0.411**	**22.17**	**0.310**	**0.501**	**4.08**	**0.207**	**0.334**
4.4	**21.73**	**0.179**	**0.611**	**3.79**	**0.119**	**0.407**	**22.30**	**0.283**	**0.484**	**4.17**	**0.189**	**0.323**
4.5	**21.85**	**0.163**	**0.606**	**3.87**	**0.109**	**0.404**	**22.43**	**0.257**	**0.470**	**4.25**	**0.172**	**0.313**
4.6	**21.97**	**0.148**	**0.602**	**3.95**	**0.099**	**0.402**	**22.56**	**0.233**	**0.457**	**4.34**	**0.155**	**0.304**
4.7	**22.10**	**0.134**	**0.599**	**4.03**	**0.089**	**0.399**	**22.70**	**0.210**	**0.445**	**4.43**	**0.140**	**0.297**
4.8	**22.23**	**0.121**	**0.596**	**4.12**	**0.080**	**0.398**	**22.84**	**0.188**	**0.436**	**4.52**	**0.125**	**0.290**
4.9	**22.36**	**0.109**	**0.594**	**4.21**	**0.073**	**0.396**	**22.98**	**0.169**	**0.428**	**4.62**	**0.113**	**0.285**
5.0	**22.50**	**0.099**	**0.592**	**4.30**	**0.066**	**0.395**	**23.13**	**0.152**	**0.421**	**4.72**	**0.101**	**0.281**
5.1	**22.65**	**0.091**	**0.591**	**4.40**	**0.060**	**0.394**	**23.29**	**0.138**	**0.417**	**4.82**	**0.092**	**0.278**
5.2	**22.80**	**0.084**	**0.590**	**4.50**	**0.056**	**0.393**	**23.45**	**0.127**	**0.413**	**4.93**	**0.085**	**0.275**
5.3	**22.96**	**0.080**	**0.590**	**4.60**	**0.054**	**0.393**	**23.62**	**0.119**	**0.411**	**5.04**	**0.080**	**0.274**
5.4	**23.12**	**0.079**	**0.589**	**4.71**	**0.052**	**0.393**	**23.79**	**0.115**	**0.409**	**5.16**	**0.077**	**0.273**
5.5	**23.29**	**0.078**	**0.589**	**4.83**	**0.052**	**0.393**	**23.98**	**0.113**	**0.409**	**5.29**	**0.075**	**0.273**
5.6	**23.48**	**0.079**	**0.589**	**4.95**	**0.053**	**0.393**	**24.18**	**0.113**	**0.409**	**5.42**	**0.075**	**0.273**
5.7	**23.67**	**0.081**	**0.590**	**5.08**	**0.054**	**0.393**	**24.39**	**0.114**	**0.409**	**5.56**	**0.076**	**0.273**
5.8	**23.87**	**0.083**	**0.590**	**5.22**	**0.056**	**0.393**	**24.61**	**0.115**	**0.410**	**5.71**	**0.077**	**0.273**
5.9	**24.09**	**0.085**	**0.590**	**5.36**	**0.057**	**0.393**	**24.85**	**0.117**	**0.410**	**5.86**	**0.078**	**0.273**
6.0	**24.32**	**0.087**	**0.590**	**5.52**	**0.058**	**0.394**	**25.10**	**0.117**	**0.410**	**6.03**	**0.078**	**0.273**
6.1	**24.57**	**0.089**	**0.591**	**5.68**	**0.059**	**0.394**	**25.37**	**0.117**	**0.410**	**6.21**	**0.078**	**0.273**
6.2	**24.84**	**0.090**	**0.591**	**5.86**	**0.060**	**0.394**	**25.66**	**0.116**	**0.410**	**6.41**	**0.077**	**0.273**
6.3	**25.13**	**0.091**	**0.591**	**6.05**	**0.060**	**0.394**	**25.98**	**0.116**	**0.410**	**6.62**	**0.077**	**0.273**
6.4	**25.44**	**0.093**	**0.591**	**6.26**	**0.062**	**0.394**	**26.32**	**0.119**	**0.411**	**6.85**	**0.079**	**0.274**
6.5	**25.78**	**0.097**	**0.592**	**6.49**	**0.065**	**0.395**	**26.69**	**0.128**	**0.413**	**7.09**	**0.085**	**0.275**
6.6	**26.15**	**0.105**	**0.593**	**6.74**	**0.070**	**0.396**	**27.10**	**0.145**	**0.419**	**7.36**	**0.097**	**0.279**
6.7	**26.56**	**0.118**	**0.596**	**7.00**	**0.079**	**0.397**	**27.54**	**0.174**	**0.430**	**7.66**	**0.116**	**0.287**
6.8	**27.00**	**0.139**	**0.600**	**7.30**	**0.093**	**0.400**	**28.02**	**0.215**	**0.448**	**7.98**	**0.143**	**0.299**
6.9	**27.48**	**0.167**	**0.607**	**7.62**	**0.111**	**0.405**	**28.55**	**0.270**	**0.477**	**8.33**	**0.180**	**0.318**
7.0	**28.01**	**0.204**	**0.619**	**7.97**	**0.136**	**0.412**	29.13	0.338	0.518	8.72	0.225	0.345
7.1	**28.59**	**0.250**	**0.635**	**8.36**	**0.167**	**0.424**	29.76	0.421	0.576	9.14	0.280	0.384
7.2	29.23	0.306	0.659	8.79	0.204	0.440	30.47	0.519	0.651	9.61	0.346	0.434
7.3	29.94	0.372	0.693	9.26	0.248	0.462						

Table A1. (*Continued.*)

	A_{IV} regression						A_V regression					
log(A_i)	log(M_0)	$\sigma^R_{\log M_0}$	$\sigma^P_{\log M_0}$	M	σ^R_M	σ^P_M	log(M_0)	$\sigma^R_{\log M_0}$	$\sigma^P_{\log M_0}$	M	σ^R_M	σ^P_M
1.0							20.63	0.717	0.992	3.05	0.478	0.661
1.1							20.71	0.693	0.975	3.10	0.462	0.650
1.2							20.79	0.670	0.959	3.16	0.447	0.639
1.3							20.87	0.647	0.943	3.21	0.431	0.629
1.4							20.95	0.624	0.927	3.26	0.416	0.618
1.5							21.03	0.601	0.912	3.32	0.401	0.608
1.6							21.11	0.578	0.897	3.37	0.385	0.598
1.7							21.19	0.555	0.882	3.43	0.370	0.588
1.8							21.27	0.532	0.868	3.48	0.355	0.579
1.9							21.35	0.510	0.855	3.53	0.340	0.570
2.0	20.06	0.571	0.786	2.67	0.381	0.524	21.43	0.487	0.841	3.59	0.325	0.561
2.1	20.16	0.551	0.771	2.74	0.367	0.514	21.51	0.465	0.829	3.64	0.310	0.552
2.2	20.26	0.530	0.757	2.81	0.354	0.505	21.60	0.443	0.816	3.70	0.295	0.544
2.3	20.36	0.510	0.743	2.87	0.340	0.495	21.68	0.421	0.805	3.75	0.280	0.536
2.4	20.46	0.490	0.729	2.94	0.327	0.486	21.76	0.399	0.794	3.81	0.266	0.529
2.5	20.56	0.470	0.716	3.01	0.313	0.477	21.85	0.377	0.783	3.86	0.252	0.522
2.6	20.66	0.449	0.703	3.08	0.300	0.468	21.93	0.356	0.773	3.92	0.237	0.515
2.7	20.77	0.429	0.690	3.14	0.286	0.460	**22.02**	**0.335**	**0.764**	**3.98**	**0.223**	**0.509**
2.8	20.87	0.410	0.678	3.21	0.273	0.452	**22.10**	**0.315**	**0.755**	**4.03**	**0.210**	**0.503**
2.9	20.97	0.390	0.666	3.28	0.260	0.444	**22.19**	**0.294**	**0.747**	**4.09**	**0.196**	**0.498**
3.0	21.07	0.370	0.655	3.35	0.247	0.436	**22.28**	**0.275**	**0.739**	**4.15**	**0.183**	**0.493**
3.1	21.18	0.351	0.644	3.42	0.234	0.429	**22.37**	**0.256**	**0.732**	**4.21**	**0.170**	**0.488**
3.2	21.28	0.332	0.634	3.49	0.221	0.422	**22.46**	**0.237**	**0.726**	**4.27**	**0.158**	**0.484**
3.3	21.39	0.313	0.624	3.56	0.208	0.416	**22.55**	**0.219**	**0.720**	**4.33**	**0.146**	**0.480**
3.4	21.50	0.294	0.615	3.63	0.196	0.410	**22.64**	**0.202**	**0.715**	**4.39**	**0.135**	**0.477**
3.5	**21.61**	**0.275**	**0.606**	**3.71**	**0.184**	**0.404**	**22.73**	**0.186**	**0.711**	**4.46**	**0.124**	**0.474**
3.6	**21.72**	**0.257**	**0.598**	**3.78**	**0.171**	**0.399**	**22.83**	**0.171**	**0.707**	**4.52**	**0.114**	**0.471**
3.7	**21.83**	**0.239**	**0.591**	**3.85**	**0.159**	**0.394**	**22.93**	**0.157**	**0.704**	**4.59**	**0.105**	**0.469**
3.8	**21.94**	**0.222**	**0.584**	**3.93**	**0.148**	**0.389**	**23.03**	**0.145**	**0.701**	**4.65**	**0.097**	**0.467**
3.9	**22.06**	**0.205**	**0.578**	**4.01**	**0.137**	**0.385**	**23.13**	**0.134**	**0.699**	**4.72**	**0.089**	**0.466**
4.0	**22.18**	**0.188**	**0.572**	**4.09**	**0.126**	**0.381**	**23.24**	**0.125**	**0.697**	**4.79**	**0.084**	**0.465**
4.1	**22.30**	**0.172**	**0.567**	**4.17**	**0.115**	**0.378**	**23.35**	**0.118**	**0.696**	**4.87**	**0.079**	**0.464**
4.2	**22.42**	**0.157**	**0.562**	**4.25**	**0.105**	**0.375**	**23.47**	**0.114**	**0.695**	**4.94**	**0.076**	**0.464**
4.3	**22.55**	**0.143**	**0.559**	**4.33**	**0.095**	**0.372**	**23.59**	**0.110**	**0.695**	**5.02**	**0.074**	**0.463**
4.4	**22.68**	**0.130**	**0.555**	**4.42**	**0.086**	**0.370**	**23.71**	**0.109**	**0.695**	**5.11**	**0.073**	**0.463**
4.5	**22.81**	**0.117**	**0.553**	**4.51**	**0.078**	**0.368**	**23.84**	**0.109**	**0.695**	**5.19**	**0.073**	**0.463**
4.6	**22.95**	**0.106**	**0.550**	**4.60**	**0.071**	**0.367**	**23.97**	**0.110**	**0.695**	**5.28**	**0.073**	**0.463**
4.7	**23.10**	**0.097**	**0.549**	**4.70**	**0.065**	**0.366**	**24.12**	**0.111**	**0.695**	**5.38**	**0.074**	**0.463**
4.8	**23.25**	**0.089**	**0.547**	**4.80**	**0.059**	**0.365**	**24.27**	**0.112**	**0.695**	**5.48**	**0.075**	**0.463**
4.9	**23.40**	**0.083**	**0.546**	**4.90**	**0.055**	**0.364**	**24.42**	**0.113**	**0.695**	**5.58**	**0.075**	**0.464**
5.0	**23.57**	**0.078**	**0.546**	**5.01**	**0.052**	**0.364**	**24.59**	**0.114**	**0.695**	**5.69**	**0.076**	**0.464**
5.1	**23.74**	**0.076**	**0.545**	**5.13**	**0.050**	**0.364**	**24.77**	**0.115**	**0.696**	**5.81**	**0.076**	**0.464**
5.2	**23.92**	**0.074**	**0.545**	**5.25**	**0.049**	**0.363**	**24.96**	**0.115**	**0.696**	**5.94**	**0.077**	**0.464**
5.3	**24.11**	**0.074**	**0.545**	**5.38**	**0.049**	**0.363**	**25.17**	**0.116**	**0.696**	**6.08**	**0.077**	**0.464**
5.4	**24.32**	**0.074**	**0.545**	**5.51**	**0.049**	**0.363**	**25.39**	**0.119**	**0.696**	**6.23**	**0.079**	**0.464**
5.5	**24.53**	**0.074**	**0.545**	**5.65**	**0.049**	**0.363**	**25.63**	**0.124**	**0.697**	**6.38**	**0.083**	**0.465**
5.6	**24.76**	**0.075**	**0.545**	**5.81**	**0.050**	**0.363**	**25.88**	**0.135**	**0.699**	**6.56**	**0.090**	**0.466**
5.7	**25.01**	**0.075**	**0.545**	**5.97**	**0.050**	**0.363**	**26.16**	**0.152**	**0.703**	**6.74**	**0.101**	**0.468**
5.8	**25.27**	**0.075**	**0.545**	**6.15**	**0.050**	**0.363**	**26.47**	**0.178**	**0.709**	**6.94**	**0.118**	**0.472**
5.9	**25.56**	**0.076**	**0.545**	**6.34**	**0.051**	**0.364**	**26.80**	**0.212**	**0.718**	**7.16**	**0.142**	**0.479**
6.0	**25.87**	**0.079**	**0.546**	**6.54**	**0.052**	**0.364**	**27.16**	**0.257**	**0.733**	**7.41**	**0.171**	**0.488**
6.1	**26.20**	**0.084**	**0.546**	**6.77**	**0.056**	**0.364**	**27.55**	**0.312**	**0.754**	**7.67**	**0.208**	**0.503**
6.2	**26.56**	**0.094**	**0.548**	**7.01**	**0.063**	**0.365**	**27.99**	**0.379**	**0.784**	**7.96**	**0.253**	**0.523**
6.3	**26.96**	**0.109**	**0.551**	**7.27**	**0.073**	**0.367**	**28.47**	**0.458**	**0.825**	**8.28**	**0.306**	**0.550**
6.4	**27.39**	**0.132**	**0.556**	**7.56**	**0.088**	**0.371**	**28.99**	**0.551**	**0.880**	**8.63**	**0.367**	**0.587**
6.5	**27.86**	**0.162**	**0.564**	**7.87**	**0.108**	**0.376**	29.58	0.659	0.951	9.02	0.439	0.634
6.6	**28.38**	**0.200**	**0.576**	**8.22**	**0.133**	**0.384**	30.22	0.783	1.041	9.45	0.522	0.694
6.7	**28.95**	**0.246**	**0.593**	**8.60**	**0.164**	**0.396**						
6.8	29.58	0.302	0.619	9.02	0.201	0.412						
6.9	30.27	0.368	0.653	9.48	0.245	0.436						
7.0												
7.1												
7.2												
7.3												

Table A1. (*Continued.*)

	A_{VI} regression						A_{VII} regression					
log(A_i)	log(M_0)	$\sigma^R_{\log M_0}$	$\sigma^P_{\log M_0}$	M	σ^R_M	σ^P_M	log(M_0)	$\sigma^R_{\log M_0}$	$\sigma^P_{\log M_0}$	M	σ^R_M	σ^P_M
0.10	20.34	0.635	0.887	2.86	0.423	0.591	23.28	0.609	0.875	4.82	0.406	0.584
0.2	20.44	0.617	0.874	2.93	0.412	0.583	23.34	0.588	0.861	4.86	0.392	0.574
0.4	20.65	0.582	0.850	3.06	0.388	0.566	23.45	0.545	0.833	4.93	0.364	0.555
0.6	20.85	0.547	0.826	3.20	0.365	0.551	23.56	0.504	0.806	5.01	0.336	0.537
0.8	21.06	0.512	0.803	3.34	0.341	0.535	23.68	0.462	0.780	5.08	0.308	0.520
1.0	21.27	0.477	0.781	3.48	0.318	0.521	23.79	0.421	0.757	5.16	0.281	0.505
1.1	21.37	0.460	0.771	3.55	0.306	0.514	23.85	0.400	0.746	5.20	0.267	0.497
1.2	21.48	0.442	0.761	3.62	0.295	0.507	23.90	0.380	0.735	5.24	0.253	0.490
1.3	21.58	0.425	0.751	3.69	0.283	0.501	23.96	0.360	0.725	5.27	0.240	0.483
1.4	21.68	0.408	0.741	3.76	0.272	0.494	24.02	0.340	0.715	5.31	0.227	0.477
1.5	21.79	0.391	0.732	3.83	0.261	0.488	24.08	0.321	0.706	5.35	0.214	0.471
1.6	21.89	0.374	0.723	3.89	0.250	0.482	24.14	0.301	0.697	5.39	0.201	0.465
1.7	22.00	0.358	0.715	3.96	0.238	0.477	24.19	0.282	0.689	5.43	0.188	0.460
1.8	22.10	0.341	0.707	4.03	0.227	0.471	24.25	0.263	0.682	5.47	0.176	0.455
1.9	22.21	0.325	0.699	4.10	0.216	0.466	24.31	0.245	0.675	5.51	0.163	0.450
2.0	22.31	0.308	0.692	4.17	0.206	0.461	24.37	0.227	0.669	5.55	0.151	0.446
2.1	22.42	0.292	0.685	4.24	0.195	0.456	24.43	0.210	0.663	5.59	0.140	0.442
2.2	22.52	0.277	0.678	4.32	0.184	0.452	24.49	0.193	0.658	5.63	0.129	0.439
2.3	22.63	0.261	0.672	4.39	0.174	0.448	24.55	0.177	0.654	5.67	0.118	0.439
2.4	22.73	0.246	0.666	4.46	0.164	0.444	24.61	0.162	0.650	5.71	0.108	0.433
2.5	22.84	0.231	0.661	4.53	0.154	0.440	24.68	0.149	0.646	5.75	0.099	0.431
2.6	22.95	0.216	0.656	4.60	0.144	0.437	24.74	0.137	0.644	5.79	0.091	0.429
2.7	23.06	0.202	0.651	4.67	0.135	0.434	24.80	0.126	0.642	5.84	0.084	0.428
2.8	23.16	0.189	0.647	4.74	0.126	0.431	24.87	0.118	0.640	5.88	0.079	0.427
2.9	23.27	0.176	0.644	4.81	0.117	0.429	24.93	0.112	0.639	5.92	0.075	0.426
3.0	23.38	0.164	0.640	4.89	0.109	0.427	25.00	0.109	0.638	5.97	0.073	0.426
3.1	23.49	0.152	0.637	4.96	0.102	0.425	25.07	0.108	0.638	6.01	0.072	0.426
3.2	23.60	0.142	0.635	5.03	0.095	0.423	25.14	0.110	0.639	6.06	0.073	0.426
3.3	23.71	0.133	0.633	5.11	0.089	0.422	25.21	0.114	0.639	6.11	0.076	0.426
3.4	23.83	0.125	0.631	5.18	0.083	0.421	25.28	0.119	0.640	6.16	0.079	0.427
3.5	23.94	0.118	0.630	5.26	0.079	0.420	25.36	0.125	0.641	6.21	0.083	0.428
3.6	24.06	0.113	0.629	5.34	0.075	0.419	25.44	0.132	0.643	6.26	0.088	0.428
3.7	24.17	0.109	0.629	5.42	0.073	0.419	25.52	0.139	0.644	6.31	0.093	0.429
3.8	24.29	0.107	0.628	5.49	0.071	0.419	25.60	0.146	0.646	6.37	0.098	0.431
3.9	24.41	0.106	0.628	5.57	0.071	0.419	25.69	0.153	0.647	6.43	0.102	0.432
4.0	24.53	0.106	0.628	5.66	0.071	0.419	25.78	0.159	0.649	6.49	0.106	0.433
4.1	24.66	0.108	0.628	5.74	0.072	0.419	25.88	0.165	0.650	6.55	0.110	0.434
4.2	24.79	0.110	0.629	5.82	0.073	0.419	25.98	0.170	0.652	6.62	0.114	0.434
4.3	24.92	0.112	0.629	5.91	0.075	0.419	26.09	0.175	0.653	6.69	0.117	0.435
4.4	25.05	0.115	0.630	6.00	0.076	0.420	26.20	0.179	0.654	6.77	0.119	0.436
4.5	25.19	0.117	0.630	6.09	0.078	0.420	26.32	0.183	0.655	6.85	0.122	0.437
4.6	25.33	0.120	0.630	6.19	0.080	0.420	26.45	0.187	0.656	6.93	0.125	0.437
4.7	25.47	0.122	0.631	6.28	0.081	0.421	26.58	0.192	0.658	7.02	0.128	0.438
4.8	25.63	0.124	0.631	6.38	0.083	0.421	26.73	0.200	0.660	7.12	0.133	0.440
4.9	25.78	0.126	0.632	6.49	0.084	0.421	26.88	0.211	0.663	7.22	0.141	0.442
5.0	25.95	0.128	0.632	6.60	0.085	0.421	27.05	0.228	0.669	7.33	0.152	0.446
5.1	26.12	0.131	0.633	6.71	0.087	0.422	27.23	0.251	0.677	7.46	0.167	0.452
5.2	26.30	0.135	0.634	6.83	0.090	0.422	27.43	0.283	0.690	7.59	0.189	0.460
5.3	26.49	0.142	0.635	6.96	0.094	0.423	27.65	0.325	0.708	7.73	0.217	0.472
5.4	26.68	0.152	0.637	7.09	0.101	0.425	27.88	0.378	0.734	7.89	0.252	0.489
5.5	26.90	0.168	0.641	7.23	0.112	0.428	28.14	0.443	0.769	8.06	0.295	0.513
5.6	27.12	0.189	0.647	7.38	0.126	0.432	28.42	0.522	0.817	8.25	0.348	0.545
5.7	27.36	0.219	0.656	7.54	0.146	0.438	28.73	0.614	0.879	8.45	0.410	0.586
5.8	27.61	0.256	0.670	7.71	0.171	0.447	29.07	0.723	0.958	8.68	0.482	0.639
5.9	27.89	0.302	0.689	7.89	0.202	0.459	29.44	0.849	1.056	8.93	0.566	0.704
6.0	28.18	0.358	0.715	8.09	0.239	0.477	29.85	0.994	1.176	9.20	0.663	0.784
6.1	28.50	0.425	0.751	8.30	0.283	0.501	30.31	1.160	1.320	9.51	0.774	0.880
6.2	28.84	0.503	0.798	8.53	0.336	0.532						
6.3	29.22	0.594	0.858	8.78	0.396	0.572						
6.4	29.62	0.699	0.934	9.05	0.466	0.623						
6.5	30.07	0.820	1.027	9.35	0.547	0.685						

Table A1. (*Continued.*)

A_{VIII} regression							I_{max} regression						
$\log(A_i)$	$\log(M_0)$	$\sigma^R_{\log M_0}$	$\sigma^P_{\log M_0}$	M	σ^R_M	σ^P_M	I_{max}	$\log(M_0)$	$\sigma^R_{\log M_0}$	$\sigma^P_{\log M_0}$	M	σ^R_M	σ^P_M
0.10	24.10	0.659	0.807	5.37	0.440	0.538	I (*felt*)	19.87	0.639	1.006	2.54	0.426	0.671
0.2	24.15	0.632	0.785	5.40	0.421	0.524	II	20.42	0.422	0.884	2.91	0.281	0.589
0.3	24.19	0.605	0.764	5.43	0.403	0.509	III	**21.02**	**0.254**	**0.818**	**3.32**	**0.169**	**0.545**
0.4	24.24	0.578	0.743	5.46	0.385	0.495	III-IV	**21.34**	**0.191**	**0.800**	**3.53**	**0.127**	**0.533**
0.5	24.28	0.551	0.722	5.49	0.368	0.481	IV	**21.67**	**0.142**	**0.790**	**3.75**	**0.095**	**0.527**
0.6	24.33	0.525	0.702	5.52	0.350	0.468	IV-V	**22.02**	**0.111**	**0.785**	**3.98**	**0.074**	**0.523**
0.7	24.37	0.499	0.683	5.55	0.332	0.455	V	**22.38**	**0.097**	**0.783**	**4.22**	**0.064**	**0.522**
0.8	24.42	0.473	0.664	5.58	0.315	0.442	V-VI	**22.74**	**0.093**	**0.783**	**4.46**	**0.062**	**0.522**
0.9	24.46	0.447	0.646	5.61	0.298	0.430	VI	**23.12**	**0.094**	**0.783**	**4.72**	**0.063**	**0.522**
1.0	24.51	0.421	0.628	5.64	0.281	0.419	VI-VII	**23.52**	**0.095**	**0.783**	**4.98**	**0.064**	**0.522**
1.1	24.55	0.396	0.612	5.67	0.264	0.408	VII	**23.92**	**0.096**	**0.783**	**5.25**	**0.064**	**0.522**
1.2	24.60	0.372	0.596	5.70	0.248	0.397	VII-VIII	**24.34**	**0.100**	**0.783**	**5.53**	**0.067**	**0.522**
1.3	24.65	0.348	0.581	5.73	0.232	0.388	VIII	**24.77**	**0.115**	**0.785**	**5.81**	**0.077**	**0.524**
1.4	**24.70**	**0.324**	**0.568**	**5.76**	**0.216**	**0.379**	VIII-IX	**25.21**	**0.145**	**0.790**	**6.11**	**0.097**	**0.527**
1.5	**24.74**	**0.302**	**0.555**	**5.80**	**0.201**	**0.370**	IX	**25.67**	**0.192**	**0.800**	**6.41**	**0.128**	**0.534**
1.6	**24.79**	**0.280**	**0.544**	**5.83**	**0.187**	**0.362**	IX-X	**26.13**	**0.253**	**0.817**	**6.72**	**0.169**	**0.545**
1.7	**24.84**	**0.259**	**0.533**	**5.86**	**0.173**	**0.355**	X	**26.61**	**0.329**	**0.844**	**7.04**	**0.220**	**0.563**
1.8	**24.89**	**0.239**	**0.524**	**5.89**	**0.160**	**0.349**	X-XI	27.10	0.418	0.882	7.37	0.279	0.588
1.9	**24.94**	**0.221**	**0.516**	**5.93**	**0.148**	**0.344**	XI	27.60	0.520	0.935	7.70	0.347	0.623
2.0	**24.99**	**0.205**	**0.509**	**5.96**	**0.137**	**0.339**	XI-XII	28.12	0.633	1.002	8.05	0.422	0.668
2.1	**25.04**	**0.191**	**0.504**	**5.99**	**0.127**	**0.336**	XII	28.65	0.759	1.086	8.40	0.506	0.724
2.2	**25.09**	**0.179**	**0.499**	**6.03**	**0.120**	**0.333**							
2.3	**25.14**	**0.171**	**0.496**	**6.06**	**0.114**	**0.331**							
2.4	**25.20**	**0.165**	**0.494**	**6.10**	**0.110**	**0.330**							
2.5	**25.25**	**0.162**	**0.493**	**6.14**	**0.108**	**0.329**							
2.6	**25.31**	**0.163**	**0.494**	**6.17**	**0.109**	**0.329**							
2.7	**25.37**	**0.166**	**0.495**	**6.21**	**0.111**	**0.330**							
2.8	**25.43**	**0.172**	**0.497**	**6.25**	**0.114**	**0.331**							
2.9	**25.49**	**0.179**	**0.499**	**6.29**	**0.119**	**0.333**							
3.0	**25.56**	**0.187**	**0.502**	**6.34**	**0.125**	**0.335**							
3.1	**25.62**	**0.196**	**0.506**	**6.38**	**0.131**	**0.337**							
3.2	**25.69**	**0.206**	**0.509**	**6.43**	**0.137**	**0.340**							
3.3	**25.76**	**0.215**	**0.513**	**6.48**	**0.143**	**0.342**							
3.4	**25.84**	**0.224**	**0.517**	**6.53**	**0.149**	**0.345**							
3.5	**25.92**	**0.232**	**0.520**	**6.58**	**0.154**	**0.347**							
3.6	**26.00**	**0.239**	**0.524**	**6.64**	**0.159**	**0.349**							
3.7	**26.09**	**0.245**	**0.526**	**6.70**	**0.163**	**0.351**							
3.8	**26.19**	**0.249**	**0.528**	**6.76**	**0.166**	**0.352**							
3.9	**26.29**	**0.252**	**0.530**	**6.83**	**0.168**	**0.353**							
4.0	**26.40**	**0.254**	**0.531**	**6.90**	**0.170**	**0.354**							
4.1	**26.51**	**0.256**	**0.531**	**6.97**	**0.170**	**0.354**							
4.2	**26.64**	**0.257**	**0.532**	**7.06**	**0.171**	**0.355**							
4.3	**26.77**	**0.258**	**0.533**	**7.15**	**0.172**	**0.355**							
4.4	**26.91**	**0.262**	**0.535**	**7.24**	**0.175**	**0.356**							
4.5	**27.07**	**0.270**	**0.539**	**7.35**	**0.180**	**0.359**							
4.6	**27.24**	**0.285**	**0.546**	**7.46**	**0.190**	**0.364**							
4.7	**27.43**	**0.310**	**0.560**	**7.59**	**0.207**	**0.373**							
4.8	**27.63**	**0.348**	**0.581**	**7.72**	**0.232**	**0.388**							
4.9	**27.86**	**0.399**	**0.614**	**7.87**	**0.266**	**0.409**							
5.0	**28.10**	**0.467**	**0.660**	**8.04**	**0.311**	**0.440**							
5.1	28.37	0.552	0.723	8.22	0.368	0.482							
5.2	28.67	0.656	0.804	8.41	0.437	0.536							
5.3	29.00	0.779	0.908	8.63	0.519	0.605							
5.4	29.36	0.924	1.034	8.88	0.616	0.690							
5.5	29.77	1.092	1.187	9.14	0.728	0.791							
5.6	30.21	1.286	1.368	9.44	0.857	0.912							
5.7													
5.8													
5.9													
6.0													

Table A1. (*Continued.*)

	N_{st}(ISS/ISC)						N_{20}(ISS/ISC) ≥ 20°Δ					
log(N/N_{mx})	log(M_0)	$\sigma^R_{\log M_0}$	$\sigma^P_{\log M_0}$	M	σ^R_M	σ^P_M	log(M_0)	$\sigma^R_{\log M_0}$	$\sigma^P_{\log M_0}$	M	σ^R_M	σ^P_M
-3.00	22.39	0.275	0.760	4.23	0.183	0.507	22.21	0.223	0.670	4.11	0.148	0.447
-2.00	22.45	0.237	0.748	4.27	0.158	0.498	22.39	0.169	0.654	4.23	0.113	0.436
-1.75	22.51	0.215	0.741	4.30	0.143	0.494	22.50	0.147	0.649	4.30	0.098	0.433
-1.50	22.59	0.184	0.732	4.36	0.123	0.488	22.67	0.122	0.644	4.41	0.081	0.429
-1.45	22.62	0.177	0.731	4.38	0.118	0.487	22.71	0.117	0.643	4.44	0.078	0.429
-1.40	22.64	0.169	0.729	4.40	0.113	0.486	22.75	0.112	0.642	4.47	0.075	0.428
-1.35	22.67	0.161	0.727	4.42	0.107	0.485	22.80	0.107	0.641	4.50	0.071	0.427
-1.30	22.71	0.153	0.725	4.44	0.102	0.484	22.85	0.102	0.640	4.53	0.068	0.427
-1.25	22.74	0.145	0.724	4.46	0.096	0.482	22.90	0.098	0.640	4.57	0.065	0.426
-1.20	22.78	0.136	0.722	4.49	0.091	0.481	22.96	0.094	0.639	4.61	0.062	0.426
-1.15	22.83	0.127	0.720	4.52	0.085	0.480	23.03	0.090	0.638	4.65	0.060	0.426
-1.10	22.88	0.119	0.719	4.55	0.079	0.479	23.10	0.086	0.638	4.70	0.057	0.425
-1.05	22.93	0.110	0.717	4.59	0.073	0.478	23.17	0.083	0.637	4.75	0.055	0.425
-1.00	22.99	0.102	0.716	4.63	0.068	0.478	23.25	0.081	0.637	4.80	0.054	0.425
-0.98	23.02	0.099	0.716	4.65	0.066	0.477	23.29	0.080	0.637	4.83	0.053	0.425
-0.96	23.05	0.096	0.715	4.67	0.064	0.477	23.32	0.079	0.637	4.85	0.053	0.425
-0.94	23.08	0.093	0.715	4.68	0.062	0.477	23.36	0.079	0.637	4.87	0.052	0.425
-0.92	23.11	0.090	0.715	4.70	0.060	0.476	23.40	0.078	0.637	4.90	0.052	0.425
-0.90	23.14	0.087	0.714	4.73	0.058	0.476	23.44	0.078	0.637	4.92	0.052	0.424
-0.88	23.17	0.085	0.714	4.75	0.057	0.476	23.48	0.077	0.637	4.95	0.051	0.424
-0.86	23.20	0.083	0.714	4.77	0.055	0.476	23.52	0.077	0.637	4.98	0.051	0.424
-0.84	23.24	0.081	0.714	4.79	0.054	0.476	23.56	0.077	0.637	5.01	0.051	0.424
-0.82	23.28	0.079	0.713	4.82	0.053	0.476	23.60	0.077	0.637	5.04	0.051	0.424
-0.80	23.32	0.078	0.713	4.84	0.052	0.476	23.65	0.077	0.637	5.07	0.051	0.424
-0.78	23.36	0.077	0.713	4.87	0.051	0.475	23.69	0.077	0.637	5.10	0.051	0.424
-0.76	23.40	0.076	0.713	4.90	0.051	0.475	23.74	0.077	0.637	5.13	0.051	0.424
-0.74	23.44	0.076	0.713	4.93	0.050	0.475	23.79	0.077	0.637	5.16	0.051	0.424
-0.72	23.49	0.075	0.713	4.96	0.050	0.475	23.84	0.077	0.637	5.20	0.051	0.424
-0.70	23.54	0.075	0.713	4.99	0.050	0.475	23.90	0.077	0.637	5.23	0.051	0.424
-0.68	23.58	0.076	0.713	5.02	0.050	0.475	23.95	0.077	0.637	5.27	0.051	0.424
-0.66	23.64	0.076	0.713	5.06	0.051	0.475	24.01	0.077	0.637	5.30	0.051	0.424
-0.64	23.69	0.077	0.713	5.09	0.051	0.475	24.06	0.077	0.637	5.34	0.051	0.424
-0.62	23.75	0.077	0.713	5.13	0.052	0.475	24.12	0.077	0.637	5.38	0.052	0.424
-0.60	23.81	0.078	0.713	5.17	0.052	0.476	24.19	0.077	0.637	5.42	0.052	0.424
-0.58	23.87	0.079	0.713	5.21	0.053	0.476	24.25	0.077	0.637	5.47	0.052	0.424
-0.56	23.93	0.080	0.714	5.25	0.053	0.476	24.31	0.077	0.637	5.51	0.051	0.424
-0.54	24.00	0.081	0.714	5.30	0.054	0.476	24.38	0.077	0.637	5.55	0.051	0.424
-0.52	24.07	0.082	0.714	5.35	0.055	0.476	24.45	0.077	0.637	5.60	0.051	0.424
-0.50	24.14	0.083	0.714	5.39	0.055	0.476	24.52	0.076	0.637	5.65	0.051	0.424
-0.48	24.22	0.083	0.714	5.44	0.056	0.476	24.60	0.076	0.637	5.70	0.050	0.424
-0.46	24.30	0.084	0.714	5.50	0.056	0.476	24.67	0.075	0.636	5.75	0.050	0.424
-0.44	24.38	0.084	0.714	5.55	0.056	0.476	24.75	0.074	0.636	5.80	0.050	0.424
-0.42	24.46	0.084	0.714	5.61	0.056	0.476	24.83	0.074	0.636	5.86	0.049	0.424
-0.40	24.55	0.084	0.714	5.67	0.056	0.476	24.92	0.073	0.636	5.91	0.048	0.424
-0.38	24.65	0.084	0.714	5.73	0.056	0.476	25.00	0.071	0.636	5.97	0.048	0.424
-0.36	24.74	0.083	0.714	5.80	0.056	0.476	25.09	0.070	0.636	6.03	0.047	0.424
-0.34	24.85	0.083	0.714	5.86	0.055	0.476	25.19	0.069	0.636	6.09	0.046	0.424
-0.32	24.95	0.082	0.714	5.94	0.054	0.476	25.28	0.068	0.636	6.15	0.045	0.424
-0.30	25.06	0.081	0.714	6.01	0.054	0.476	25.38	0.066	0.635	6.22	0.044	0.424
-0.28	25.18	0.080	0.713	6.09	0.053	0.476	25.48	0.065	0.635	6.29	0.043	0.424
-0.26	25.30	0.079	0.713	6.17	0.053	0.476	25.58	0.064	0.635	6.35	0.042	0.423
-0.24	25.43	0.079	0.713	6.25	0.053	0.476	25.69	0.063	0.635	6.43	0.042	0.423
-0.22	25.56	0.080	0.714	6.34	0.053	0.476	25.80	0.062	0.635	6.50	0.041	0.423
-0.20	25.69	0.082	0.714	6.43	0.055	0.476	25.91	0.062	0.635	6.58	0.041	0.423
-0.18	25.84	0.086	0.714	6.52	0.057	0.476	26.03	0.062	0.635	6.65	0.042	0.423
-0.16	25.98	0.091	0.715	6.62	0.061	0.477	26.15	0.064	0.635	6.74	0.042	0.423
-0.14	26.14	0.099	0.716	6.73	0.066	0.477	26.28	0.066	0.635	6.82	0.044	0.424
-0.12	26.30	0.109	0.717	6.83	0.073	0.478	26.41	0.070	0.636	6.90	0.046	0.424
-0.10	26.47	0.122	0.719	6.95	0.081	0.480	26.54	0.074	0.636	6.99	0.049	0.424
-0.08	26.65	0.137	0.722	7.06	0.091	0.481	26.68	0.080	0.637	7.08	0.053	0.425
-0.06	26.83	0.155	0.726	7.19	0.103	0.484	26.82	0.087	0.638	7.18	0.058	0.425
-0.04	27.02	0.176	0.731	7.31	0.117	0.487	26.96	0.096	0.639	7.28	0.064	0.426
-0.02	27.22	0.199	0.737	7.45	0.133	0.491	27.11	0.106	0.641	7.38	0.070	0.427
0.00	27.43	0.226	0.744	7.59	0.151	0.496	27.27	0.117	0.643	7.48	0.078	0.428

Table A2. ISS and ISC station reporting history (annual maximum number of stations reporting an earthquake).

	International Seismological Summary (ISS)			
Year	N_{mx}	N_{mx} Event	N_{20mx}	N_{20mx} Event
1913	72	Tonga: 06/26: 7.7: s	72	—same—
14	64	New Guinea: 05/26: 8.0: s	64	—same—
15	54	northern Kurils: 05/01: 7.9: s	53	—same—
16	53	Turkey: 01/24: 7.1: s	53	Solomon Islands: 01/01: 7.6: s
17	57	Kermadec: 11/16: 7.3: s	56	Kermadec: 05/01: 8.0: s
18	84	Celebes Sea: 08/15: 8.2: s	81	—same—
19	81	Tonga: 04/30: 8.3: s	80	—same—
1920	78	Tibet: 12/16: 8.3: s	77	New Britain: 02/02: 7.5: s
21	83	Java: 09/11: 7.3: s	82	—same—
22	102	central Chile: 11/11: 7.3: s	96	—same—
23	102	Japan: 11/05: 8.0: s	99	Kamchatka: 02/03: 8.6: s
24	98	Macquarie ridge: 06/26: 8.3: s	97	—same—
25	108	Banda Sea: 11/10: 7.1: s	106	—same—
26	117	Macquarie ridge: 10/03: 7.3: s	113	New Guinea: 10/26: 7.4: s
27	131	Tibet: 05/22: 7.7: s	124	—same—
28	136	Mexico: 10/09: 7.4: s	127	—same—
29	148	western Aleutians: 12/17: 7.6: s	148	—same—
1930	162	Japan: 11/25: 6.9: s	141	Himalayan arc: 07/02: 7.0: s
31	198	Japan: 11/02: 7.4: s	173	Asia (Altai): 11/25: 8.1: s
32	187	near Japan: 11/13: 7.0: d	165	Mexico (Rivera): 06/03: 7.9: s
33	242	Japan: 03/02: 8.4: s	195	Baffin Bay, Canada: 11/20: 7.0: s
34	204	Himalaya (Bihar): 01/15: 8.1: s	196	—same—
35	231	Pakistan: 05/30: 8.1: s	221	—same—
36	256	Kamchatka: 06/30: 7.3: s	240	Molucca passage: 04/01: 7.6: s
37	258	south Kurils: 02/21: 7.4: s	240	Tibet: 01/07: 7.6: s
38	274	Japan: 11/05: 7.9: s	196	eastern Aleutians: 11/10: 8.4: s
39	179	Japan: 05/01: 7.0: s	171	central Chile: 01/25: 7.6: s
1940	195	Japan: 07/10: 7.3: d	153	northern Peru: 05/24: 7.7: s
41	176	Japan: 11/18: 7.7: s	160	Andaman (w. Java): 06/26: 7.7: s
42	155	Japan: 11/26: 7.4: d	134	Columbia-Ecuador: 05/14: 7.8: s
43	166	Japan: 06/13: 7.1: s	155	Banda Sea: 11/06: 7.5: s
44	174	Japan: 12/07: 8.1: s	133	New Britain: 05/25: 7.4: s
45	143	Makran (Pakistan): 11/27: 8.0: s	132	—same—
46	173	Japan: 12/20: 8.1: s	141	—same—
47	167	Japan: 11/04: 7.1: s	152	New Guinea: 04/02: 7.2: s
48	195	Japan: 04/17: 7.2: s	163	eastern Aleutians: 05/14: 7.4: s
49	210	Queen Charlotte F.: 08/22: 8.0: s	197	Solomon Islands: 10/19: 7.5: s
1950	243	Japan: 02/28: 7.8: d	225	Banda Sea: 10/08: 7.5: s
51	260	Japan: 07/11: —: d	240	Indian Oc.(SW ridge): 12/08: 7.5: s
52	313	Japan: 03/04: 8.1: s	277	Solomon Islands: 12/06: 7.3: s
53	329	Izu-Bonin arc: 11/25: 7.9: s	318	Vanuatu Islands: 11/04: 7.5: s
54	317	Burma: 03/21: 7.4: d	309	—same—
55	333	Philippines: 03/31: 7.7: s	317	—same—
56	350	Japan: 10/11: 7.6: s	342	Tonga: 05/23: 7.5: d

Table A2. (*Continued.*)

Year	N_{mx}	N_{mx} Event	N_{20mx}	N_{20mx} Event
		International Seismological Summary (ISS)		
57	391	Asia (Altai): 12/04: 8.1: s	366	Santa Cruz Islands: 12/17: 7.5: d
58	410	south Kurils: 11/06: 8.4: s	360	Peru: 07/26: 7.6: d
59	409	Kamchatka: 05/04: 8.0: s	378	—same—
1960	389	Japan: 03/20: 7.8: s	380	Vanuatu Islands: 03/08: 7.2: d
61	377	Japan: 02/26: 7.7: s	345	South Sandwich Isl.: 09/08: 7.7: d
62	388	Japan: 04/12: 7.2: s	370	Banda Sea: 05/15: 7.2: s
63	409	northern Kurils: 03/16: 7.3: s	369	Peru: 08/15: 7.7: d
		International Seismological Centre (ISC)		
64	360	Japan: 06/16: 7.6: s	261	—same—
65	384	Japan: 10/25: 6.8: d	295	—same—
66	350	central Chile: 12/28: 7.7: s	334	—same—
67	441	Tonga: 10/09: —: d	428	—same—
68	456	Mariana Islands: 10/07: —: d	381	Molucca Passage: 08/10: 7.6: s
69	451	Japan: 01/19: —: d	388	Sumatra: 11/21: 7.6: s
1970	468	Japan: 12/07: —: d	388	northern Peru: 12/10: 7.1: s
71	457	Japan: 12/07: —: d	401	northern Sumatra: 02/04: —: s
72	539	Izu-Bonin Islands: 12/04: 7.6: s	426	—same—
73	540	North Korea: 09/29: —: d	421	—same—
74	500	Izu-Bonin Islands: 11/29: —: d	430	northern Chile: 01/02: —: d
75	545	Sea of Japan: 01/29: —: d	468	Burma: 07/08: —: d
76	580	Tangshan, NE China: 07/28: 7.5: s	485	Chile-Bolivia border: 11/30: —: d
77	622	Sea of Japan: 03/09: 6.9: d	552	Tonga: 06/22: 8.1: s
78	654	Kuril Islands: 12/06: 7.8: d	523	—same—
79	618	North Korea: 08/16: 6.7: d	522	Loyalty Islands: 05/01: 7.4: s
1980	615	Kuril Islands: 02/23: 7.1: s	519	Tonga: 04/13: 7.6: d
81	661	Japan: 05/08: 6.5: d	523	Kuril Islands: 02/23: 6.6: s
82	692	Japan: 03/21: 6.9: s	582	Banda Sea: 06/22: 7.5: d
83	744	Japan: 05/26: 7.7: s	625	New Ireland region: 03/18: 7.7: d
84	819	Japan: 09/18: 6.9: s	723	Philippines: 03/05: 7.3: d
85	748	Hindu-Kush region: 07/29: 7.4: d	697	—same—
86	803	Aleutian Islands: 05/07: 8.0: s	789	—same—
87	886	Sea of Japan: 05/07: 6.8: d	734	—same—
88	887	Gulf of Alaska: 03/06: 7.8: s	819	Burma-India border: 08/06: 7.3: d
89	845	Japan: 11/01: 7.4: s	735	western Brazil: 05/05: 7.1: d
1990	1,008	Sakhalin Island: 05/12: 7.2: d	849	—same—
91	887	Kuril Islands: 12/22: 7.6: s	800	Fiji region: 06/09: 7.0: d
92	920	Japan: 08/24: 6.1: d	845	Vanuatu Islands: 10/11: 7.4: d
93	993	Japan (Hokkaido): 07/12: 7.7: s	845	S. Marianas (Guam): 08/08: 7.8: s

Note: Event description format: locale: month/day: moment magnitude: shallow (s) or deep (d). **M** from either Pacheco and Sykes (G49, 1992), Harvard Univ. (G31, 1977-1994), or taken as M_{GR} from Gutenberg and Richter (1954) or Rothé (1969). Designations s and d follow the same sources.

Table A3. log(M_0)–log(A_i) SCR database: (a) North America; (b) global.

(a)

Event #	logM_o (U) [source: Part I]	M	I_{max} [S]	A_{felt}(U)	A_{III}(U)	A_{IV}(U)	A_V(U)	A_{VI}(U)	A_{VII}(U)	A_{VIII}(U)	[S]	Q
						[log (MMI areas in km^2)]						
NA-25-0301	25.70(2.6)	6.43	9 [21]	6.41(1.1)	6.19(1.2)	5.83(1.3)	5.14(1.7)	4.80(2.0)	4.30(2.4)	3.37(3.7)	[22]	f-g
			8 [05]	6.44(1.1)	6.11(1.2)	5.85(1.3)	5.18(1.7)	4.82(2.0)	3.72(2.4)	3.18(3.7)	[20]	f-g
				6.52(1.2)	--------	5.80(1.4)	--------	--------	--------	--------	[27]	p
			8.5	**6.42(1.1)**	**6.15(1.2)**	**5.84(1.3)**	**5.16(1.7)**	**4.81(2.0)**	**4.01(2.4)**	**3.27(3.7)**		
NA-29-0812	23.35(1.8)	4.87	8 [05]	**5.95(1.2)**	--------	**5.24(1.4)**	**3.94(2.1)**	**3.08(4.1)**	--------	--------	[26]	g
				5.56(1.4)	--------	--------	4.45(2.9)	--------	†3.20(8.9)	--------	[07]	f-p
				5.45(1.4)	--------	--------	--------	--------	--------	--------	[29]	p
NA-29-1118	26.92(1.8)	7.25	10[05]	6.79(1.2)	6.62(1.2)	6.45(1.3)	5.92(1.7)	5.85(2.0)	--------	--------	[22]	p
				6.70(1.2)	6.65(1.2)	6.32(1.3)	5.95(1.7)	5.43(2.0)	--------	--------	[20]	p
			10	**6.74(1.2)**	**6.64(1.2)**	**6.38(1.3)**	**5.94(1.7)**	**5.43(2.0)**	--------	--------		
NA-35-1101	25.36(1.9)	6.21	7 [22]	**6.33(1.1)**	**6.17(1.2)**	**5.89(1.2)**	**5.11(1.6)**	**4.60(2.0)**	**2.88(2.4)**	--------	[22]	g
				6.42(1.3)	--------	5.86(1.5)	--------	--------	--------	--------	[27]	p
NA-39-1019	24.00(3.5)	5.30	6 [22]	**6.18(1.3)**	**5.76(1.3)**	**5.20(1.5)**	**4.51(2.4)**	**3.75(4.5)**	--------	--------	[22]	f
NA-40-1220	24.20(4.0)	5.43	7 [05]	**5.62(1.2)**	--------	**5.24(1.4)**	**4.56(2.2)**	**3.85(3.4)**	**2.61(4.8)**	--------	[26]	f-g
				6.05(1.3)	**5.79(1.3)**	5.34(1.4)	4.67(2.4)	3.42(4.1)	--------	--------	[29]	f
				5.90(1.3)	--------	4.95(1.6)	--------	--------	--------	--------	[27]	p
NA-44-0905	24.73(3.0)	5.79	8 [05]	**6.06(1.2)**	--------	**5.53(1.3)**	**5.02(2.0)**	**4.28(2.8)**	**3.74(3.8)**	**2.92(5.1)**	[26]	f-g
			9 [29]	--------	**5.91(1.2)**	5.57(1.3)	5.07(2.0)	4.36(2.8)	3.78(3.8)	3.07(5.1)	[22]	f-g
				6.19(1.3)	--------	5.68(1.5)	--------	4.58(3.9)	--------	--------	[29]	p
				6.16(1.3)	--------	5.54(1.5)	--------	--------	--------	--------	[27]	p
NA-62-0202	22.40(1.3)	4.23	6 [17]	**4.94(1.3)**	--------	--------	**3.60(2.5)**	**2.21(5.1)**	--------	--------	[29]	g
NA-63-0303	23.04(1.6)	4.66	6 [17]	**5.33(1.2)**	--------	**4.81(1.4)**	--------	**3.46(4.3)**	--------	--------	[26]	g
				5.34(1.2)	--------	--------	**4.57(2.2)**	3.88(4.3)	--------	--------	[29]	g
				5.46(1.2)	--------	--------	4.38(2.2)	3.78(4.3)	--------	--------	[07]	g
NA-65-1021	22.98(1.3)	4.62	6 [15]	5.64(1.2)	--------	--------	4.13(2.2)	3.40(4.3)	--------	--------	[29]	g
				5.40(1.3)	--------	5.08(1.6)	--------	3.92(6.4)	--------	--------	[07]	f
			6	**5.55(1.3)**	--------	**5.08(1.6)**	**4.13(2.2)**	**3.60(5.0)**	--------	--------		
NA-66-0101	22.40(1.3)	4.23	6 [17]	**4.67(1.3)**	--------	--------	**3.13(2.5)**	--------	--------	--------	[29]	g
NA-67-0604	22.49(1.3)	4.29	6 [05]	**4.75(1.3)**	--------	--------	**3.99(2.1)**	--------	--------	--------	[29]	g
NA-67-0613	22.18(1.3)	4.09	6 [17]	**3.85(1.3)**	--------	--------	**2.81(2.6)**	--------	--------	--------	[29]	g
NA-68-1109	24.11(1.2)	5.37	7 [09]	**6.19(1.2)**	--------	**5.71(1.3)**	**5.17(2.1)**	**4.19(3.0)**	**3.61(4.0)**	--------	[09]	g
				--------	--------	--------	--------	4.70(3.0)	3.81(4.0)	--------	[29]	g
NA-69-0101	22.56(1.6)	4.34	6 [29]	**4.92(1.2)**	--------	--------	**4.14(2.4)**	--------	--------	--------	[29]	g
NA-69-1120	22.86(1.6)	4.54	6 [17]	**5.53(1.2)**	**5.33(1.3)**	**4.47(1.4)**	----	--------	--------	--------	[03]	g
				5.54(1.2)	--------	--------	**4.29(2.2)**	--------	--------	--------	[29]	g
NA-70-1117	22.20(1.3)	4.10	6 [29]	**4.99(1.3)**	--------	--------	**4.25(2.6)**	--------	--------	--------	[29]	g
NA-72-0915	22.23(1.6)	4.12	6 [17]	**5.36(1.3)**	--------	--------	--------	--------	--------	--------	[29]	g
NA-73-0615	22.79(1.3)	4.49	6 [30]	5.36(1.2)	--------	4.89(1.4)	4.21(2.2)	--------	--------	--------	[29]	g
				5.06(1.4)	4.89(1.4)	4.16(1.7)	3.40(2.8)	--------	--------	--------	[30]	f
			6	**5.25(1.3)**	**4.89(1.4)**	**4.65(1.6)**	**4.00(2.5)**	--------	--------	--------		
NA-73-1130	22.18(1.9)	4.09	6 [04]	5.15(1.3)	--------	4.93(1.5)	4.37(2.6)	--------	--------	--------	[29]	g
			6 [17]	4.80(1.3)	--------	--------	4.33(2.6)	1.13(5.5)	--------	--------	[04]	g
			6	**5.15(1.3)**	--------	**4.93(1.5)**	**4.35(2.6)**	**1.13(5.5)**	--------	--------		
NA-74-0215	22.60(1.9)	4.37	5 [29]	**4.98(1.3)**	--------	**4.68(1.5)**	**3.80(2.4)**	--------	--------	--------	[06]	g
				4.67(1.3)	--------	--------	--------	--------	--------	--------	[29]	g
NA-75-0613	21.66(1.3)	3.74	6 [26]	**4.23(1.5)**	--------	**3.68(2.0)**	--------	--------	--------	--------	[29]	f
NA-75-0709	22.51(1.6)	4.31	6 [29]	**4.91(1.3)**	--------	**4.70(1.5)**	**4.28(2.4)**	**2.87(5.0)**	--------	--------	[29]	g
NA-75-0712	22.23(1.7)	4.12	4 [11]	**5.15(1.3)**	**4.82(1.4)**	**3.82(1.7)**	--------	--------	--------	--------	[11]	f-g
NA-76-0325a	22.99(1.3)	4.63	6 [29]	**5.45(1.3)**	--------	--------	**4.98(2.5)**	**3.77(5.4)**	--------	--------	[29]	f-g
NA-78-0218	21.90(1.8)	3.90	5 [15]	--------	**4.71(1.3)**	**3.86(1.6)**	**2.82(2.7)**	--------	--------	--------	[12]	g
NA-78-0616	22.81(1.4)	4.51	5 [15]	**5.04(1.2)**	--------	--------	**3.65(2.2)**	--------	--------	--------	[06]	g
				4.72(1.2)	--------	--------	3.54(2.2)	--------	--------	--------	[29]	g
NA-79-0819	23.18(1.5)	4.75	5 [10]	--------	**4.75(1.3)**	**4.44(1.4)**	**3.81(2.1)**	--------	--------	--------	[10]	g
NA-80-0727	23.63(1.3)	5.05	7 [29]	**5.82(1.2)**	--------	**5.46(1.3)**	**4.71(2.1)**	**4.06(4.0)**	--------	--------	[26]	g
				5.81(1.2)	--------	--------	4.74(2.1)	4.06(4.0)	--------	--------	[29]	g
				5.83(1.4)	--------	--------	†3.86(2.6)	†3.44(5.5)	**2.60(7.8)**	--------	[14]	f
NA-82-0109a	24.28(1.2)	5.49	6 [29]	--------	**5.71(1.3)**	**5.36(1.4)**	**4.89(2.3)**	**3.38(3.7)**	--------	--------	[29]	f

Table A3. (*Continued.*)

Event #	logM_o (U) [source: Part I]	M	I_{max} [S]	A_{felt}(U)	A_{III}(U)	A_{IV}(U)	A_V(U)	A_{VI}(U)	A_{VII}(U)	A_{VIII}(U)	[S]	Q
						[log (MMI areas in km²)]						
NA-82-0109b	23.19(1.4)	4.76	6 [29]	**5.14(1.4)**	--------	**4.05(1.8)**	**3.70(3.0)**	--------	--------	--------	[02]	f-p
				--------	**4.90(1.3)**	--------	--------	--------	--------	--------	[23]	f-g
NA-82-0111	23.67(1.3)	5.08	6 [29]	5.45(1.4)	--------	**4.91(1.6)**	**4.50(2.8)**	**3.45(6.0)**	--------	--------	[02]	f-p
				5.35(1.3)	--------	--------	--------	--------	--------	--------	[29]	f
NA-82-0119	22.56(1.6)	4.34	6 [29]	**5.13(1.3)**	--------	--------	**4.22(2.4)**	**2.76(4.6)**	--------	--------	[29]	g
NA-82-0121	22.67(1.4)	4.41	6 [29]	--------	**4.54(1.3)**	--------	**2.81(2.3)**	--------	--------	--------	[29]	g
NA-82-0331	22.20(2.0)	4.1	4 [T2]	**4.96(1.5)**	--------	**4.58(2.0)**	**3.90(3.8)**	--------	--------	--------	[02]	f-p
NA-82-0402	21.60(2.0)	3.7	3 [T2]	**4.50(1.6)**	--------	**3.90(2.2)**	--------	--------	--------	--------	[02]	f-p
NA-82-0616	22.05(2.0)	4.0	4 [T2]	**4.85(1.4)**	--------	**4.50(1.9)**	**3.90(3.9)**	--------	--------	--------	[02]	f-p
NA-82-0713	20.85(2.0)	3.2	4 [T2]	**4.25(1.8)**	--------	**3.70(2.4)**	--------	--------	--------	--------	[02]	f-p
NA-82-0813	21.30(2.0)	3.5	4 [T2]	**4.66(1.7)**	--------	**4.25(2.3)**	--------	--------	--------	--------	[02]	f-p
NA-83-1007	23.36(1.2)	4.87	6 [15]	**5.81(1.2)**	--------	**5.52(1.4)**	**4.76(2.1)**	**3.17(4.1)**	--------	--------	[26]	g
				5.81(1.2)	--------	--------	4.79(2.1)	3.42(4.1)	--------	--------	[29]	g
NA-84-0908	23.46(1.6)	4.94	5 [26]	**4.83(1.3)**	--------	--------	**3.93(2.6)**	--------	--------	--------	[24]	f
NA-86-0131	23.32(1.8)	4.85	6 [26]	5.50(1.2)	--------	5.09(1.4)	4.38(2.1)	2.94(4.2)	--------	--------	[26]	g
				5.54(1.2)	--------	5.12(1.4)	4.45(2.1)	3.02(4.2)	--------	--------	[25]	g
			6	**5.52(1.2)**	--------	**5.10(1.4)**	**4.41(2.1)**	**3.02(4.2)**	--------	--------		
NA-86-0712	22.65(1.5)	4.40	6 [26]	**5.01(1.3)**	--------	**4.24(1.5)**	**3.51(2.3)**	**2.48(4.6)**	--------	--------	[19]	g
NA-87-0610	23.49(1.3)	4.96	6 [18]	**5.68(1.2)**	--------	--------	**4.80(2.1)**	**3.20(4.0)**	--------	--------	[18]	g
NA-88-0907	22.30(1.5)	4.17	6 [26]	--------	--------	--------	**4.22(2.6)**	**2.74(5.5)**	--------	--------	[28]	g
				5.01(1.5)	--------	--------	--------	--------	--------	--------	[26]	p
NA-88-1125	24.82(1.3)	5.85	7 [08]	**6.52(1.2)**	--------	**6.16(1.3)**	**5.68(1.8)**	**5.12(2.4)**	--------	--------	[08]	g
NA-89-1225b	25.11(1.3)	6.04	----	**5.90(1.3)**	--------	5.45(1.5)	**4.85(2.2)**	--------	--------	--------	[02]	f-p
					--------	**5.55(1.4)**	--------	--------	--------	--------	[31]	f
NA-90-0926	22.48(2.0)	4.29	6 [15]	**5.16(1.3)**	--------	**4.71(1.5)**	**4.13(2.4)**	**3.13(4.9)**	--------	--------	[16]	g
NA-90-1019	22.92(2.0)	4.58	5 [13]	--------	--------	5.74(1.4)	4.21(2.2)	--------	--------	--------	[13]	g
				5.81(1.5)	--------	†6.10(1.9)	4.85(3.4)	--------	--------	--------	[02]	p
			5	**5.81(1.5)**	--------	**5.74(1.4)**	**4.40(2.4)**	--------	--------	--------		
NA-91-0504	22.54(1.7)	4.33	6 [15]	**4.96(1.3)**	--------	**4.56(1.5)**	**4.06(2.5)**	**2.97(5.1)**	--------	--------	[16]	g
NA-94-0116	22.08(1.7)	4.02	**6.5**[01]	--------	**4.09(1.3)**	**3.52(1.5)**	**2.69(2.6)**	**1.70(6.0)**	--------	--------	[††]	g

(††C. Sharnberger, written communication, 1995)

([T2] indicates source is Table 2, Part I)

(b)

Event #	logM_o (U) [source: Part I]	M	I_{max} [S]	A_{felt}(U)	A_{III}(U)	A_{IV}(U)	A_V(U)	A_{VI}(U)	A_{VII}(U)	A_{VIII}(U)	[S]	Q
						[log (MMI areas in km²)]						
AFRICA												
AF-39-0622	25.77(2.3)	6.48	9 [36]	**6.32(1.2)**	--------	**6.03(1.3)**	**5.78(1.8)**	**4.87(2.2)**	--------	--------	[04]	f
				6.31(1.3)	--------	--------	--------	--------	**2.80(2.9)**	**2.43(4.8)**	[65]	f-p
AF-45-0912	25.15(2.5)	6.07	8 [04]	--------	**5.57(1.3)**	--------	--------	--------	--------	--------	[04]	p
AF-55-0912	25.66(2.3)	6.41	-----	--------	----	*5.89(1.4)	*5.68(2.1)	*5.20(2.8)	*4.92(3.3)	--------	[20]	p
AF-69-0929	25.65(1.4)	6.40	9 [48]	**6.30(1.2)**	**5.88(1.2)**	**5.61(1.3)**	**5.04(1.8)**	**4.30(2.3)**	**3.37(2.9)**	**2.98(4.5)**	[16]	f
AF-83-1222	25.41(1.5)	6.24	9 [04]	--------	**6.12(1.3)**	--------	**5.45(2.4)**	--------	--------	--------	[04]	p

*not used for regression; most of isoseismal area in excluded crust along the Red Sea rift

ANTARCTICA and ASIA none

AUSTRALIA

AU-66-0503	22.74(1.8)	4.46	5 [15]	--------	**5.01(1.3)**	**4.67(1.5)**	**3.16(2.3)**	--------	--------	--------	[15]	g
AU-68-1014	25.92(1.3)	6.58	9 [19]	--------	**6.12(1.2)**	**5.81(1.3)**	**5.18(1.5)**	**4.24(1.8)**	**3.09(2.1)**	**2.53(3.2)**	[15]	g
AU-73-0309	23.76(1.9)	5.14	**6.5**[15]	--------	--------	**5.48(1.3)**	**4.66(2.0)**	--------	--------	--------	[15]	g
AU-79-0602	25.19(1.2)	6.09	9 [15]	**6.03(1.2)**	--------	**5.66(1.2)**	**4.69(1.7)**	**3.53(2.1)**	**2.41(2.6)**	**2.06(3.9)**	[15]	g
AU-82-1121	23.03(1.7)	4.65	6 [13]	--------	**5.15(1.3)**	**4.82(1.4)**	**4.15(2.2)**	--------	--------	--------	[53]	g
AU-88-0122a	25.45(1.3)	6.27	7 [35]	--------	**6.24(1.2)**	**5.87(1.2)**	**5.43(1.6)**	**4.21(2.0)**	**3.74(2.4)**	--------	[35]	g
AU-88-0122b	25.61(1.4)	6.37	7 [35]	--------	**6.24(1.1)**	**5.87(1.2)**	**5.43(1.6)**	**4.21(1.9)**	**3.74(2.3)**	--------	[35]	g
AU-88-0122c	25.91(1.2)	6.57	8 [35]	**6.44(1.1)**	--------	**6.11(1.2)**	**5.76(1.5)**	**4.46(1.8)**	--------	--------	[40]	g

Table A3. (*Continued.*)

Event #	logM_o (U) [source: Part I]	M	I_{max} [S]	A_{felt}(U)	A_{III}(U)	A_{IV}(U)	A_V(U)	A_{VI}(U)	A_{VII}(U)	A_{VIII}(U)	[S]	Q
						[log (MMI areas in km^2)]						
CHINA												
CH-62-0318	25.11(1.6)	6.04	8 [10]	--------	--------	5.61(1.4)	5.10(2.0)	4.01(2.7)	2.72(3.5)	1.40(5.5)	[22]	f
				--------	--------	--------	--------	4.20(2.1)	2.97(2.7)	1.97(4.0)	[64]	g
			8	--------	--------	**5.61(1.4)**	**5.10(2.0)**	**4.11(2.4)**	**2.85(3.1)**	**1.69(4.8)**		
CH-69-0725	24.71(1.8)	5.77	8 [22]	--------	--------	--------	--------	3.60(2.8)	2.99(3.8)	2.19(5.1)	[22]	f-g
				--------	--------	--------	--------	3.61(2.8)	3.06(3.8)	2.41(5.1)	[64]	f-g
			8	--------	--------	--------	--------	**3.60(2.8)**	**3.03(3.8)**	**2.30(5.1)**		
CH-69-1217	23.24(1.5)	4.79	----	--------	--------	**4.99(1.8)**	**4.77(3.2)**	--------	--------	--------	[64]	p
CH-69-1220	23.16(1.5)	4.74	----	--------	--------	**4.79(1.8)**	**4.47(3.2)**	--------	--------	--------	[64]	p
CH-74-0422	24.04(1.4)	5.33	7 [10]	--------	--------	--------	3.52(2.0)	2.94(3.4)	1.93(4.4)	--------	[64]	g
				--------	5.20(1.3)	4.76(1.5)	3.55(2.0)	2.97(3.4)	2.00(4.4)	--------	[23]	g
			7	--------	**5.20(1.3)**	**4.76(1.5)**	**3.54(2.0)**	**2.96(3.4)**	**1.97(4.4)**	--------		
CH-79-0709	24.22(1.3)	5.45	8 [23]	--------	**5.60(1.2)**	**5.22(1.3)**	**4.80(1.9)**	**3.38(3.0)**	**2.60(4.0)**	**1.48(5.1)**	[23]	g
CH-84-0521	25.17(1.4)	6.08	----	--------	--------	**5.32(1.4)**	**4.84(2.0)**	**3.78(3.2)**	--------	--------	[32]	f
CH-87-0802	23.56(1.4)	5.01	7 [63]	--------	--------	--------	**3.99(2.3)**	3.10(4.7)	**1.82(6.5)**	--------	[38]	f-g
EUROPE												
EU-78-0903	23.70(1.8)	5.10	**7.5**[29]	--------	**5.56(1.3)**	**5.23(1.5)**	**4.79(2.6)**	3.83(5.5)	3.11(7.8)	--------	[50]	f
				--------	--------	--------	--------	**3.75(4.0)**	**3.11(5.5)**	--------	[29]	g
EU-83-1108	23.20(2.0)	4.77	7 [34]	--------	**5.11(1.4)**	**4.26(1.5)**	--------	--------	--------	--------	[03]	p
				5.17(1.4)	†4.41(1.5)	†3.87(1.8)	**3.35(3.3)**	--------	--------	--------	[33]	f
				--------	--------	--------	--------	**2.59(7.5)**	**1.96(10.0)**	--------	[02]	p
EU-86-0205	23.11(1.4)	4.71	6 [48]	--------	**5.52(1.4)**	**5.25(1.7)**	**4.82(3.0)**	--------	--------	--------	[30]	f-p
EU-88-0808	24.43(1.8)	5.59	----	--------	**5.81(1.4)**	**5.55(1.5)**	--------	--------	--------	--------	[30]	p
EU-89-0123	23.76(1.4)	5.14	5 [30]	--------	**5.58(1.4)**	**5.29(1.6)**	**4.83(2.8)**	--------	--------	--------	[30]	f-p
EU-92-0413	24.04(1.4)	5.33	8 [48]	5.88(1.2)	5.61(1.3)	5.16(1.4)	4.64(2.2)	3.84(4.0)	--------	--------	[62]	f-g
				5.73(1.2)	5.46(1.3)	5.14(1.4)	4.50(2.2)	3.81(4.0)	--------	--------	[**]	f-g
				--------	5.61(1.3)	5.33(1.4)	4.51(2.2)	3.52(4.0)	2.74(5.5)	--------	[**]	f-g
				--------	--------	--------	--------	3.66(4.0)	2.88(5.5)	--------	[**]	f-g
			8	**5.88(1.2)**	**5.54(1.3)**	**5.16(1.4)**	**4.58(2.2)**	**3.82(4.0)**	**2.81(5.5)**	--------		
								(**G. Houtgast, written communication, 1993)				
INDIA												
IN-56-0721	25.08(1.8)	6.02	**9** [59]	**5.91(1.3)**	**5.41(1.3)**	**5.01(1.5)**	**4.51(2.4)**	**3.73(3.2)**	**3.55(4.4)**	**3.17(7.0)**	[59]	p
IN-67-1210	25.51(1.6)	6.31	**8.5**[08]	**6.19(1.2)**	--------	**5.65(1.3)**	**5.00(1.7)**	3.30(2.2)	2.60(2.8)	--------	[08]	f-g
				--------	--------	--------	--------	**3.31(2.0)**	**2.79(2.4)**	**1.67(3.6)**	[27]	g
IN-69-0413	24.66(1.4)	5.74	7.5 [25]	5.96(1.3)	--------	5.31(1.6)	5.01(3.0)	4.53(4.0)	--------	--------	[47]	p
			7 [47]	6.39(1.2)	--------	5.61(1.4)	5.20(2.2)	4.67(3.3)	--------	--------	[08]	f
			7.5	**6.20(1.3)**	--------	**5.46(1.5)**	**5.11(2.6)**	**4.60(3.7)**	--------	--------		
IN-70-0323	24.14(1.4)	5.39	7 [26]	**4.94(1.3)**	**4.61(1.3)**	**4.35(1.5)**	**3.84(2.6)**	3.16(4.3)	--------	--------	[08]	f-p
				--------	--------	--------	--------	**2.95(3.2)**	**2.04(4.2)**	--------	[26]	g
IN-93-0929	25.31(1.3)	6.17	**9** [++]	--------	**6.16(1.5)**	**5.77(1.5)**	**5.04(2.0)**	**4.44(2.3)**	†3.63(4.0)	†3.15(6.6)	[++]	f
				--------	--------	--------	--------	--------	**3.17(2.5)**	**2.67(3.5)**	[++]	g
								(++ B. K. Rastogi, written communication, 1994)				
SOUTH AMERICA												
SA-80-1120	23.85(1.3)	5.20	7 [05]	**6.10(1.3)**	--------	**5.18(1.5)**	**4.66(2.5)**	**3.51(4.9)**	**3.12(6.8)**	--------	[06]	f
			6 [48]									

† denotes values not used for regression. Final values used in the regressions are in **bold**.

M_o in dyne-cm. Taken from the selected value in Part I, Table B2 or Table 2. **M** is the corresponding moment magnitude.

S: source. Primary reference for the quoted value of I_{max} or A_i (appendix bibliography, either N (North America) or G (global) prefix.

Q: quality of source isoseismal map. g = good, f = fair, p = poor. See text for detailed explanation.

U: uncertainty in log(M_o) and log(A_i) expressed as multiplicative error factor. U is from Part I for log(M_o) and from Table 1 for log(A_i).

Table A4. Other regression data: (a) events with seismic moment from teleseismic magnitudes; (b) large SCR border events with SCR isoseismal areas.

Event (event number)	log(M_o) [S]	T	Selected logM_o (U)	M	I_{max} [S]	A_{felt}(U)	A_{III}(U)	A_{IV}(U)	A_V(U)	A_{VI}(U)	A_{VII}(U)	A_{VIII}(U)	[S]	Q
								[log (MMI areas in km^2)]						
Nan'ao SE China	26.99 [28]	ms	26.99 (2.2)	7.29	**10** [22]	--------	--------	6.36(1.2)	--------	5.24(1.7)	4.66(2.3)	4.10(3.6)	[09]	f-p
(CH-18-0213)	27.16 [01]	ms				--------	--------	----	--------	5.29(2.0)	4.81(2.3)	--------	[24]	p
	26.82 [49]	ms				6.50(1.2)	--------	----	--------	5.41(1.7)	4.82(2.0)	4.30(3.0)	[22]	f
						6.50(1.2)	--------	**6.36(1.2)**	--------	**5.31(1.8)**	**4.76(2.2)**	**4.20(3.3)**		
Meeberrie WA	26.17 [28]	ms	25.95 (2.0)	6.60	**8** [15]	--------	**6.32(1.2)**	**6.13(1.2)**	**5.64(1.5)**	**5.14(1.7)**	**4.54(1.9)**	**4.01(2.9)**	[15]	g
(AU-41-0429)	25.73 [14]	ms												
Sichuan-Hubei	23.60 [P1]	mb	23.60 (2.5)	5.03	**7** [23]	--------	--------	--------	**3.07(2.2)**	**2.56(4.4)**	**1.81(6.0)**	--------	[23]	f-g
(CH-79-0521)														
North Wales UK	23.53 [P1]	mb	23.72 (1.8)	5.11	6 [61]	--------	4.98(1.2)	4.56(1.3)	3.78(2.0)	--------	--------	--------	[46]	g
(EU-84-0719)	23.81 [P1]	ms				--------	5.38(1.3)	5.02(1.5)	3.94(2.6)	3.14(4.5)	--------	--------	[61]	f
	†23.00 [60]	wb			**6**	--------	**5.18(1.3)**	**4.79(1.4)**	**3.86(2.3)**	**3.14(4.5)**	--------	--------		
Nhill Victoria	23.17 [P1]	mb	23.17 (2.5)	4.75	6 [41]	**5.23(1.2)**	--------	**4.83(1.4)**	**4.15(2.1)**	**3.04(4.2)**	--------	--------	[41]	g
(AU-87-1222)														
Ayers Rock NT	24.13 [P1]	ms	24.25 (1.8)	5.47	**7** [45]	**5.20(1.2)**	--------	**4.89(1.4)**	**4.39(2.3)**	**3.56(3.7)**	**2.81(5.1)**	--------	[45]	f
(AU-89-0528)	24.50 [P1]	mb												
Newcastle NSW	24.19 [P1]	mb	24.19 (2.5)	5.43	8 [43]	--------	5.47(1.2)	5.04(1.3)	4.56(2.1)	3.83(3.3)	--------	--------	[43]	f-g
(AU-89-1227)	†23.45 [34]	ms				--------	--------	--------	--------	--------	2.18(4.4)	1.40(5.4)	[58]	f-g
						--------	--------	--------	--------	--------	2.19(4.4)	1.32(5.4)	[44]	f-g
						--------	--------	--------	--------	--------	2.77(3.7)	1.54(4.5)	[52]	g
						--------	†5.65(1.4)	†5.45(1.5)	†4.98(2.7)	†4.68(4.6)	†4.00(6.4)	†3.57(8.0)	[52]	p
					8	--------	**5.47(1.2)**	**5.04(1.3)**	**4.56(2.1)**	**3.83(3.3)**	**2.38(4.2)**	**1.42(5.1)**		
Bishops Castle UK	23.10 [P1]	mb	23.10 (2.5)	4.70	6 [48]	**5.38(1.3)**	**5.13(1.4)**	**4.79(1.6)**	**4.16(2.7)**	**3.20(6.0)**	--------	--------	[51]	f
(EU-90-0402)														
Arnhem Ld. NT	23.96 [P1]	ms	24.04 (1.8)	5.32	-----	**5.67(1.2)**	**5.44(1.3)**	**5.15(1.4)**	**4.69(2.2)**	--------	--------	--------	[42]	f-g
(AU-92-0930)	24.19 [P1]	mb												

† not used; U uncertainty expressed as MEF; Q quality

[S] Source: Appendix reference no. (G-prefix); [P1] denotes Part I regression on average of ISC [G34] and NEIC [G48] values

T technique: mb from Part I regression on teleseismic body-wave magnitude m_b (period ~1 sec)
ms from Part I regression on teleseismic surface-wave magnitude M_S (period ~20 sec)
wb from waveform modeling–body waves

bold: log(A_i) or I_{max} data values used in the regression analyses

(b)

Event (event number)	log(M_o) [S]	T	Selected logM_o (U)	M	I_{max} [S]	A_{felt}(U)	A_{III}(U)	A_{IV}(U)	A_V(U)	A_{VI}(U)	A_{VII}(U)	A_{VIII}(U)	[S]	Q
								[log (MMI areas in km^2)]						
Bihar, Himalaya	28.04 [11]	ss	28.22(2.4)	8.11	10 [11]	**6.77(1.1)**	--------	**6.53(1.2)**	--------	**6.08(1.5)**	5.49(1.8)	--------	[54]	f
(IN-34-0115)	†27.97 [07]	ss				--------	--------	--------	**6.31(1.4)**	--------	**5.51(1.8)**	**5.03(2.5)**	[55]	f
	†28.64 [57]	ss												
San Juan, Andes	27.11 [37]	wb	27.19(1.3)	7.43	9 [17]	--------	**6.51(1.1)**	**6.14(1.2)**	**5.78(1.5)**	**5.42(1.7)**	†4.90(1.9)	†4.24(2.9)	[17]	f
(SA-77-1123)	27.27 [31]	ct												
	26.53 [12]	wb												
Outer Sunda Arc	28.48 [39]	bi	28.51(1.3)	8.31	-----	**7.10(1.1)**	**6.91(1.1)**	**6.64(1.2)**	--------	--------	--------	--------	[21]	f
(AU-77-0819)	28.38 [56]	mt												
	28.56 [31]	ct												
	28.63 [18]	ws												

symbols and **bold** same as Table A4(a) except

T: technique
wb waveform modeling, teleseismic body waves
ws waveform modeling, teleseismic surface waves
ss spectral amplitude, surface waves
bi body-wave inversion
mt moment tensor inversion (best double couple)
ct centroid, moment tensor inversion (best double couple)

APPENDIX REFERENCES

North American references [Table A3(a); N prefix]

N01 Armbruster, J.G., Seeber, L., Barstow, N., Kim, W.Y. & Horton, S., 1994. The Jan 1994 Wyomissing Hills earthquakes (Mblg = 4.0 & 4.6) in southeastern Pennsylvania: a 2 km-long northwest-striking fault illuminated by aftershocks, *EOS, Trans. Am. geophys. Un.*, **75,** spring mtg. suppl., 237, (abstract).

N02 Atkinson, G.M., 1993. Earthquake source spectra in eastern North America, *Bull. seism. Soc. Am.*, **83,** 1778–1798.

N03 Bollinger, G.A., 1973. Seismicity of the southeastern United States, *Bull. seism. Soc. Am.*, **63,** 1785–1808.

N04 Bollinger, G.A., Langer, C.J. & Harding, S.T., 1976. The eastern Tennessee earthquake sequence of October through December, 1973, *Bull. seism. Soc. Am.*, **66,** 525–547.

N05 Coffman, J. & von Hake, C.A., 1973. *Earthquake History of the United States—Revised Edition (through 1970), Publication* **41-1,** U.S. Dept. of Commerce, Nat. Oceanic Atmos. Admin., Boulder, CO.

N06 Davis, S.D., Pennington, W.D. & Carlson, S.M., 1989. *A Compendium of Earthquake Activity in Texas,* Geological Circ. 89-3, Bur. Econ. Geol., Univ. Texas, Austin, TX.

N07 Docekal, J., 1970. *Earthquakes of the Stable Interior, with Emphasis on the Midcontinent,* PhD Dissert., Univ. of Nebraska, Lincoln, NE.

N08 Drysdale, J.A. & Cajka, M.G., 1989. Intensity distribution of the 1988 M6 Saguenay earthquake, *Seism. Res. Lett.*, **60,** 142, (abstract).

N09 Gordon, D.W., Bennett, T.J., Herrmann, R.B. & Rogers, A.M., 1970. The south-central Illinois earthquake of November 9, 1968: macroseismic studies, *Bull. seism. Soc. Am.*, **60,** 953–971.

N10 Hasegawa, H.S. & Wetmiller, R.J., 1980. The Charlevoix earthquake of 19 August 1979 and its seismo-tectonic environment, *Earthq. Notes,* **51(4),** 23–37.

N11 Horner, R.B., Stevens, A.E., Hasegawa, H.S. & LeBlanc, G., 1978. Focal parameters of the July 12, 1975, Maniwaki, Québec, earthquake—an example of intraplate seismicity in eastern Canada, *Bull. seism. Soc. Am.*, **68,** 619–640.

N12 Horner, R.B., Wetmiller, R.J. & Hasegawa, H.S., 1979. The St. Donat, Quebec, earthquake sequence of February 18–23, 1978, *Can. J. Earth Sci.*, **16,** 1892–1898.

N13 Lamontagne, M., Hasegawa, H.S., Forsyth, D.A., Buchbinder, G.G.R. & Cajka, M., 1994. The Mont-Laurier, Québec, earthquake of 19 October 1990 and its seismotectonic environment, *Bull. seism. Soc. Am.*, **84,** 1506–1522.

N14 Mauk, F.J., Christensen, D.C. & Henry, S., 1982. The Sharpsburg, Kentucky, earthquake 27 July 1980: main shock parameters and isoseismal maps, *Bull. seism. Soc. Am.*, **72,** 221–236.

N15 National Earthquake Information Center (NEIC), 1963–1994. *Preliminary Determination of Epicenters,* USGS monthly publ., Golden, CO.

N16 National Earthquake Information Service (NEIS). Computer file of intensity data, various earthquakes, USGS, Golden, CO.

N17 Nuttli, O.W. & Brill, K.G., 1981. Catalog of central United States earthquakes since 1800 of $m_b \geq 3.0$, Part II and Appendix B-2, in *An Approach to Seismic Zonation for Siting Nuclear Electric Power Generating Facilities in the Eastern United States,* pp. 97–143, B2-1–B2-31, eds Barstow, N.L., Brill, K.G., Nuttli, O.W. & Pomeroy, P.W., *NUREG/CR-1577,* US Nuclear Regulatory Comm., Washington, DC.

N18 Reagor, G. & Brewer, L.R., 1987. Preliminary isoseismal map and intensity distribution for the southeastern Illinois earthquake of June 10, 1987, *USGS Open-File Rpt.,* **87-578.**

N19 Schwartz, S.Y. & Christensen, D.H., 1988. The 12 July 1986 St. Marys, Ohio earthquake and recent seismicity in the Anna, Ohio seismogenic zone, *Seism. Res. Lett.*, **59,** 57–62.

N20 Seeber, L. & Armbruster, J.G., 1981. The 1886 Charleston, South Carolina earthquake and the Appalachian detachment, *J. geophys. Res.*, **86,** 7874–7894.

N21 Smith, W.E.T., 1962. Earthquakes of eastern Canada and adjacent areas, 1534–1927, *Publ. Dominion Observatory,* **26,** 269–301.

N22 Smith, W.E.T., 1966. Earthquakes of eastern Canada and adjacent areas, 1928–1959, *Publ. Dominion Observatory,* **32,** 87–121.

N23 Stevens, A.E. (ed.), 1983. *Miramichi, New Brunswick, Canada earthquake sequence of 1982—a preliminary report,* Earthq. Eng. Res. Inst., Berkeley, CA.

N24 Stover, C.W., 1985. Preliminary isoseismal map and intensity distribution for the Laramie Mountains, Wyoming, earthquake of October 18, 1984, *USGS Open-File Rpt.,* **85-137.**

N25 Stover, C.W., 1986. Preliminary isoseismal map for the northeastern Ohio earthquake of January 31, 1986, *USGS Open-File Rpt.,* **86-356.**

N26 Stover, C.W. & Coffman, J.L., 1993. *Seismicity of the United States, 1568–1989 (Revised), USGS Prof. Paper,* **1527.**

N27 Street, R.L. & Lecroix, A., 1979. An empirical study of New England seismicity: 1727–1977, *Bull. seism. Soc. Am.*, **69,** 159–175.

N28 Street, R.L., Taylor, K., Jones, D., Harris, J., Steiner, G., Zekulin, A. & Zhang, D., 1993. The 4.6 $m_{b,Lg}$ northeastern Kentucky earthquake of September 7, 1988, *Seism. Res. Lett.*, **64,** 187–200.

N29 US Coast & Geodetic Survey (US Geological Survey), 1928–1986. *United States Earthquakes,* Ann. publ. USCGS (USGS), Dept. of Commerce (Interior), Washington, DC.

N30 Wetmiller, R.J., 1975. The Québec–Maine border earthquake, 15 June 1973, *Can. J. Earth Sci.*, **12,** 1917–1928.

N31 Wetmiller, R.J. *et al.*, 1992. Canadian Seismic Agreement—Ann. Rept July 1989–June 1990, *NUREG/CR-4753,* US Nuc. Reg. Comm., Washington, DC.

Global (non-North American) SCR References [Tables A3(b) and A4; G-prefix]

G01 Abe, K., 1981. Magnitudes of large shallow earthquakes from 1904 to 1980, *Phys. Earth planet. Inter.*, **27,** 72–92.

G02 Ahorner, L., Camelbeeck, T., De Becker, M., Flick, J., Ritsema, R., Houtgast, G. & Vogt, J., 1985. Macroseismic map of the Liège earthquake of November 8, 1983, in *Seismic Activity in Western Europe,* pp. 297–300, ed. Melchior, P., D. Reidel Publ. Co., Dordrecht, The Netherlands.

G03 Ahorner, L. & Pelzing, R., 1985. The source characteristics of the Liège earthquake on November 8, 1983, from digital recordings in West Germany, in *Seismic Activity in Western Europe,* pp. 263–290, ed. Melchior, P., D. Reidel Publ. Co., Dordrecht, Holland.

G04 Ambraseys, N.N. & Adams, R.D., 1986. Seismicity of West Africa, *Ann. Geophys.*, **4B,** 679–702.

G05 Assumpção, M., Suárez, G., & Veloso, J.A., 1985. Fault plane solutions of intraplate earthquakes in Brazil: some constraints on the regional stress field, *Tectonophysics,* **113,** 283–293.

G06 Berrocal, J., Assumpção, M., Antezana, R., Dias Neto, C.M., Ortega, R. & França, H., 1983. Seismic activity in Brazil in the period 1560–1980, *Earthq. Predict. Res.*, **2,** 191–208.

G07 Brune, J. & King, C., 1967. Excitation of mantle Rayleigh waves of period 100 seconds as a function of magnitude, *Bull. seism. Soc. Am.*, **57,** 1355–1365.

G08 Chaudhury, H.M., Bhattacharya, S.N. & Basu, S.R., 1970. Recent earthquake activity in India, in *Proc. Fourth Symp. Earthq. Eng.,* India Meteorological Dept., New Delhi, 382–388 & 415–418.

G09 Chen, E., Su, T. & Hung, Y.-Y., 1985. Preliminary study of the earthquake at Nanai, Guangdong Province in 1918 and its background of genetic structure, *J. South Chinese Seism.*, **5,** 1–16, (in Chinese).

G10 Chen, P. & Nuttli, O.W., 1984. Estimates of magnitudes and short-period wave attenuation of Chinese earthquakes from modified Mercalli intensity data, *Bull. seism. Soc. Am.*, **74,** 957–968.

G11 Chen, W.-P. & Molnar, P., 1977. Seismic moments of major earthquakes and the average rate of slip in central Asia, *J. geophys. Res.*, **82,** 2945–2969.

G12 Chinn, D.S. & Isacks, B.L., 1983. Accurate source depths and focal mechanisms of shallow earthquakes in western South America and in the New Hebrides island arc, *Tectonics,* **2,** 529–563.

G13 Denham, D., Gibson, G., Smith, R.S. & Underwood, R., 1985. Source mechanisms and strong ground motion from the 1982 Wonnangatta and the 1966 Mount Hotham earthquakes, *Austr. J. Earth Sci.*, **32,** 37–46.

G14 Everingham, I.B., Denham, D. & Greenhalgh, S.A., 1987. Surface-wave magnitudes of some early Australian earthquakes, *Bur. Mineral Res. J. Austr. Geol. Geophys.*, **10,** 253–259.

G15 Everingham, I.B., McEwin, A.J. & Denham, D., 1982. Atlas of isoseismal maps of Australian earthquakes, *Bull.*, **214,** Bur. Mineral Res., Geol. and Geophys., Canberra.

G16 Geological Survey of South Africa, 1974. *Earthquake of 29 Sept 1969 in the Southwest Cape Province: Seismic History of the S-W Cape Province,* Seism. Ser., **14,** Pretoria, RSA, (in Afrikaans).

G17 Giuliano, A., Amado, J. & Vargas, A., 1982. Analisis de los espectros de ductilidad correspondientes al terremoto de San Juan del 23 de Noviembre de 1977, *Publicacion Techica No. 8,*

Instituto Nacional de Prevencion Sismica, Argentina, (in Spanish).

G18 Given, J.W. & Kanamori, H., 1980. The depth extent of the 1977 Sumbawa, Indonesia earthquake, *EOS, Trans. Am. geophys. Un.*, **61,** 1044, (abstract).

G19 Gordon, R.R. & Lewis, J.D., 1980. The Meckering and Calingiri Earthquakes, October 1968 and March 1970, *Geol. Surv. West. Austr. Bull.*, **126**.

G20 Gorshkov, G.P., 1963. The seismicity of Africa, in *A Review of the Natural Resources of the African Continent,* pp. 101–151, UNESCO, Internat. Documents Ser., Columbia University Press, New York, NY.

G21 Gregson, P.J., Paull, E.P. & Gaull, B.A., 1979. The effects in Western Australia of a major earthquake in Indonesia on 19 August 1977, *Bur. Mineral Res. J. Austr. Geol. Geophys.*, **4,** 135–140.

G22 Gu, G. (ed.), 1983a. *Catalog of Chinese Earthquakes 1831 BC–1969 AD*, Science Press, Beijing, (in Chinese).

G23 Gu, G. (ed.), 1983b. *Catalog of Chinese Earthquakes 1970–1979,* Science Press, Beijing, (in Chinese).

G24 Guo, Z. & Ma, Z., 1988. *Research on Major Earthquakes in China—Part 1,* Seismological Publishing Company, Beijing, (in Chinese).

G25 Gupta, H.K., Mohan, I. & Narain, H., 1970. Godavari Valley earthquake sequence of April 1969, *Bull. seism. Soc. Am.*, **60,** 601–615.

G26 Gupta, H.K., Mohan, I. & Narain, H., 1972. The Broach earthquake of March 23, 1970, *Bull. seism. Soc. Am.*, **62,** 47–61.

G27 Gupta, H., Narain, H., Rastogi, B.K. & Mohan, I., 1969. A study of the Koyna earthquake of December 10, 1967, *Bull. seism. Soc. Am.*, **59,** 1149–1162.

G28 Gutenberg, B. & Richter, C.F., 1954. *Seismicity of the Earth and Associated Phenomena,* 2nd edn, Princeton University Press, Princeton, NJ.

G29 Haessler, H., Hoang-Trong, P., Schick, R., Schneider, G. & Strobach, K., 1980. The September 3, 1978 Swabian Jura earthquake, *Tectonophysics,* **68,** 1–14.

G30 Hansen, R.A., Bungum, H. & Alsaker, A., 1989. Three recent larger earthquakes offshore Norway, *Terra Nova,* **1,** 284–295.

G31 Harvard University, 1977–1944. *Centroid, Moment Tensor Catalog,* computer event file, Cambridge, MA.

G32 He, C. & Zhang, T., 1990. The south Huanghai Sea, Jiangsu Province earthquake of M6.2 of May 21, 1984, in *Earthquake Cases in China (1981–1985),* pp. 190–223, Seismological Press, Beijing.

G33 Houtgast, G., 1985. Macroseismic observations of the Liège earthquake of November 8, 1983 in the Netherlands, in *Seismic Activity in Western Europe,* pp. 311–312, ed. Melchior, P., D. Reidel Publ. Co., Dordrecht, Holland.

G34 International Seismological Centre (ISC), 1964–1993. *Bull. Int. Seism. Centre,* Monthly publ. ISC, Newbury, UK.

G35 Jones, T.D., Gibson, G., McCue, K., Denham, D., Gregson, P.J. & Bowman, J.R., 1991. Three large earthquakes rupture the Australian Precambrian shield near Tennant Creek, Northern Territory on 22 January, 1988, *Bur. Mineral Res. J. Austr. Geol. Geophys.*, **12,** 339–343.

G36 Junner, N.R., 1941. The Accra earthquake of 22nd June, 1939, *Gold Coast Geol. Surv. Bull.*, **13,** 3–41.

G37 Kadinsky-Cade, K. & Reilinger, R., 1985. Surface deformation associated with the November 23, 1977, Caucete, Argentina, earthquake sequence, *J. geophys. Res.*, **90,** 12 691–12 700.

G38 Lei, T.-C., Wang, Y.-D. & Ou, B.-S., 1991. Surface rupture pattern by the Xunwu earthquake of magnitude 5.5 on August 2, 1987, *Seismol. Geol.*, **13,** 353–360, (in Chinese).

G39 Lynnes, C. & Lay, T., 1988. Source process of the great 1977 Sumba earthquake, *J. geophys. Res.*, **93,** 13 407–13 420.

G40 McCue, K., 1990. Australia's large earthquakes and Recent fault scarps, *J. struct. Geol.*, **12,** 761–766.

G41 McCue, K., Gibson, G. & Wesson, V., 1990. The earthquake near Nhill, western Victoria, on 22 December 1987 and the seismicity of eastern Australia, *Bur. Mineral Res. J. Austr. Geol. Geophys.*, **11,** 415–420.

G42 McCue, K. & Michael-Leiba, M., 1993. Australia's deepest known earthquake, *Seism. Res. Lett.*, **64,** 201–206.

G43 McCue, K., Wesson, V. & Gibson, G., 1990. The Newcastle, New South Wales, earthquake of 28 December 1989, *Bur. Mineral Res. J. Austr. Geol. Geophys.* **11,** 559–567.

G44 Melchers, R.E. & Page, A.W., 1992. The Newcastle earthquake, *Proc. Inst. Civ. Engrs Structs & Bldgs,* **94,** 143–156.

G45 Michael-Leiba, M., Love, D., McCue, K. & Gibson, G., 1994. The Uluru (Ayers Rock), Australia, earthquake of 28 May 1989, *Bull. seism. Soc. Am.*, **84,** 209–214.

G46 Muir Wood, R. & Woo, G., 1985. The British earthquake of 19 July 1984, *Geol. Today,* **1,** 4–5.

G47 Mukherjee, M.K., 1981. Evolution of Anklesvar anticline, Cambay basin, India, *Am. Assoc. Petrol. Geol. Bull.*, **65-2,** 336–343.

G48 National Earthquake Information Center (NEIC), 1963–1994. *Preliminary Determination of Epicenters,* USGS monthly publ., Golden, CO.

G49 Pacheco, J.F. & Sykes, L.R., 1992. Seismic moment catalog of large shallow earthquakes, 1900 to 1989, *Bull. seism. Soc. Am.*, **82,** 1306–1349.

G50 Procházková, D. *et al.*, 1979. Macroseismic field of the earthquake of September 3, 1978, in the Swabian Jura, *J. Geophys.*, **46,** 343–347.

G51 Ritchie, M.E.A., Musson, R.M.W. & Woodcock, N.H., 1990. The Bishop's Castle earthquake of 2 April 1990, *Terra Nova,* **2,** 390–400.

G52 Rynn, J.M.W., 1991. The 1989 Newcastle earthquake—the source, the size, the observations—lessons for Australia, in *What We Have Learnt from the Newcastle Earthquake, Proc.,* ed. Rynn, J.M.W., University of Queensland, Australia.

G53 Rynn, J.M.W., Denham, D., Greenhalgh, S., Jones, T., Gregson, P.J., McCue, K.F. & Smith, R.S., 1987. *Atlas of Isoseismal Maps of Australian Earthquakes,* Bur. Mineral Res., Geol. and Geophys., *Bull.* **222,** Canberra, ACT.

G54 Seeber, L. & Armbruster, J.G., 1981a. The 1886 Charleston, South Carolina earthquake and the Appalachian detachment, *J. geophys. Res.*, **86,** 7874–7894.

G55 Seeber, L. & Armbruster, J.G., 1981b. Great detachment earthquakes along the Himalayan arc and long-term forecasting, in *Earthquake Prediction, An International Review,* pp. 259–277, eds Simpson, D.W. & Richards, P.G., Am. Geophys. Un., Maurice Ewing Series 4.

G56 Silver, P. & Jordan, T., 1983. Total-moment spectra of fourteen large earthquakes, *J. geophys. Res.*, **88,** 3273–3293.

G57 Singh, D.D. & Gupta, H.K., 1980. Source dynamics of two great earthquakes of the Indian subcontinent: The Bihar-Nepal earthquake of January 15, 1934 and the Quetta earthquake of May 30, 1935, *Bull. seism. Soc. Am.*, **70,** 757–773.

G58 Somerville, M.R., 1991. Seismic amplification determined from microtremor monitoring at alluvial and rock sites in Newcastle, in *What We Have Learnt from the Newcastle Earthquake, Proc.,* ed. Rynn, J.M.W., University of Queensland, Australia.

G59 Tandon, A.N., 1959. The Rann of Cutch earthquake of 21 July 1956, *Indian J. Meteor. Geophys.*, **10,** 137–146.

G60 Trodd, H., Warburton, P. & Pooley, C.I., 1985. The great British earthquake of 1984 seen from afar, *Geophys. J. R. astr. Soc.*, **83,** 809–812.

G61 Turbitt, T. *et al.*, 1985. The North Wales earthquake of 19 July 1984, *J. geol. Soc. London,* **142,** 567–571.

G62 van Eck, T., Ahorner, L. & Paulssen, H., 1993. The earthquake of the century in northwestern Europe: The Roermond, The Netherlands, earthquake of April 13, 1992, *Earthq. Volc.*, **24,** 15–26.

G63 Wei, B.-Z. & Chung, W.-Y., 1993. Regional waveform constraints on the source parameters of the Xunwu, China, earthquake of August 2, 1987 with implications for mid-plate seismotectonics, *Phys. Earth planet. Inter.*, **78,** 57–68.

G64 Xie, Y. & Cai, M. (eds), 1983. *The Collection of Earthquake Data in China History,* Science Publishing Co., Beijing.

G65 Yarwood, D.R. & Doser, D.I., 1990. Deflection of oceanic transform motion at a continental margin as deduced from waveform inversion of the 1939 Accra, Ghana earthquake, *Tectonophysics,* **172,** 341–349.